AD-A159 739 ATMOSPHERIC ELECTRICITY HAZARDS THREAT ENVIRONMENT 1/3
DEFINITION(U) BOEING MILITARY AIRPLANE CO SEATTLE WA
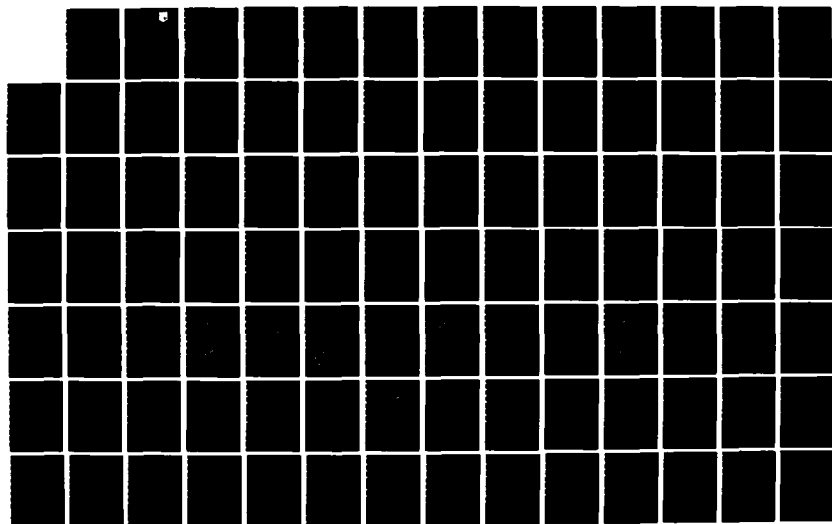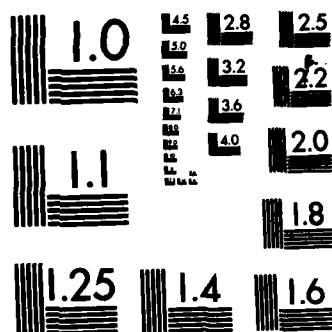B G MELANDER ET AL. AUG 85 AFWAL-TR-85-3052
UNCLASSIFIED F33615-82-C-3406 F/G 1/2 NL

MICROCOPY RESOLUTION TEST CHART
NATIONAL BUREAU OF STANDARDS-1963-A

AFWAL-TR-85-3052

AD-A159 739

# ATMOSPHERIC ELECTRICITY HAZARDS THREAT ENVIRONMENT DEFINITION

B.G. MELANDER
BOEING MILITARY AIRPLANE COMPANY
SEATTLE, WASHINGTON 98124

AUGUST 1985

FINAL REPORT FOR PERIOD AUG 82 - MARCH 1984

APPROVED FOR PUBLIC RELEASE; DISTRIBUTION UNLIMITED

DTIC
ELECTE
S   OCT 0 4 1985
E   D

FLIGHT DYNAMICS LABORATORY
AIR FORCE WRIGHT AERONAUTICAL LABORATORIES
AIR FORCE SYSTEMS COMMAND
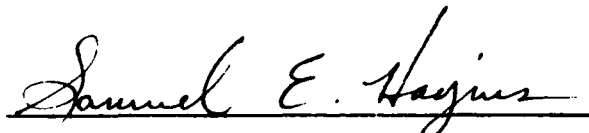WRIGHT-PATTERSON AIR FORCE BASE, OHIO 45433

85  10  03  135

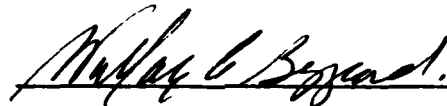This report has been reviewed by the Office of Public Affairs (ASD/PA) and is releasable to the National Technical Information Service (NTIS). At NTIS, it will be available to the general public, including foreign nations.

This technical report has been reviewed and is approved for publication.
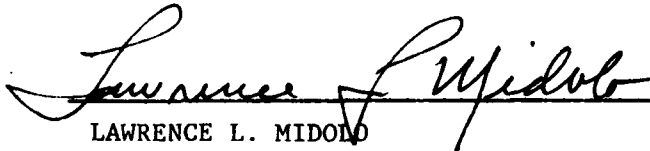
SAMUEL E. HAGINS, 2Lt, USAF
AEHP Project Engineer
Advanced Development Programs Branch

WALLACE C. BUZZARD, Chief
Advanced Development Programs Branch
Vehicle Equipment Division

FOR THE COMMANDER

LAWRENCE L. MIDOLO
Acting Chief
Vehicle Equipment Division

"If your address has changed, if you wish to be removed from our mailing list, or if the addressee is no longer employed by your organization please notify AFWAL/FIEA, W-PAFB, OH 45433 to help us maintain a current mailing list".

Copies of this report should not be returned unless return is required by security considerations, contractual obligations, or notice on a specific document.

AD-A159 739

# REPORT DOCUMENTATION PAGE

| 1a. REPORT SECURITY CLASSIFICATION | 1b. RESTRICTIVE MARKINGS |
|---|---|
| UNCLASSIFIED | |

| 2a. SECURITY CLASSIFICATION AUTHORITY | 3. DISTRIBUTION/AVAILABILITY OF REPORT |
|---|---|
| | Approved for Public release; distribution unlimited. |
| 2b. DECLASSIFICATION/DOWNGRADING SCHEDULE | |

| 4. PERFORMING ORGANIZATION REPORT NUMBER(S) | 5. MONITORING ORGANIZATION REPORT NUMBER(S) |
|---|---|
| | AFWAL-TR-85-3052 |

| 6a. NAME OF PERFORMING ORGANIZATION | 6b. OFFICE SYMBOL (If applicable) | 7a. NAME OF MONITORING ORGANIZATION |
|---|---|---|
| Boeing Military Airplane Co. | | Air Force Wright Aeronautical Laboratories Flight Dynamics Laboratory (AFWAL/FIEA) |

| 6c. ADDRESS (City, State and ZIP Code) | 7b. ADDRESS (City, State and ZIP Code) |
|---|---|
| Seattle, Washington 98124 | Wright-Patterson AFB, OH 45433 |

| 8a. NAME OF FUNDING/SPONSORING ORGANIZATION | 8b. OFFICE SYMBOL (If applicable) | 9. PROCUREMENT INSTRUMENT IDENTIFICATION NUMBER |
|---|---|---|
| Flight Dynamics Laboratory | AFWAL/FIEA | F33615-82-C-3406 |

| 8c. ADDRESS (City, State and ZIP Code) | 10. SOURCE OF FUNDING NOS. | | | |
|---|---|---|---|---|
| | PROGRAM ELEMENT NO. | PROJECT NO. | TASK NO. | WORK UNIT NO. |
| Wright-Patterson AFB, OH 45433 | 63205F | 2507 | 02 | 01 |

11. TITLE (Include Security Classification) Atmospheric Electricity Hazards Threat Environment Definition

12. PERSONAL AUTHOR(S)
Melander, B. G. , Cooley, W. W.

| 13a. TYPE OF REPORT | 13b. TIME COVERED | 14. DATE OF REPORT (Yr., Mo., Day) | 15. PAGE COUNT |
|---|---|---|---|
| Interim | FROM Aug 82 TO Mar 84 | August 1985 | 145 |

16. SUPPLEMENTARY NOTATION

| 17. | COSATI CODES | | 18. SUBJECT TERMS (Continue on reverse if necessary and identify by block number) |
|---|---|---|---|
| FIELD | GROUP | SUB. GR. | Aircraft Lightning Threat Atmospheric Electricity |
| 03 | 01 | | |
| | | | |

19. ABSTRACT (Continue on reverse if necessary and identify by block number)

This document provides definition of the atmospheric electricity threat environment as part of the Atmospheric Electricity Hazards Protection (AEHP) program under Air Force contract F33615-82-C-3406. This issue contains an initial atmospheric electricity threat to be used for aircraft based on measurement of (1) the lightning threat at the ground, and (2) the static electrification threat at altitude. The experimental basis for this threat is critically reviewed. Recommendations are made for future work in atmospheric electricity environments to refine and improve understanding of aircraft AEH environments.

| 20. DISTRIBUTION/AVAILABILITY OF ABSTRACT | 21. ABSTRACT SECURITY CLASSIFICATION |
|---|---|
| UNCLASSIFIED/UNLIMITED ☒ SAME AS RPT. ☐ DTIC USERS ☐ | UNCLASSIFIED |

| 22a. NAME OF RESPONSIBLE INDIVIDUAL | 22b. TELEPHONE NUMBER (Include Area Code) | 22c. OFFICE SYMBOL |
|---|---|---|
| 2Lt S. Haging | (513) 255-2527 | AFWAL/FIEA |

**DD FORM 1473, 83 APR** EDITION OF 1 JAN 73 IS OBSOLETE.

# FOREWORD

| Accession For | |
|---|---|
| NTIS GRA&I | X |
| DTIC TAB | ☐ |
| Unannounced | ☐ |
| Justification | |

By_____
Distribution/
Availability Codes
Avail and/or
Dist    Special

**A-1**

DTIC
COPY
INSPECTED
8

iii

# TABLE OF CONTENTS

# LIST OF FIGURES

## LIST OF FIGURES (continued)

# LIST OF FIGURES (continued)

# LIST OF TABLES

# 1.0 INTRODUCTION

The objectives of the Atmospheric Electricity Hazards Protection (AEHP) program are to develop design criteria, guidelines, and qualification test procedures for mitigating any atmospheric electricity vulnerabilities of electronic equipment in future advanced aircraft structures. The emphasis is on indirect effects of lightning/static electrification and their induced electrical transients in aircraft wiring rather than direct arc/spark effects.

Potential hazards to electronics equipment within an aircraft encountering natural atmospheric electricity depends strongly on the interaction of airframe structure with a lightning strike and its associated electromagnetic fields. The physical processes whereby electrical transients are induced by lightning or static electricity within an air vehicle wiring installation are significantly different than processes previously considered for structural damage due to directly attached lightning. The most important difference for electronic effects is the need to consider rate-of-rise parameters for currents and fields because inductive and capacitive coupling dominates internal transients when circuitry is isolated from vehicle structure. Peak values and time duration of current and fields are also important in determining voltages and currents within the structure. Pulse energy is also important in determining the rating for transient protective devices that may be required to absorb energy from the lightning induced transients.

Physical understanding of the experimental data sources that define lightning and static electrification environments are important in determining the critical rate of rise parameters. These parameters are especially important for determining currents and electromagnetic fields associated with aircraft interaction with the AEH threat environments.

## 1.1 OBJECTIVE AND SCOPE

The objective of this document is to provide definition of the AEHP program threat environment. This threat document will be revised periodically to provide the "best" current definition of AEH threats. This issue summarizes the initial atmospheric electricity threat to be used for definition of the lightning threat at the ground. The experimental basis for this threat is critically reviewed. Comparisons with statistical data are made as well as

1

comments on the validity of this data. Comments on on-going lightning/static electrification data collection programs are made. This data will impact the final threat definition. An initial threat definition is needed to support the Phase I environmental impact tests. A final AEH threat definition will arise out of additional studies of existing data as well as new data as it becomes available.

## 1.2    THREAT SUMMARY

The problem of determining the atmospheric electricity (AE) threat to aircraft in flight has been examined for many years. More recently due to research into advanced composite material having poor electrical properties compared to metals, interest has increased in better definition of the AE threat to aircraft and electrical/electronic equipment. The severity of the threat will determine the equipment protection necessary for aircraft all weather operation.

Natural atmospheric electricity presents two separate hazards:  lightning and static discharges due to aircraft charging. The mechanism of a natural cloud-to-ground lightning discharge is illustrated in Figure 1.1. When sufficient charge accumulates in the lower part of a cloud to cause an electric field which exceeds the ionization threshold of air, an electrical discharge is initiated toward the earth. Because the discharge requires a finite amount of charge and time for the channel resistance to lower to the arc phase, the discharge proceeds in a sequence of steps, pausing periodically to allow the previous channel section to become fully conducting. This mechanism is known as the stepped (or step) leader process.

The natural electrical phenomena occurring with lightning discharges vary in number and intensity. A statistical basis is needed to define a threat because of this variability. A moderate threat level is defined as the expected levels from a typical lightning flash. Severe lightning is defined as a reasonable worst-case level expected to occur during the service life of an aircraft. The maximum rate-of-rise and peak current values that represent the severe lightning threat are currently subjects of on-going current research into lightning hazards to aircraft in flight.

There is currently insufficient statistical data from efforts to measure lightning currents on aircraft in flight that allow definition of a worst-case

threat. Recent in flight data from the NASA Storm Hazards program has shown a worst-case value of 80 kA/μs for low level current from a cloud-to-cloud strike.

The best available statistical data on lightning currents is data measured on the ground. Currently published data on cloud-to-ground lightning currents measured on the ground show that 180 kA/μs is the largest rate of rise directly measured. Recently obtained data on lightning currents inferred from measured electric fields are as high as 400 kA/μs. Both of these measurements are subject to uncertainties in the measuring techniques. These limitations will be discussed in Chapter 2. The best engineering judgment at present is that 200 kA/μs adequately represents the worst-case expected for an aircraft in flight and is defined as the severe level for AEH threat. Additional research is needed to resolve the difference between the defined severe threat and the distant field measurements.

The defined parameters for the AEH lightning threats to aircraft are shown in Table 1-1.

TABLE 1-1   AEH LIGHTNING THREAT PARAMETERS

| SINGLE STROKE THREAT | PEAK CURRENT | MAXIMUM RATE OF RISE | TIME TO HALF AMPLITUDE | ACTION INTEGRAL |
|---|---|---|---|---|
| Moderate (Expected) | 20 kA | 50 kA/μs | 50μsec | $1.5 \times 10^4$ A$^2$-sec |
| Severe | 200 kA | 200 kA/μs | 50μsec | $1.5 \times 10^6$ A$^2$-sec |

Multiple Stroke Events - Flash (Moderate and Severe)

| | | | | |
|---|---|---|---|---|
| o Transient Duration | 50-500 μsec | | o Duration of Flash | 2 sec |
| o Interstroke Interval | 10-100 msec | | o Number of Strokes | 24 |

A second threat to aircraft from atmospheric electricity occurs due to aircraft charging effects. As an aircraft moves through the air, it can become charged. This can result in discharges either by streamering, corona or arcs and sparks.

3

Figure 1.2 shows these discharges from various sections of an aircraft. Arcs and sparks can create direct damage effects especially in fuel tanks. Proper grounding and bonding can usually eliminate these problems. Noise problems from corona or streamering phenomena is not so easily eliminated. These noise levels must be established as a part of the total atmospheric threat levels to aircraft. The static electrification threat is vehicle dependent as described in Sections 6 and 7.

The organization of this document is as follows. Lightning threat is discussed in Chapters 2 and 3. Chapter 2 describes the literature review and discusses the choice of the best data for threat definition. Chapter 3 outlines the ground lightning threats, both moderate and severe, and discusses their correlation with available data. Chapter 4 discusses the applicability of lightning models as a tool in extrapolating the lightning threat to aircraft altitudes. Chapter 5 reviews the static electrification threats from streamers and corona. Chapter 6 lists parametric threat levels for both lightning and static electrification. Chapter 7 will discuss meterological phenomenon and will be completed for the final threat documentation. Chapter 9 summarizes the document content and makes recommendations for future work.

4

STEPPED LEADER CHANNEL
APPROACHING AIRCRAFT

LEADER CHANNEL
PASSING THROUGH AIRCRAFT

RETURN STROKE PASSING
BACK TOWARD CLOUD
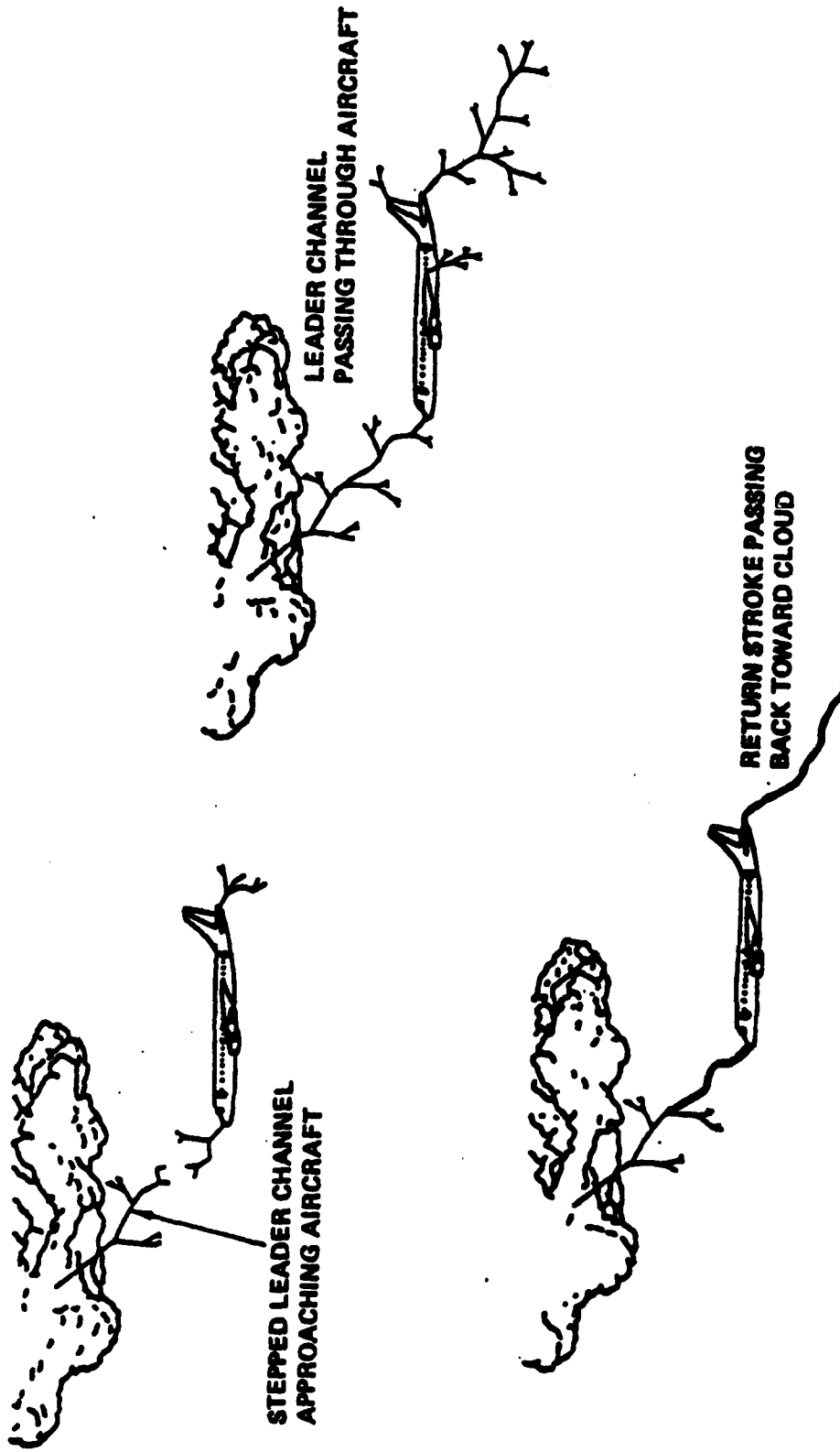
Figure 1.1

**Lightning Flash Striking an Aircraft**

INDUCTION PULSES
PRODUCED BY
CHARGED PARTICLES
PASSING ANTENNA

CORONA
DISCHARGES
FROM
EXTREMITIES

STREAMERS ON
INSULATING
SURFACES

SPARKS BETWEEN
UNBONDED METAL
SECTIONS
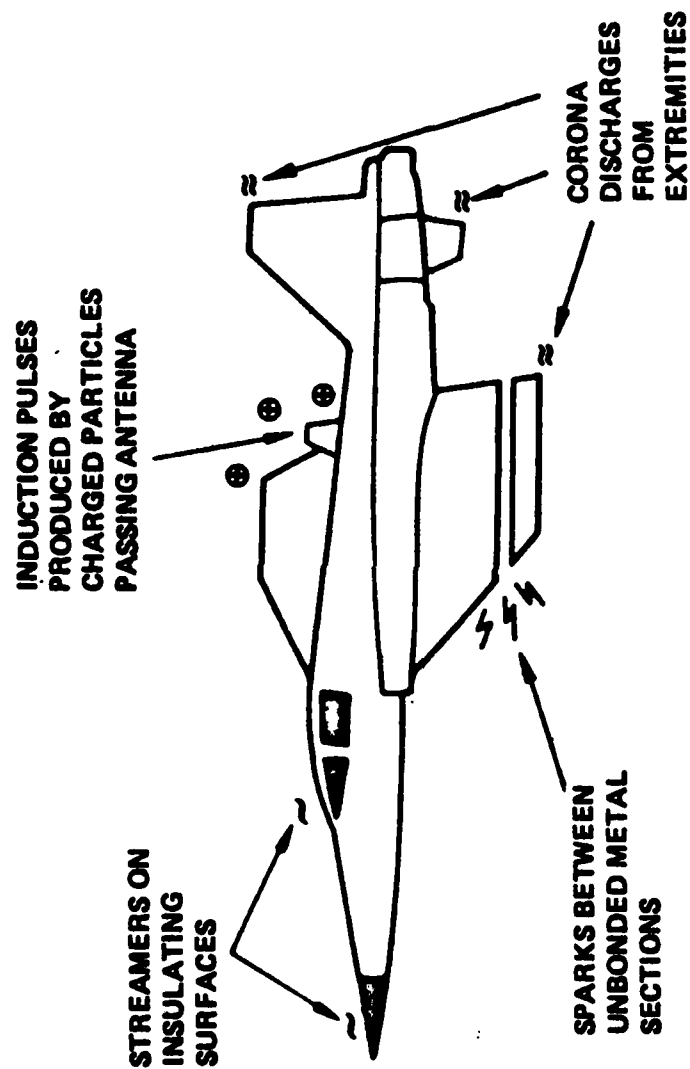
Figure 1.2
Noise Generation Sources

6

## 2.0 REVIEW OF AVAILABLE LIGHTNING DATA

### 2.1 INTRODUCTION

Lightning is a transient, high current electric discharge. The most common source of lightning arises from the electric charge separation in ordinary thunderstorm clouds (cumulonimbus). Well over half of all lightning discharges occur within the cloud (intracloud discharges). Cloud-to-ground lightning (sometimes called streaked or forked lightning) has been studied more extensively than other forms of lightning because of its practical interest (e.g., as the cause of disturbances in power and communication systems, strikes to aircraft and the ignition of forest fires) and because it is more easily observed with optical instruments. Cloud-to-cloud and cloud-to-air discharges are less common than intracloud or cloud-to-ground lightning.

Lightning strikes to aircraft are thought to involve both cloud-to-ground discharges (at low altitudes) and intracloud events (at high altitudes). The lightning data discussed in the present document includes only cloud-to-ground events. This data will be used to establish a ground based threat. A later version of this document will examine the airborne threat which will include cloud events.

A typical cloud-to-ground discharge starts with a preliminary breakdown within a cloud followed by a stepped leader initiating the first stroke (see Figure 2.1). Leader steps are usually $1\mu s$ long, tens of meters in length, with a pause between steps of $50\mu s$. The typical leader current is the order of 1 kA.

As the leader nears an aircraft, it enhances the local fields. Discharges off the extremities of the aircraft are produced when the field values reach air ionization levels. When the stepped leader connects to one of the aircraft discharges, it becomes merely a part of one step as the stepped leader proceeds to ground or another charged cloud.

As the leader tip nears the ground, an upward moving discharge is initiated at the ground (see Figure 2.2). The leader channel is discharged as a ground potential wave, the return stroke, propagates up the ionized leader path. The return stroke has a much higher current than a leader, an average of 20 kA

7

with maximum up to 200 kA and a rise time of few microseconds. The return stroke may be followed by a dart leader which initiates a subsequent stroke (see Figure 2.3). Subsequent strokes have faster rise times but comparable rates of change to return strokes. Many additional complete discharges called multiple strokes can take place. In general, these subsequent strokes have smaller magnitudes. Establishing the size of these threats is the first part of establishing an AEH threat.

## 2.2   DATA SOURCES

The data needed for estabishing aircraft lightning threat parameters are measurements of direct lightning strike currents and EM fields on aircraft at altitude. Lightning strike data measured on aircraft are not yet well understood because of the limited number of validated measurements. Two recent programs to gather more strike data at altitude are the NASA Storm Hazards Research F-106 and USAF C-130. This data will be used to aid in understanding the threat level at altitude.

The available data necessary to establish an aircraft lightning threat characterization is limited. Of all the types of lightning processes (leader, dart leader, J & K changes, preliminary breakdown, etc.), the most critical processes to aircraft safety are thought to be first return and subsequent strokes due to high current levels, high current rise rates and high energy inputs into aircraft systems. Data on these processes are for the most part confined to ground measurements of electric and magnetic fields, current waveforms, and stroke velocities (see Chapter 2 reference list for each topic).

Ground parameters are thought to be the worst case situation for lightning threats. Current and field amplitudes and rate of rise are thought to decrease with altitude. Hence, the most severe lightning threat to aircraft is a severe lightning strike on the ground.

The initial lightning threat outlined in this document is based on these ground measurements. The final threat will take into account altitude effects including in flight data.

## 2.3   DATA APPLICABILITY

The present threat definition is based on ground based direct current measurements. The data sets used were taken from available statistical studies on measured lightning current parameters.

8

Lightning current parameters derived from distant EM field measurements were not used in the initial threat definition. The statistics were not yet available when establishing the threat.

The errors associated with both direct current measurements and currents derived from field values should be established. This will allow a more complete and thorough use of the presently available data.

The following sections describe the major experimental efforts. The author date references are for chronology. Specific data sources are identified in the chapter where the data is discussed.

### 2.3.1 Berger, Garbagnati

Berger (1975) in Switzerland and Garbagnati (1982) in Italy have made a series of direct current measurements using towers on mountain tops. Berger's data is measured on a 70 m tower on top of Mount San Salvadore which is 914 m above sea level. Garbagnati's measurements are from 40 m towers on Italian mountains near San Salvadore. Berger's latest data is comprised of 101 negative and 26 positive first strokes and 135 subsequent strokes. Garbagnati has 103 negative and 5 positive first strokes and 175 subsequent strokes.

Uncertainties associated with both Berger and Garbagnati's data arise from the fact that both used towers on rocky mountain tops. The presence of the tower may have two effects on the data taken. The presence of the tower may influence the statistics of the lightning strikes. For example, larger amplitude strokes are thought to strike tall towers. The distance over which a structure attracts a downward leader is a function of the charge on the leader which, in turn, is related to the amplitude of the current in the return stroke (Golde, 1977). It would thus follow that lightning strikes to open ground should have a greater proportion of lower currents while taller structures might be expected to be subjected to a higher number of more intense currents. Another statistical fluctuation may be in the number of positive strokes seen. Evidence exists that positive flashes may increase with altitude (Berger, 1975; Erikson, 1978). If this trend holds true to aircraft altitudes, then any statistics taken near the ground will not be the statistics at altitude. The statistics of lightning strikes to aircraft are the statistics of interest here. Any way of measuring lightning strike statistics other than from strikes to the specific aircraft under mission

9

conditions will not reflect the true statistics of interest. Obviously, compromises on this issue will have to be made and some estimates of the errors involved should be established.

The presence of a tower in direct current measurements also affects the measurements themselves. The maximum rise rate is effected by the tower inductance and ground impedance effects. This would tend to lower the observed rise rates. The magnitude of this effect needs to be established. The early time portion of the waveform may also be effected due to the presence of the upward-going leaders which may lead to slower rise times for tall objects (Cianos and Pierce, 1972). Both effects could imply the current rise rates measured on towers are too low.

The leader effect should be more pronounced for first return strokes than for subsequent strokes since subsequent strokes are not thought to have long upward propagating leaders. Both Berger and Garbagnati's data show much higher rates of rise for subsequent than first return strokes while Uman (1973) and Weidman and Krider (1978, 1980) report no difference in current rates of rise derived from fields.

### 2.3.2 Uman and Krider
Uman and Krider have spent many years measuring electric and magnetic fields of various types of lightning (e.g. Lin et al 1979, Tiller et al 1976, Uman et al, 1976, Uman et al 1973, Weidman et al 1981). They have found much higher field rise times (under a microsecond) than have been seen in direct current measurements. The fast rise times were seen in measurements over salt water. Propagation over salt water does not attenuate the high frequencies as severely as earth. The reported upper frequency limit of these measurements is 20 MHz (Weidman et al 1981) due to wave action influencing measurements above 20 MHz. This data is very useful in establishing validity of a physical current model from which EM fields can be calculated and compared to the measured results.

To use this data in estabishment of a lightning current threat, the uncertainty associated with deriving currents from EM field measurements must be established. First, uncertainties arise from the measurements due to equipment limitations, resonance effects, propagation effects, etc. Second and more serious are uncertainties due to the assumptions in the current

models and the number of parameters needed to fit the data. The first type of uncertainty can be readily quantified. The second needs to be examined. In Uman's model, current is assumed to propagate up the channel at constant velocity. The channel is taken to be vertical with the initiation of the stroke at the ground. Three types of current profiles (uniform or leader current, breakdown current and corona current) have been incorporated to fit simultaneous electric and magnetic fields at two distances. The pulse velocity is an input to the model and is not well known. Assuming the velocity to be constant with height may also add uncertainties to the results. The corona current shape is somewhat arbitrary as stated by Lin et al (1980). The non-uniqueness of the current decomposition is a major problem and the uncertainties due to this have not yet established. The assumption that the initiation point is at the ground and not some distance above has been argued (C. Baum private communication) to introduce a factor of two error due to the two return front waves produced above ground. Lastly, the effect of the assumptions that the column is vertical and straight must be taken into account. Due to the above assumptions, error bars on measured field data and lightning current model assumptions must be established before the data can be incorporated into the AEHP lightning threat definition.

### 2.3.3  Others

Other data sources are listed in the Chapter 2 reference list (taken from a review by Uman and Krider, 1981). Only a few names will be specifically mentioned here. The recent review by Uman and Krider (1981) contains an extensive review of the lightning literature.

Data summarized by Cianos and Pierce (1972) was used in establishing the initial lightning threat. This data was a compilation of work prior to 1972 and is limited by the rise time resolution used in the data collection. This skews the results toward longer rise times and lower rise rates.

Data collected and reviewed by Popolansky (1972) include not only results obtained on tall chimneys and lightning rods but also the negative and positive first strokes recorded by Berger, totaling 624 waveforms. The resulting cumulative frequency distribution curve produces a median value of 28 kA. Berger et al (1975) conclude that the median values obtained on Mount San Salvatore and on tall chimneys in open country are similar. However, it should be pointed out that the slopes of the curves of best fit for these two data sets do not coincide completely (see Figures 3.9 and 3.10, next chapter).

11

Anderson and Erikson (1978) in South Africa measured lightning currents on a tower located in open country. Unlike Berger and Garbagnati, the measurements were taken on relatively flat terrain. Only a small number of strokes (eleven) were analyzed with a maximum current rise rate of 180 kA/$\mu$s for a subsequent stroke. This is a higher level both in absolute value and relative percentage than Berger and Garbagnati's measurements. With so few events, however, definite comparisons are premature.

Recently current waveforms are being measured in aircraft in flight by NASA (see Pitts 1981 and Pitts and Thomas 1981). To date cloud discharges dominate their results. The 1983 program will attempt to measure some cloud-to-ground strikes.

Return and subsequent stroke velocity data have been measured using luminosity data (e.g. Orville, 1968; Boyle and Orville, 1976; Lin et al, 1979; Hubert and Mouget, 1980; Jordan and Uman, 1980; Weidman and Krider, 1980). The data has a wide variation of velocities ranging from $2 \times 10^7$ m/sec to $2 \times 10^8$ m/sec. Typically the data only allows calculation of an average velocity found by knowing the distance traveled divided by the elapsed time. This data can be used to compare lightning model results for height variation of velocities. This data can also be used to estimate some of the uncertainty present in calculating current waveforms from field measurements.

## 2.4 CONCLUSIONS

To correctly assess the ground lightning threat, the available data sets (Berger, Garbagnati, Uman, Eriksson, Cianos and Pierce and Popalansky) must be critically assessed as to accuracy and limitations. The earlier data (Cianos and Pierce and Popalansky) do not reflect the recent fast rise times measured and so are biased to smaller rise rates. Both tower current data and current values derived from field measurements are subject to uncertainties. These uncertainties need to be quantitatively assessed before used as a basis for the final current threat levels.

## 2.5 BIBLIOGRAPHY

The following bibliography of AEH phenomena is included for locating sources of AEH data. The entries were obtained from a literature review initially collected by M. Uman and E. P. Krider.

### 2.5.1 Return Stroke Measured Fields

Baum, C.E., Breen, E.L., O'Neill, J.P., Moore, C.B., and Hall, D.L., Measurement of electromagnetic properties of lightning with 10 nano-second resolution, in Lightning Technology, NASA Conference Publication 2128, FAA-RD-80-30, April 1980, pp. 39-84.

Baum R.K., Airborne lightning characterization, in Lightning Technologoy, NASA Conference Publication 2128, FAA-RD-80-30, April 1980, pp. 153-172.

Fisher, R.J., and Uman, M.A., Measured electric fields risetimes for first and subsequent lightning return strokes, J. Geophy. Res., 77, 399-407, 1972.

Gupta, S.N., Distribution of peaks in atmospheric radio noise, IEEE Trans. on Electromagnetic Compatibility, EMC-15, 100-103, 1973.

Hart, J.E., V.L.F. radiation from multiple stroke lightning, J. Atmosperic Terrest. Phys., 29, 1011-1014, 1967.

Himley, R.O., VLF radiation from subsequent return strokes in multiple stroke lightning, J. Atmospheric Terrest. Phys., 31, 749-753, 1969.

Levine, D.M., and Krider, E.P., The temporal structure of HF and VHF radiation during Florida Lightning return strokes, Geophys. Res. Lett., 4, 13-16, 1977.

Lin, Y.T., Uman, M.A., Tiller, J.A., Brantley, R.D., Krider, E.P. and Weidman, C.D., Characterization of lightning return stroke electric and magnetic fields from simultaneous two-station measurements, J. Geophys. Res., 84, 6307-6314, 1979.

Nakai, T., On the time and amplitude properties of electric field near sources of lightning in the VLF, LF, and HF bands, Radio Science, 12, 389-396, 1977.

Nanevicz, J.E., and Vance, E.F., Analysis of electrical transients created by lightning SRI4026, NASA Contractor Report 159308, July 1980.

Pitts, F.L., Electromagnetic measurement of lightning strikes to aircraft, AIAA 19th Aerospace Sciences Meeting, St. Louis, Jan. 1981.

Pitts, F.L., and Thomas, M.E., 1980 direct strike lightning data, NASA Technical Memorandum 81946, Langley Research Center, Hampton, VA, February 1981.

Tiller, J.A., Uman, M.A., Lin, Y.T., Brantley, R.D., and Krider, E.P., Electric field statistics for close lightning return strokes near Gainesville, Florida, J. Geophys. Res., 81, 4430-4434, 1976.

Uman, M.A., Brantley, R.D., Tiller, J.A., Lin, Y.T., Krider, E.P., and McLain, D.K., Correlated electric and magnetic fields from lightning return strokes, J. Geophys. Res., 80, 373-376, 1976a.

Uman, M.A., McLain, D.K., Fisher, R.J., and Krider, E.P., Electric field intensity of the lightning return stroke, J. Geophys. Res. 78, 3523-3529, 1973.

Uman, M.A., Swanberg, C.E., Tiller, J.A., Lin, Y.T., and Krider, E.P., Effects of 200 km propagation on Florida lightning return stroke electric fields, Radio Science, 11, 985-990, 1976b.

## 2.5.2 Return Stroke Frequency Spectra

Barlow, J.S., Frey, Jr., G.W., and Newman, J.B., Very low frequency noise power from the lightning discharge, J. Franklin Inst., 27, 145-163, 1954.

Bradley, P.A., The spectra of lightning discharges at very low frequenceis, J. Atmospheriec Terrest. Phys., 26, 1069-1073, 1964.

Bradley, P.A., The VLF energy spectra of first and subsequent return strokes of multiple lightning discharge to ground, J. Atmospheric Terrest. Phys., 27, 1045-1053, 1965.

Croom, D.L., The spectra of atmoshperics and propagation of very low frequency radio waves, PH.D. Thesis, University of Cambridge, England, 1961.

Croom, D.L., The frequency spectra and attentuation of atmospherics in the range 1-15 kc/s, J. Atmospheric and Terrest. Phys., 26, 1015-1046, 1964.

Dennis, A.S., and Pierce, E.T., The return stroke of the lightning flash to earth as a source of VLF atmospherics, Radio Science, 68D, 779-794, 1964.

Galejs, J., Amplitude statistics of lightning discharge currents and ELF and VLF radio noise, J. Geophys. Res., 72, 2943-2953, 1967.

Harwood, J., and Harden, B.N., The measurement of atmospheric radio noise by an aural comparison methods in the range 15-500 kc/s, Proc. Inst. of Elec. Eng. (London), B107, 53-59, 1960.

Horner, F., Narrow band atmospherics from two local thunderstorms, J. Atmospheric Terrest. Phys., 21, 13-25, 1961.

Horner, F., Atmospherics of near lightning discharges, in Radio Noise of Terrestial Origin, F. Horner (ed.), American Elsevier Publishing Company, New York, 16-17, 1962.

Horner, F., Radio noise from thunderstorms, in Advances in Radio Research, 2, J.A. Saxton (ed.), Academic Press, New York, 122-215, 1964.

Horner, F., and Bradley, P.A., The spectra of atmospherics from near lightning, J. Atmospheric Terrest. Phys., 26, 1155-1166, 1964.

Levine, D., and Krider, E.P., The temporal structure of HF and VHF radiation during Florida lightning return strokes, Geophys. Res. Lett., 4, 13-16, 1977.

Marney, G.O., and Shanmugam, K., Effect on channel orientation on the frequency spectrum of lightning discharges, J. Geophys. Res., 76, 4198-4202, 1971.

Maxwell, E.L., Atmospheric noise from 20 Hz to 30 KHz, Radio Science, 2, 637-644, 1967.

Maxwell, E.L., and Stone, D.L., Natural noise fields from 1 cps to 100 kc, IEEE Trans. on Antenna and Propagation, AP-11, 339-343, 1963.

Obayashi, T., Measured frequency spectra of VLF atmospherics, J. Res. National Bureau of Standards, 64D, 41-48, 1960.

Serhan, G.I., Uman, M.A., Childers, D.G., and Lin, Y.T., The RF spectra of first and subsequent lightning return strokes in the 1-200 km range, Radio Science, 1980.

Steptoe, B.J., Some observations on the spectrum and propagation of atmospherics, Ph.D. thesis, University of London, England, 1958.

Taylor, W.L., Radiation field characteristics of lightning discharges in the bank 1 kc/s to 100 kc/s, J. Res. National Bureau of Standards, 67D, 539-550, 1963.

Taylor, W.L., and Jean, A.G., Very low frequency radiation spectra of lightning discharges, J. Res. National Bureau of Standards, 63D, 199-204, 1959.

Watt, A.D., and Maxwell, E.L., Characteristics of atmospherics noise from 1 to 100 kc, Proc. Inst. Radio Engineers, 45, 55-62, 1957.

Williams, J.C., Thunderstorms and VLF radio noise, Ph.D. thesis, Harvard University, Cambridge, Mass., 1959.

### 2.5.3 Frequency Spectra, Review Papers

Jones, H.L., Calkins, R.L., and Hughes, W.L., A review of the frequency spectrum of cloud-to-ground and cloud-to-cloud lightning, IEEE Trans. on Geoscience Electronics, GE-5, 1, 26-30, 1967.

Kimpara, A., Electromagnetic energy radiated from lightning, in Problems of Atmospheric and Space Electricity, S.C. Coroniti (ed.), American Elesevier Publishing Company, New York, 1965, 352-365.

Oetzel, G.N., and Pierce, E.T., Radio emissions from close lightning, in Planetary Electrodynamics, 1, S.C. Coroniti and J. Hughes (eds.), Gordon and Breach, New York, 1969, 543-570.

Oh, L.L., Measured and calculated spectral amplitude distribution of lightning sferics, IEEE Trans. Electromagnetic Compatability, EMC-11, 125-130, 1969.

Pierce, E.T., Spherics (sferics), in Encyclopedia of Atmospheric Sciences and Astrogeology, R.W. Fairbridge (ed.), Reinhold Publishing Co., 1967a, 935-939.

Pierce, E.T., Atmospherics - their characteristics at the source and propagation, Progress in Radio Science 1963-1966, Pt. 1, Inter. Scientific Radio Union, Berkeley, California, 987-1039, 1967b.

Pierce, E.T., Atmospherics and radio noise, in Lightning, 1, Physics of Lightning, R.H. Golde (ed.), Academic Press, New York, 1977, 351-384.

## 2.5.4 Return Stroke Current

Berger, K., Die messeinrichtungen for die blitzforschung auf dem Monte San Salvatore, Bull. Schweiz. Elektrotech. Ver., 46, 193-204, 1955.

Berger, K., Extreme blitzstrome und blitzschutz, Bull. ASE/USC, 71, 460-464, 1980.

Berger, K., Front duration and current steepness of lightning strokes to earth, Gas Discharges and the Electricity Supply Industry, (eds.) J.S. Forrest, P.R. Howard, and D.J. Littler, Butterworth, London, 1962, pp. 63-73.

Berger, K. Gewitterforschung auf dem Monte San Salvatore, Elektrotechnik, Z-A, 82, 249-260, 1967.

Berger, K., Lightning research in Switzerland, Weather, 2, 231-238, 1947.

Berger K., Methoden und resultate der blistzforschung auf dem Monte San Salvatore bei Lugano in dem jahren 1963-1971, Bull. Schweiz. Elektrotech. Ver., 63, 1403-1422, 1972.

Berger, K., Novel observations on lightning discharges: results of research on Mount San Salvatore, J. Franklin Inst., 283, 478-525, 1967.

Berger, K., Resultate der blitzmessungen der jahre 1947-1954 auf dem Monte San Salvatore, Bull. Schweiz. Electrotech. Ver., 46, 405-424, 1955.

Berger, K., Anderson, R.B., and Kroninger, H., Parameters of lightning flashes, Electra, 80, 23-37, 1975.

Berger, K., and Vogelsanger, E., Messungen und resultate der blitzforschung der jahre 1955-1963, auf dem Monte San Salvatore, Bull. Schweiz. Elecktrotech. Ver., 56, 2-22, 1965.

Berger, K., and Vogelsanger, E., New results of lightning observations, in Coroniti, S.C., and Hughes, J. (ed.), Planetary Electrodynamics, 1, Gordon and Breach, New York, 489-510. 1969.

Clifford, D.W., Krider, E.P., and Uman, M.A., A case for submicrosecond risetime current pulses for use in aircraft induced coupling studies, 1979 IEEE-EMC Conference, IEEE Report 79CH-1383-9 EMC, Library of Congress Catalog No. 78-155514.

Davis, R., and Standring, W.G., Discharge currents associated with kite balloons, Proc. Roy. Soc. (Longdon), A191, 304-322, 1947.

Eriksson, A.J., Lightning and tall structures, Trans. South African IEE, 69, pt. 8, 238-252, 1978.

Fieux, R.P., Gary, C.H., Hutzler, B.P., Eybert-Bernard, A.R., Hubert, P.L., Meesters, A.C., Perroud, P.H., Hamelin, J.H., Person, J.M., Research on artificially triggered lightning in France, IEEE Trans. on Power Apparatus and systems, PAS-97, 725-733, 1978.

Garbagnati, E., Giudice, E., Lopiparo, G.B., Measurement of lightning currents in Italy - Results of a statistical evaluation, Elektrotechnishe Zeitschrift etz-a, 99, 664-668, 1978.

Garbagnati, E., Giudice, E., Lopiparo, G.B., and Magagnoli, U., Relieve delle caratteristiche dei fulmini in Italia. Risultati ottenuti negli anni 1970-1973, L'Elettrotecnica, LXII, 237-249, 1975.

Gilchrist, J.H., and Thomas, J.B., A model for the current pulses of cloud-to-ground lightning discharges, J. Franklin Inst., 299, 199-210, 1975.

Hagenguth, J.H., and Anderson, J.G., Lightning to the Empire State Building - Pt. 3, AIEE, 71 (pt. 3), 641-649, 1952.

Hylten-Cavallius, N., and Stromberg, A., The amplitude, time to half-value, and the steepness of the lightning currents, ASEA J., 29, 129-134, 1956.

Hylten-Cavallius, N., and Stromberg, A., Field measurement of lightning currents, Elteknik, 2, 109-113, 1959.

Poplansky, F., Frequency distribution of amplitudes of lightning currents, Electra, 22, 139-147, 1972.

McCann, D.G., The measurement of lightning currents in direct stokes, Trans. AIEE, 63, 1157-1164, 1944.

McEachron, K.B., Lightning to the Empire State Building, J. Franklin Inst., 227, 149-217, 1939.

McEachron, K.B., Wave shapes of successive lightning current peaks, Electrical World, 56, 428-431, 1940.

McEachron, K.B., Lightning to the Empire State Building, Trans. AIEE, 60, 885-889, 1941.

Petterson, B.J., and Wood, W.R., Measurements of lightning strikes to aircraft, Report No. SC-M-67-549, Sandia Labs, Albuquerque, NM, 1968.

Pitts, F.L., Electromagnetic measurement of lightning strikes to aircraft, AIAA 19th Aeorspace Sciences Meeting, St. Louis, Jan. 1981.

Pitts, F.L., and Thomas, M.E., 1980 direct strike lightning data, NASA Technical Memorandum 81946, Langley Research Center, Hampton, VA, February, 1981.

Sargent, M.A, The frequency distribution of current magnitude of lightning strokes to tall structures, IEEE Trans. on Power Apparatus and Systems, PAS - 2224-22229, 1972.

Szpor, S., Comparison of Polish to American lightning records, IEEE Trans. on Power Apparatus and Systems, PAS - 88, 646-652, 1969.

Szpor, S., Courbes internationales des courants de foudre, Acta Geophysica Polonica, 19, 365-369, 1971.

Uman, M.A., McLain, D.K., Fisher, R.J., and Krider, E.P., Currents in Florida lightning strokes, J. Geophys. Res., 78, 3530-3537, 1973.

Weidman, C.D., and Krider, E.P., The fine structure of lightning return stroke wave forms, J. Geophys. Res., 83, 6239-6247, 1978.

Weidman, C.D., and Krider, E.P., Submicrosecond risetimes in lightning return stroke fields, Geophys. Res. Lett., 7, 955-958, 1980.

Weidman, C.D., Krider, E.P., Uman, M.A., Lightning Amplitude Spectra in the Interval from 100kHz to 20 MHz, G.R.L., 8, 931-934, 1981.

19

## 2.5.5 Return Stroke Velocity

Boyle, J.S., and Orville, R.E., Return stroke velocity measurement in multistroke lightning flashes. J. Geophys. Res., 81, 4461-4466, 1976.

Hubert, P., and Mouget, G. Return stroke velocity measurements in two triggered lightning flashes, J. Geophys. Res., 86, 5253-5261, 1981.

Idone, V.P., and Orville, R.E., Lightning return stroke velocities in the thunderstorm research international program (TRIP), JGR, 87, 4903-4915, 1982.

Jordan, D., and Uman, M.A., Variations of light intensity with height and time from subsequent return strokes, Trans. Am. Geophys. Union, 61, 977, 1980.

Orville, R.E., A High Speed Time-Resolved Spectroscopic Study of Lightning Return Stroke, J. of Atmospheric Sciences, 25, 827-856, 1968.

Orville, R.E., Lala, G.G., and Idone, V.P., Daylight time resolved photographs of lightning, Science, 201, 59-61, 1978.

McEachron, K.B., Photographic study of lightning, AIEE Trans., 66, 577-585, 1947.

Radda, G.J., and Krider, E.P., Photoelectric measurements of lightning return stroke propagation speeds, Trans. Amer. Geophys. Union, 56, 1131, 1974; and private communication.

Saint-Privat D'Allier Research Group, Research in artificially triggered lightning in France, Proc. Third Symposium on Electromagnectic Compatibility, Rotterdam, May 1-3, 1979, Ed., T. Dvorak, ETH Zentrum, Zurich 8092.

Schonland, B.F.J., and Collens, H., Progressive lightning, Proc. Roy. So. (London), A143, 654-674, 1934.

Schonland, B.F.J., Malan, D.J., and Collens, H., Progressive Lightning II, Proc. Roy. Soc. (London), A152, 595-625, 1935.

Weidman, C.D., and Krider, E.P., Time and height resolved photoelectric measurements of lightning return strokes, Trans. Am. Geophys. Union, 61, 978, 1980.
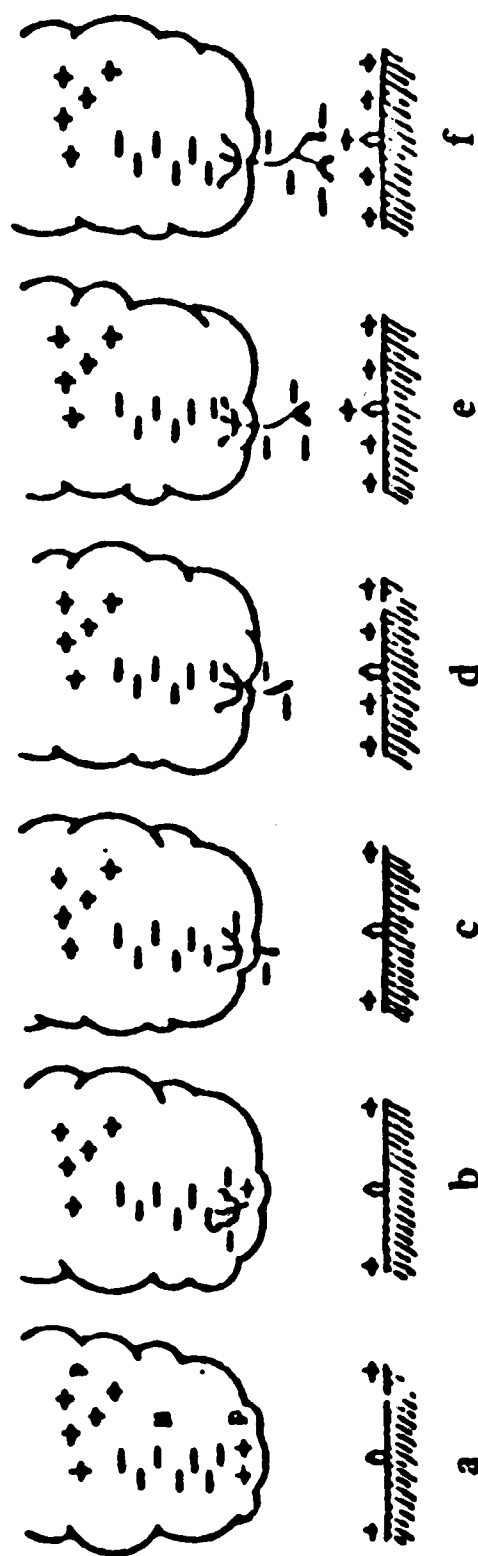
(a) Cloud charge distribution prior to lightning. (b) Discharge called "preliminary breakdown" in lower cloud. (c)-(f) Stepped-leader progression toward ground. Scale of drawing is distorted for illustrative purposes. Adapted from Uman (1971).

Figure 2.1.

Stepped-Leader Initiation and Propagation
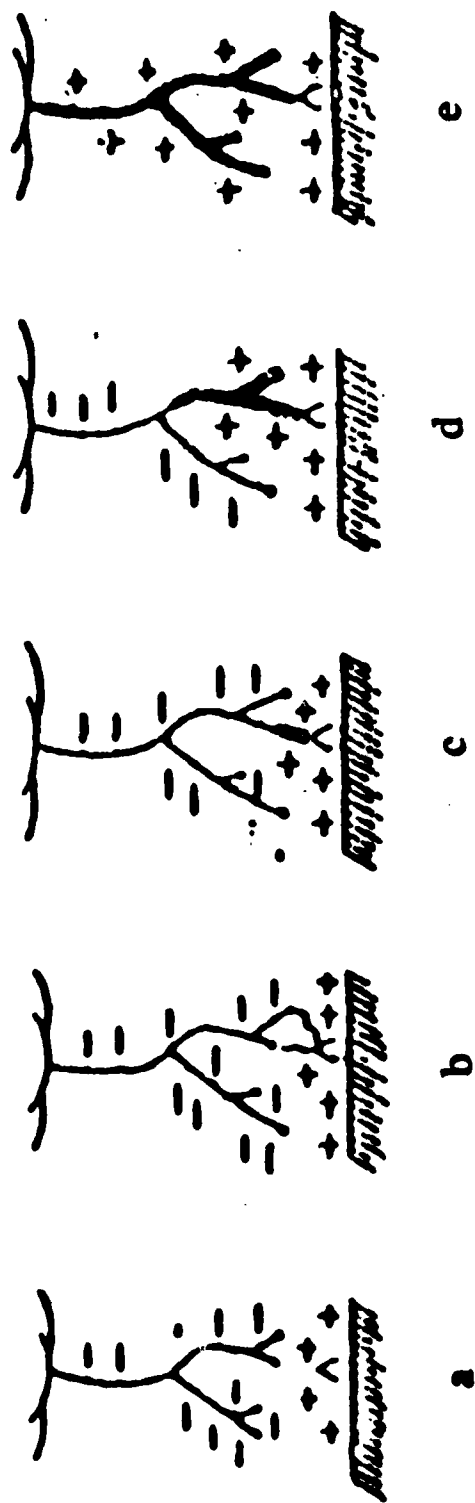
(a) Final stage of stepped-leader decent. (b) Initiation of upward moving discharges. (c)-(e) Return-stroke propagation from ground to cloud. Scale of drawing is distorted for illustrative purposes. Adapted from Uman (1971).

Figure 2.2.

Return-Stroke Initiation and Propagation
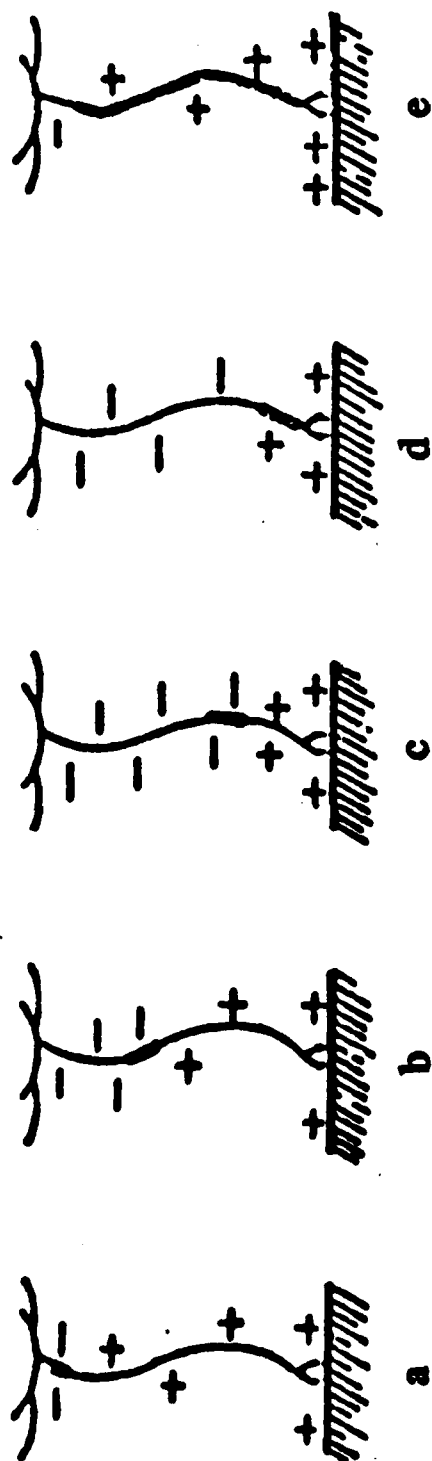
(a)-(c)  Dart leader deposits negative charge on defunct first-stroke channel.
(d)-(e)  Return-stroke propagates from ground to cloud.  Scale of drawing
is distorted for illustrative purposes.  Adapted from Uman (1971).

Figure 2.3.
Dart-Leader and Subsequent Return Stroke

23

# 3.0   INITIAL LIGHTNING CURRENT THREAT DEFINITION

The initial AEH lightning threat defined in this chapter will be shown to match well with the most recently published statistical lightning data. Two sets of parameters are used to identify a moderate or expected lightning stroke and a severe or worst-case stroke. The lightning threat is not designed to match the physical parameters of a particular lightning stroke but rather to be representative of the range of values for the many types of lightning discharges.

## 3.1   LIGHTNING THREAT

The parameters of most importance in this lightning threat were chosen because of their impact on aircraft electrical/electronic systems. These parameters include maximum current rise rate, peak current and energy input (action integral). The selected values were chosen from a review of existing data. They are shown to be consistent with statistical variations of other available data in the following sections. Other characteristics of the waveform (rise time and fall time) are determined uniquely by choosing the above three parameters since the threat model has only three independent parameters. Even so, both rise and fall times are well within the statistics of measured data.

The lightning threat must characterize both single and multiple stroke phenomena. Multiple strokes will be characterized by several single strokes with the addition of induced transient duration, inter-stroke time interval, total event time and total number of strokes. These parameters are listed in Figure 3.1.

The initial single stroke lightning threat model is a double exponential waveform representing the lightning current; the waveform and spectrum is shown in Figure 3.2. The double exponential form of the lightning threat model will be shown to adequately predict the expected electric field spectra from a combination of measured lightning discharges. This threat is to be interpreted as the current flowing in the unperturbed lightning arc channel (i.e., no aircraft interaction). In applying the threat to an aircraft, an electromagnetic coupling model is needed which includes the aircraft and channel geometry and includes the threat as an incident current waveform propagating along the channel.

24

The double exponential waveform, which is a convenient model for engineering calculations, has a historical precedent in both lightning and NEMP (Reference 3-1). The waveform parameters are selected to include the most important features of the lightning current rather than to faithfully represent any single lightning waveform. The three lightning parameters incorporated in the threat waveform are peak rate-of-rise, peak current, and action integral. The moderate and severe threats were selected to be expected and worst-case levels of the parameters based upon review of the best available measured data. Figure 3.3 shows these threat parameter values and the defining equations for the double exponential current waveform.

## 3.2    RATIONALE

No single waveform can represent all types of lightning discharges (e.g., cloud-to-ground, intracloud, positive strokes, negative first strokes, and negative subsequent strokes). It is necessary to select parameters from particular stroke types which provide reasonably conservative threat levels for all strokes. Cloud-to-ground strokes were chosen because they are generally more severe, although a less frequent threat to aircraft, than intracloud discharges. On this basis, the threat waveform parameter values were chosen as described below.

### 3.2.1    Peak Rate-of-Rise

Rise rate data displayed by Cianos and Pierce has recently been interpreted to be too low. More recent statistical data [References 3-4, 3-6, 3-8, and 3-13] has shown higher current rates of rise. The values for the initial threat determination were taken from Berger's [Reference 3-6] tower measurements. The moderate value of 50 kA/$\mu$s lie at his upper 35% mark while the severe threat of 200 kA/$\mu$s was chosen at his 1% level.

### 3.2.2    Peak Current

The peak current was chosen from the statistical study done by Cianos and Pierce [Reference 3-7]. The moderate threat level of 20 kA was chosen at their 50% level for first return strokes. The severe threat of 200 kA was chosen at their upper 1% level.

### 3.2.3    Action Integral

The action integral was also chosen from Cianos and Pierce data. Peak current values and mean rise and fall times were used to determine a moderate energy input level of $1.5 \times 10^4$ A$^2$-s and a severe level of $1.5 \times 10^6$ A$^2$-s.

## 3.3    COMPARISON TO PRIOR LIGHTNING STANDARDS

In this section the lightning threat defined in Figures 3.1 through 3.3 is compared against other industry lightning standards. Table 3.1 summarizes comparisons between previously used standards and the present threat definition. Only the severe threat is compared since the other standards represent severe strikes.

The maximum current rise rate of industrial lightning threat standards are given in Table 3.1. The values in parenthesis are obtained from the peak current value divided by the rise time for the corresponding standard. This gives an average rise time or a maximum rise time if the initial current waveform is a straight line. The straight line waveform for the initial current rise is used in the SAE-4L standards. The rise time for the AEH threat is the peak rate of rise, not an average. For a double exponential waveform these quantities are substantially different. The peak rate of rise, not the average, is the important quantity when specifying a lightning threat. This difference between peak and average rate of rise leads to the AEH higher standard for rise rate.

The peak and average rate of rise definition also leads to an AEH rise time different from other industry standards. These rise time differences are shown in Table 3.1. The longer AEH rise time is due to the double exponential waveform used. Other standards use linear ramp functions. However, the rise rate, not the rise time, is the important parameter when considering possible damage to electronic equipment.

The peak current and fall time are listed in Table 3.1. The AEH initial threat values agree with those previously used.

## 3.4    LIGHTNING THREAT COMPARISON TO MEASURED DATA

The data presented, for comparison between the AEHP defined threat and lightning measurements, is the most recent found in the literature. Each model parameter is examined separately below. Two summary tables of experimental statistics are given in Tables 3.2 and 3.3. The first table is taken from Berger (Reference 3-2). The second is from Garbagnati and Lopiparo (Reference 3-4). Tables 3.2 and 3.3 summarize the data from References 3-2 and 3-4 from which most of the data comparisons in this section were made.

26

All the AEHP threat parameters are within reasonable statistics of this database. Detailed comparisons with recent individual experimentors are given in the following subsections.

### 3.4.1 Uman-Krider Measured Field Data Comparison

A comparison is made in this section to measured electric fields presented by Uman and Krider (Reference 3-7). The comparison of a lightning current profile to electric radiation field data is not straightforward if lightning geometry, propagation effects, height dependence of lightning current, etc. are taken into account. Since the comparison presented here is meant to be preliminary, a simpler procedure will be followed. The magnetic radiation field is calculated from an infinite current carrying wire. This approximation is valid close to the wire (less than a wavelength away). This minimum distance is 300 km for 1 KHz and goes to 3 Km at 100 KHz. The electric radiation field is obtained from the magnetic radiation field assuming free space radiation. The results for both moderate and severe current profiles are plotted in Figure 3.4 against Uman and Krider's (Reference 3-7) electric field spectra for first strokes. Also plotted are NEMP results for comparison. The threat models tend to be well above the data for low frequency and straddling the data at higher frequency. The shape of the frequency spectra of the predicted fields versus the measured fields is fairly good. Of course this assumes no dispersion effects occur in propagation. This is not the case especially at higher frequencies or where the earth is very lossy. Newer measurements by Krider are over salt water having low loss propagation.

Figure 3.5 taken from Reference 3-7 shows frequency spectra from different lightning discharges. The solid line represents the first return stroke data. All the discharges shown are on top of or close to the first return stroke data. This justifies our use of AEH threat comparison to first stroke data in Figure 3.4.

### 3.4.2 Current Rise Rate

The single stroke threat model value for maximum current rise rate is given in Figure 3.3 as 50 kA/$\mu$s for a moderate stroke and 200 kA/$\mu$s for a severe one. The values correspond to the upper 35% and upper 1% as shown in data from Berger (Reference 3-2) in Figure 3.6. Note that no measurements were made with rate of rise greater than 100 kA/$\mu$s. Figure 3.7 shows older data

accumulated by Cianos and Pierce (Reference 3-5). The moderate and severe threat correspond to the upper 12% and upper 0.1% values. The Cianos and Pierce data is actually average rates of rise rather than maximum values. Thus the threat values show as higher percentiles as compared to Berger's data. Data from Garbagnati (Reference 3-4) of two different data sets (first and subsequent strokes) is shown in Figure 3.8. The moderate threat is at the 10% mark in (a) and 35% in (b). The severe threat is at 3% in (a) and 1.5% in (b). These statistical values correlate well with the choice of rise rate picked in the current threat model.

There is considerable uncertainty in the maximum rate of rise values. It should be noted that the largest current rise rates measured by Berger or Garbagnati and Lopiparo were 102 kA/μsec. This data may be low because of instrumentation bandwidth limitations and the tower heights. No data has been directly measured showing current rise rate greater than the 180 kA/μs reported by Anderson and Erickson. Anderson and Erikson (1978) in South Africa measured lightning currents on a tower located in open country. Unlike Berger and Garbagnati, the measurements were taken on relatively flat terrain. Only a small number of strokes (eleven) were analyzed with a maximum current rise rate of 180 kA/μs for a subsequent stroke. This is a higher level both in absolute value and relative percentage than Berger and Garbagnati's measurements. With so few events, however, definite comparisons are premature.

Higher rate of rise values (up to 400 kA/μs) have been reported (Reference 3-8) but are inferred from distant electric fields.

Consequently, the AEHP threat value has been adjusted upward to 200 kA/us. This is based on engineering judgement of where the real threat is expected to be. Further testing is needed to resolve the threat uncertainty but it is expected to be within a factor of two of the present AEHP threat.

### 3.4.3 Peak Current

The peak current values were taken from Poplansky's data (Reference 3) shown in Figure 3.9. The moderate (20 kA) and severe (200 kA) threat values were chosen at 60% and 1% respectively. Data in Figure 3.10 from Berger (Reference 3-2) show these values to lie at 80% and 0.1%, respectively. Figure 3.11 is data from Garbagnati (Reference 3-4). The moderate threat is at 80% in 9(a)

and 60% in 9(b). The severe threat is less than 0.1% in both figures. The moderate threat is close to a median value in Figures 3.9 and 3.11 and seems to be a good choice. All the data but Poplansky's have smaller current values near the severe threat limit. Our use of 200 kA seems justified, at least initially, on the basis of prior industry standards and because the 200 kA is above the 1% levels of Figures 3.9 and 3.11 and so includes at least the 1% level in the other data sets available.

### 3.4.4 Action Integral

The last parameter chosen in the threat definition is the energy input or action integral. Figure 3.12 shows the Berger data. The percentiles for the moderate threat energy case range from 25% to 85% for negative subsequent and first return strokes. The severe threat is at 1% of the first negative stroke and < 0.1% for the subsequent stroke. The severe threat level agrees with the first return stroke and is overly severe for subsequent.

Figure 3.13 presents data from Reference 3-4. 3.13(a) has moderate and severe threat energy levels at 82% and 1% while 3.13(b) has 48% and < 0.1% levels. The moderate threat agrees with the subsequent stroke data and is not severe enough according to first return stroke data. The severe threat level is overly severe for the subsequent and adequate for first return strokes.

### 3.4.5 Rise Time

The rise time of the threat is a consequence of fixing the maximum current rise-rate, the peak current and the action integral. Rise time is not fixed independently of these parameters. Consequently, comparing rise time to data gives an indication of the general adequacy of the form of the double exponential used to model the lightning current. Figure 3.14 from Reference 3-2 shows the moderate threat value of $2\mu s$ falling at 25% and 95% for subsequent and first strokes respectively. The severe threat of $4\mu s$ lies at the 6% and 70% mark. Figures 3.15a and b show results from Reference 3-4. Figure 3.15a shows moderate and severe percentile of 70% and 43%. Figure 3.15b shows values of 25% and 3%. The data is widely scattered over a large range of rise times. The values chosen fall within this middle range of the data.

Figure 3.16 from Reference 3-6 shows results that have very short rise times ($<1\mu s$). These results were taken over salt water. The relationship to

29

data taken over land is not completely understood but the rise time should be slower over land than over water. This data indicates that much shorter rise times may have to be included in a future threat. The impact of short rise times on the lightning threat is through the related parameter rise rate. Generally the shorter the rise time, the higher the rise rate, although the relationship is waveform dependent. Current rise rate values directly affect the amount of protection an aircraft must have to guard against lightning strike cause equipment malfunctions.

### 3.4.6  Fall Time to Half Peak

The fall time, like the rise time, is determined by the preceeding parameters so the fall time was not fit to the measured data in defining the threats. Figure 3.17 from Reference 3-2 shows the moderate and severe threat time of $50\mu s$ to lie at 30% and 80% for negative subsequent and negative first strokes respectively. Figure 3.18 has data taken from Reference 3-4. The AEHP threat fall time ranges from the 35% to 75% level in 15(a) and is 30% in 15(b). The threat value is well within the median range of the above data.

### 3.5  LIGHTNING THREAT TEST WAVEFORM

Uman (Reference 3-8) proposed lightning threat waveforms for both first return and subsequent strokes. A separate waveform for testing must be used since the double exponential form cannot easily be produced in a laboratory. The double exponential peak rate of rise may be limited by stray inductance and capacitance in a test configuration since the peak occurs at zero time. The purpose of this section is to examine the sensitivity of the time domain current waveform on the frequency spectral components. The second aim is to compare the initial AEHP lightning threat waveforms with both Uman's proposed threats and a recommended test waveform.

The choice of a representative waveform of a lightning threat useable for test and analysis must consider both time and frequency domain profiles. The use of a piecewise continuous waveform can introduce high frequency nulls which are undesireable for most analyses because of the lack of frequency content and hence response. The use of a smooth continous function for analysis is desired to generate a smooth continuous frequency spectrum with no such nulls. Real test waveforms will be smoothed by the generator turn-on and parasitic R/L/C elements. Double exponentials have been shown to bound in

both time and frequency domains more complex time domain waveforms. The purpose of a lightning test waveform is to bound both in time and frequency the important parameters of lightning.

### 3.5.1 Recommended Test Waveform

The recommended test waveform shape is a sine wave with an exponential tail. A comparison of the recommended test waveform with the double exponential threat waveform is seen in Figures 3.19 and 3.20. The time domain waveforms are shown in the first figure. The comparisons are done for a severe threat. The frequency spectra is shown in Figure 3.20. The double exponential and test waveforms match well in the frequency domain. Thus, the proposed test waveform should represent the double exponential threat well.

### 3.5.2 Comments on Uman's Threat Waveform

Figure 3.21 shows Uman's proposed lightning current waveforms for both first return and subsequent stroke (Reference 3-8). The waveforms both go to zero at $t = 0$ and $t = 300$ $\mu$s. The maximum rise rates for the two waveforms are 750 kA/$\mu$s for the severe first return stroke and 600 kA/$\mu$s for the severe subsequent stroke. Uman's severe threat rise rate values were chosen to be a factor of five larger than the moderate rise rate values derived from field data.

### 3.5.3 Waveform Sensitivity

The sensitivity of spectral content was examined for various choices of time domain waveforms similar to Uman's threat. Uman's severe first return stroke profile is shown in Figure 3.22 (solid line). The first change to this waveform was to delete the ramps running from $t = 0$ to $t = 100$ $\mu$s and from $t = 200$ to $t = 300$ $\mu$s and then to normalize the current amplitude to zero at $t = 100$ and $t = 200$ $\mu$s. The maximum rise rate was left unchanged. The second alteration was to fill in the notch present after the maximum amplitude is reached. This change is shown by a dotted line near the peak amplitude in Figure 3.22. Again the maximum rise rate was left unchanged. The spectra of the waveforms are shown in Figures 3.23 and 3.24. Figure 3.23 shows a comparison of the original waveform to one without the ramps. The only change is at the low frequency end of the spectrum as expected. No difference above 10 KHz exists. Figure 3.24 shows the waveforms with and without the notch present. Again there is very little difference over the entire spectrum.

### 3.5.4 Threat Comparison

Comparison of the initial AEHP threat with Uman's waveforms and a sample of Berger's (1975) data selected by Uman is shown in Figure 3.25-3.28. Figures 3.25 and 3.27 show the time domain waveforms while Figures 3.26 and 3.28 show the associated spectra. Both the initial AEHP threat and Berger's data envelope Uman's threat waveforms except at early time. Uman picked 750 kA/μs for his first return stroke threat and 600 for his subsequent stroke threat. Berger's example has values of 70 kA/μ for first return stroke (upper 20% of his data) and 360 kA/μs for subsequent strokes (extremely severe, less than upper 0.1% of his data). The AEHP threat values are 200 kA/μs for severe threats and 50 kA/μs for moderate threats based on both first return and subsequent stroke data. Upper bounds and reliable statistics for high rates of rise are not yet well established. Therefore, Uman's high rise rates may well be indicative of a more severe lightning stroke than the upper 1% level taken for the basis of the AEHP threat.

These high rise rates are also reflected in the frequency spectra in Figures 3.26 and 3.28. The initial AEHP threat bounds both Berger's data and Uman's waveform at lower frequencies for both first return and subsequent strokes. At higher frequencies, Uman's threat is higher than either Berger's data or the AEHP threat level. Again this is due to the rise rates chosen.

Uman's large rise rate values are chosen from current parameters derived from EM field measurements. These values are subject to uncertainty due to the deconvolution from fields to currents. This process is nonunique and many assumptions must be made as to the current waveforms. The lower AEHP threat levels are taken from tower measurements. These values are also subject to uncertainty due to tower-lightning interactions as discussed in the last chapter. Quantitative evaluations of both Uman's field data and the tower measurements must be done to establish a better statistical base for rise rate values.

### 3.5.5 High Frequency Content

The last point to be addressed here regards the high frequency shape of Uman's waveforms. Above 10 MHz a sin x/x type variation appears in the spectra with deep nulls present. This type of waveform is not useful for either testing or analysis due to these nulls. Rather what is needed are bounding curves in the time and frequency regime.

32

The sin x/x variation is caused by the multiple discontinuities in slope in Uman's time domain waveforms. For more than one discontinuity in slope, the sin x/x variation appears with the first frequency null determined by the time spacing between the discontinuities. An example of this is the waveform given in Figure 3.29 shown again Uman's severe first return stroke threat. The two frequency spectra are plotted against each other in Figure 3.30. The discontinuous waveform plotted has nulls identical to Uman's waveforms because the rise times of the steepest slope are identical (both waveforms steepest slope rise is 0.1 μs - this gives the first null at 10 MHz).

Rather than smoothing the discontinuities in Uman's waveforms which is tedious, a better approach is to bound the waveform and spectrum. An example of such a bound by a double exponential waveform (but not the initial AEHP threat waveform) is given in Figures 3.31 and 3.32. The parameters chosen for this double exponential were chosen to bound Uman's waveform at high frequencies. The general expression with the values chosen are shown below.

$$I(t) = I_0 [e^{-\alpha t} - e^{-\beta t}] \tag{1}$$

$$I_0 = 180 \text{ kA}; \alpha = 1.4 \text{ E} + 4 \text{ sec}^{-1}; \text{ and } \beta = 9.0 \text{ E} + 6 \text{ sec}^{-1}. \tag{2}$$

The peak amplitude of this waveform is 178 kA. The maximum rate of rise is very high at 1600 kA/μs. The spectral fit to Uman's waveform is excellent at high and low frequencies. Between 10 KHz and 1 MHz there is up to a factor of three difference in amplitude. This double exponential serves as an excellent example of a bounding wave in both time and frequency domains.

33

# CHAPTER 3 REFERENCES

3-1.    Golde, R.H., ed; "Lightning, Vol I: Physics of Lightning", Academic Press, 1977.

3-2.    Berger, K; Anderson, R.B.; Kroninger, H., "Parameters of Lightning Flashes", Electra, 80, 23-37, 1975.

3-3.    Popolansky, F., "Frequency Distribution of Amplitudes of Lightning Currents", Electra, 22, 139-147, 1972.

3-4.    Garbagnati, E.; Lopipard, G.B.; "Lightning Parameters - Results of 10 Years of Systematic Investigation in Italy", Proceedings of International Conference on Lightning and Static Electricity; Oxford, England, March, 1982.

3-5.    Cianos, N.; Pierce, E.T., "A Ground Lightning Environment for Engineering Usage", Stanford Research Institute Technical Report; No. 1, Project 1834, August 1972.

3-6.    Clifford, D.W.; Krider, E.P.; Uman, M.A.; "A Case for Submicrosecond Rise-Time Lightning Current Pulses for Use in Aircraft Induced-Coupling Studies", IEEE Symposium on Electromagnetic Compatability, San Diego, CA, October 1979.

3-7.    Uman, M.A.; Krider, E.P.; "A Review of Natural Lightning: Experimental Data and Modeling", IEEE EMC Transactions; p. 79-111, May 1982.

3-8.    Weidman, C. D.; Krider; "Submicrosecond Risetimes in Lightning Return-Stroke Fields", GRL, F, 955-958, November, 1980.

# Table 3.1
# Present Lightning Threats

| Present Lightning Standards | Single Stroke Lightning Parameters | | | |
| --- | --- | --- | --- | --- |
| | Maximum Rise Rate (kA/µs) | Peak Current (kA) | Rise Time (µs) (0 to Peak) | Fall Time to Half Peak Value (µs) |
| Initial AEH threat definition (severe) | 200 | 200 | 4 | 50 |
| Boeing severe (1% exceeding) (767/7757 avionics) | 200 | 200 | 4 | 50 |
| MIL B-5087—Bonding, Electrical and Lightning Protection for Aerospace Systems (1978) | (100) | 200 | 2 | 50 |
| SAE Committee AE-4L (1978) and MIL-STD (1980) | 100 | 200 | 2 | 50 |
| NASA Lightning Protection Criteria (JSC-07636, Space Shuttle Guidelines, 1975) | (100) | 200 | 2 | 50 |

# Table 3.2

## Lightning Parameters Compared to Initial Threat

Berger, et al., 1975

| Number | Parameter | Unit | Percentage exceeding tabulated value 95% | 50% | 5% | AEH Initial threat Moderate | Severe |
|---|---|---|---|---|---|---|---|
| | **Current amplitude (crest) exceeding 2 kA** | | | | | | |
| 101 | Negative first strokes and flashes | kA | 14 | 30 | 90 | 30 | 200 |
| 135 | Negative subsequent strokes | kA | 4.6 | 12 | 30 | — | — |
| 26 | Positive flashes | kA | 4.6 | 35 | 250 | — | — |
| | **Charge** | | | | | | |
| 93 | Negative first strokes | C | 1.1 | 5.2 | 24 | | |
| 122 | Negative subsequent strokes | C | 0.2 | 1.4 | 11 | | |
| 94 | Negative flashes | C | 1.3 | 7.5 | 40 | | |
| 26 | Positive flashes | C | 20 | 80 | 350 | | |
| | **Impulse charge** | | | | | | |
| 90 | Negative first strokes | C | 1.1 | 4.5 | 20 | 2.1 | 4.5 |
| 117 | Negative subsequent strokes | C | 0.22 | 0.95 | 4.0 | | |
| 26 | Positive flashes | C | 2.0 | 16 | 150 | | |
| | **Time to crest** | | | | | | |
| 89 | Negative first strokes | µs | 1.8 | 5.5 | 18 | | |
| 118 | Negative subsequent strokes | µs | 0.22 | 1.1 | 4.5 | | |
| 19 | Positive flashes | µs | 3.5 | 22 | 200 | 50 | 200 |
| | **Maximum di/dt** | | | | | | |
| 92 | Negative first strokes | kA µs⁻¹ | 5.5 | 12 | 32 | | |
| 122 | Negative subsequent strokes | kA µs⁻¹ | 12 | 40 | 120 | | |
| 21 | Positive flashes | kA µs⁻¹ | 0.2 | 2.4 | 32 | 50 | 50 |
| | **Time to half-value** | | | | | | |
| 90 | Negative first strokes | µs | 30 | 75 | 200 | | |
| 115 | Negative subsequent strokes | µs | 6.5 | 32 | 140 | | |
| 16 | Positive flashes | µs | 25 | 230 | 2,000 | | |
| | **Action integral** | | | | | | |
| 91 | Negative first strokes and flashes | A²s | $6.0 \times 10^3$ | $5.5 \times 10^4$ | $5.5 \times 10^5$ | $1.5 \times 10^{14}$ | $1.5 \times 10^6$ |
| 88 | Negative subsequent strokes | A²s | $5.5 \times 10^2$ | $6.0 \times 10^3$ | $5.2 \times 10^4$ | | |
| 26 | Positive flashes | A²s | $2.5 \times 10^4$ | $6.5 \times 10^5$ | $1.5 \times 10^7$ | | |

# Table 3.3

# Mean Values of Lightning Parameters Compared to Initial Threat

Mean values and relevant standard deviation of the lightning-current parameters. (*)

| | Negative flashes | | | | Positive flashes (**) | AEH initial threat |
| | Downward | | Upward | | | Moderate threat |
| | First strokes | Following strokes | First strokes | Following strokes | | |
|---|---|---|---|---|---|---|
| Number of strokes | 42 | 33 | 61 | 142 | 5 | — |
| Peak value (kA) | 33 (0.25) | 18 (0.22) | 7 (0.23) | 8 (0.22) | 30-180 | 20 |
| Maximum rate of rise (kA/µs) | 14 (0.38) | 33 (0.39) | 5 (0.76) | 13 (0.52) | 5-30 | 50 |
| Time to crest (µs) | 9 (0.40) | 1.1 (0.33) | 4 (0.66) | 1.3 (0.36) | 20-55 | 2.1 |
| Time to half value (µs) | 56 (0.32) | 28 (0.50) | 35 (0.37) | 31 (0.35) | 250-600 | 50 |
| Impulse charge (C) | 2.8 (0.35) | 1.4 (0.31) | 0.5 (0.30) | 0.6 (0.32) | 16-60 | — |
| Impulse energy (x $10^3$ $A^2$ s) | 44 (0.65) | 14 (0.50) | 1.8 (0.46) | 2.3 (0.51) | 450-3,000 | 16 |

(*) The mean value and the standard deviation are obtained considering a log-normal distribution for all the parameters. The mean values are expressed in the measuring unit of the parameter, while the relevant standard deviations (figures in brackets) in logarithmic units. For positive flashes, due to the low number of data, only the range of values is reported.

(**) Only the values corresponding to impulses characterized by higher peaks and longer duration have been considered.

Garbagnati and Lopiparo, 1982

37

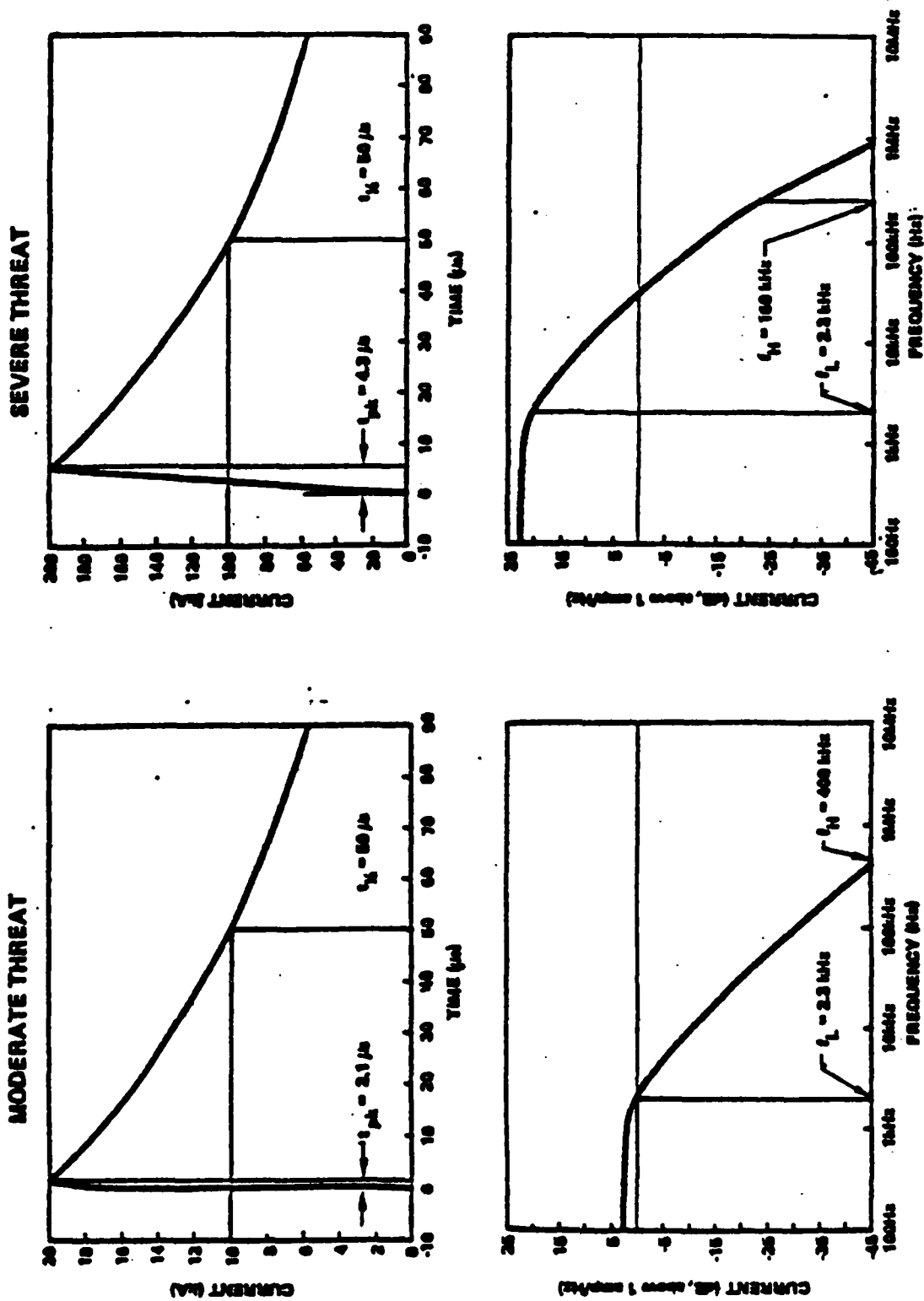| Variables | Range |
| --- | --- |
| • Duration of transient | 50 - 500 $\mu$s |
| • Inter-stroke time interval | 10 - 100 ms |
| • Time duration of lightning event | 0.01 - 2 sec |
| • Number of strokes | 1 - 24 |

Figure 3.1
Multi-Stroke Threat
(Non-Damage Effects)

Figure 3.2

Single Stroke Threat Definition

**Waveform**

$$I(t) = I_0 (e^{-\alpha t} - e^{-\beta t})$$

| | $I_0$ | $\alpha$ | $\beta$ | $t_{pk}$ | $t_{1/2}$ |
|---|---|---|---|---|---|
| Moderate: | 20.6 kA | $14.3 \times 10^3$ sec$^{-1}$ | $2.5 \times 10^6$ sec$^{-1}$ | 2.1 µs | 50 µs |
| Severe: | 206 kA | $14.3 \times 10^3$ sec$^{-1}$ | $1.0 \times 10^6$ sec$^{-1}$ | 4.3 µs | 50 µs |

**Spectrum**

$$I(f) = I_0(1/[\alpha + j2\pi f] - 1/[\beta + j2\pi f])$$

| | DC Limit | Upper Turning Frequency | Lower Turning Frequency |
|---|---|---|---|
| Moderate: | 1.4 amps/Hz | 400 kHz | 2.3 kHz |
| Severe: | 14 amps/Hz | 160 kHz | 2.3 kHz |

**Lightning Parameters**

| | Peak Current | Peak Rate-of-Rise | Action Integral |
|---|---|---|---|
| Moderate: | 20 kA | $5 \times 10^{10}$ amps/sec | $1.5 \times 10^4$ amp$^2$-sec |
| Severe: | 200 kA | $2 \times 10^{11}$ amps/sec | $1.5 \times 10^6$ amp$^2$-sec |

Figure 3.3

Definition of Single Stroke Threat
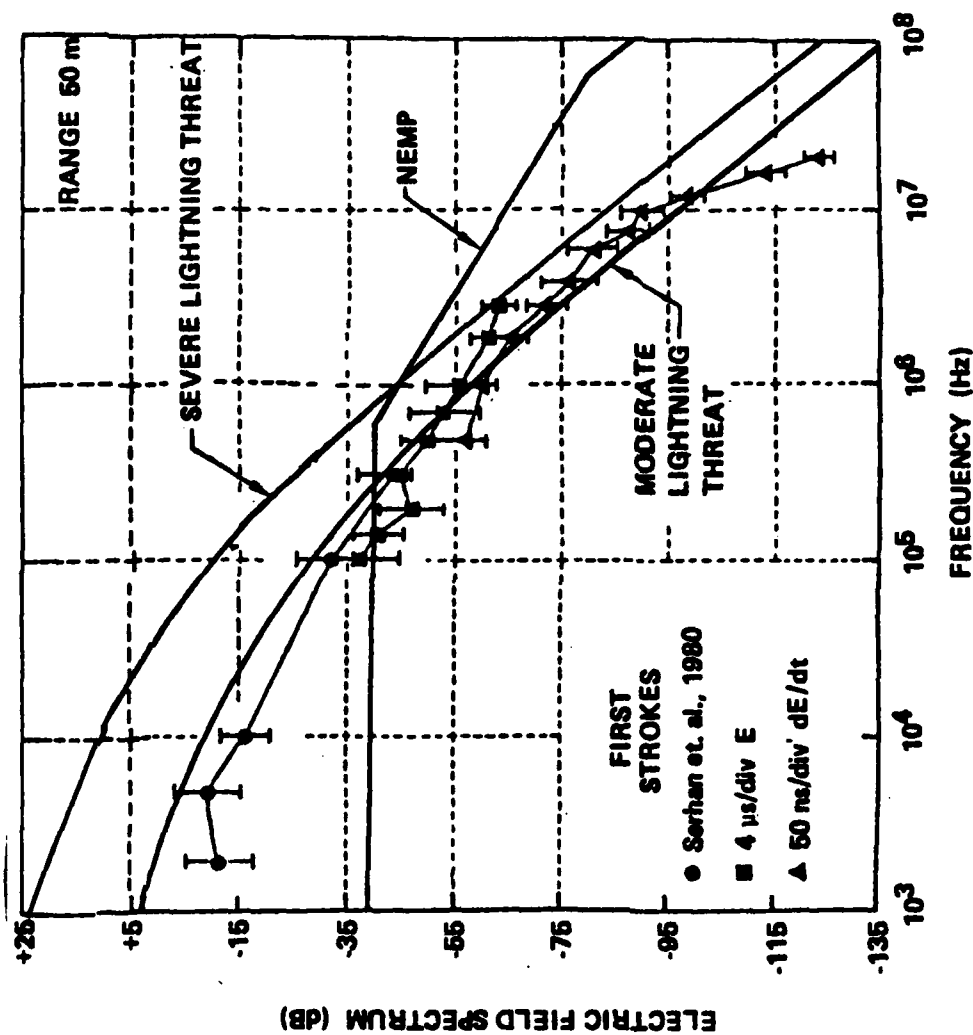(Damage Effects)

Figure 3.4
Comparison of Electric Field Data with
Initial Threat Definitions
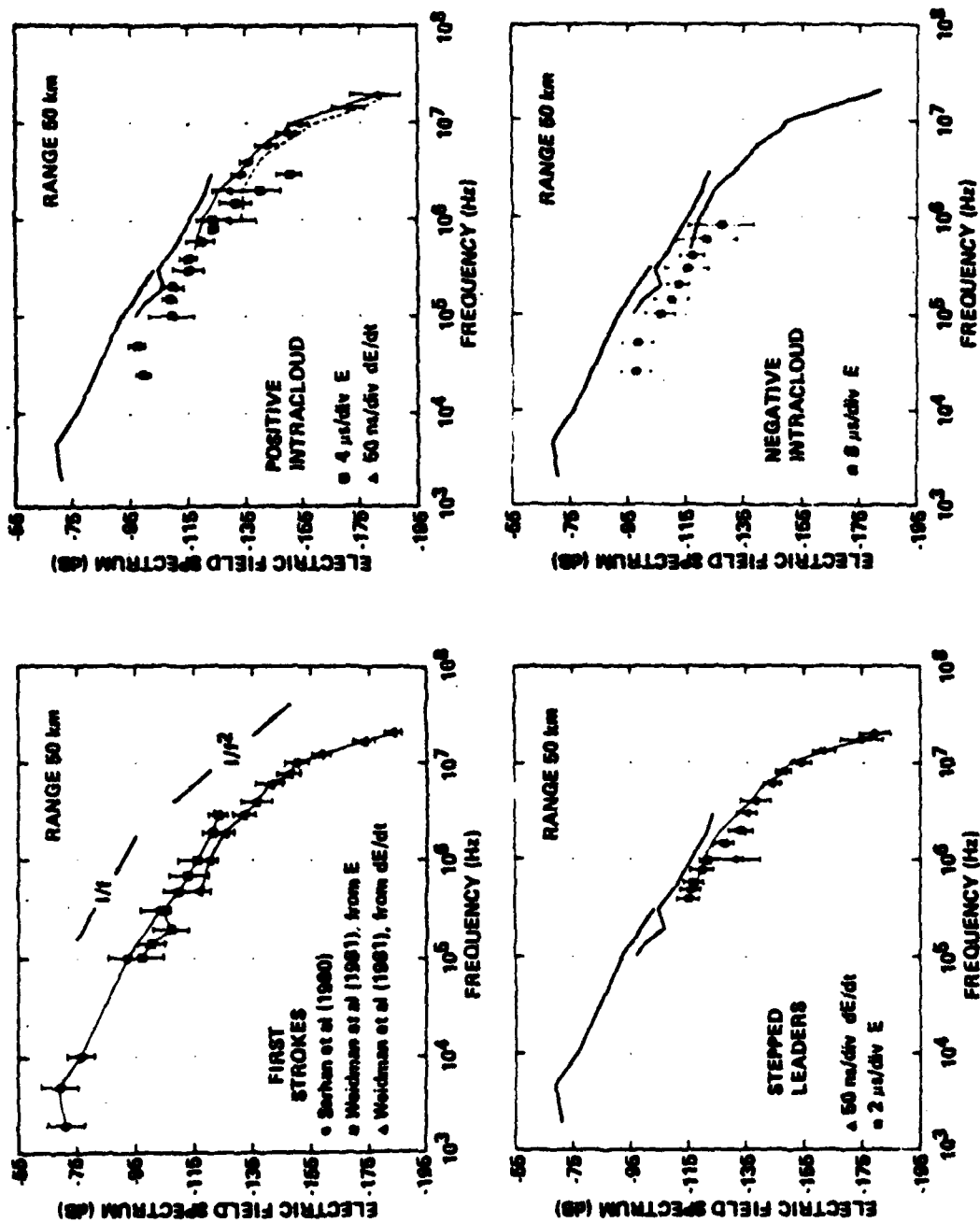
Figure 3.5

Electric Field Frequency Spectra

Figure 3.7

**DISTRIBUTION OF AVERAGE RATES OF RISE FROM CIANOS & PIERCE (1972)**
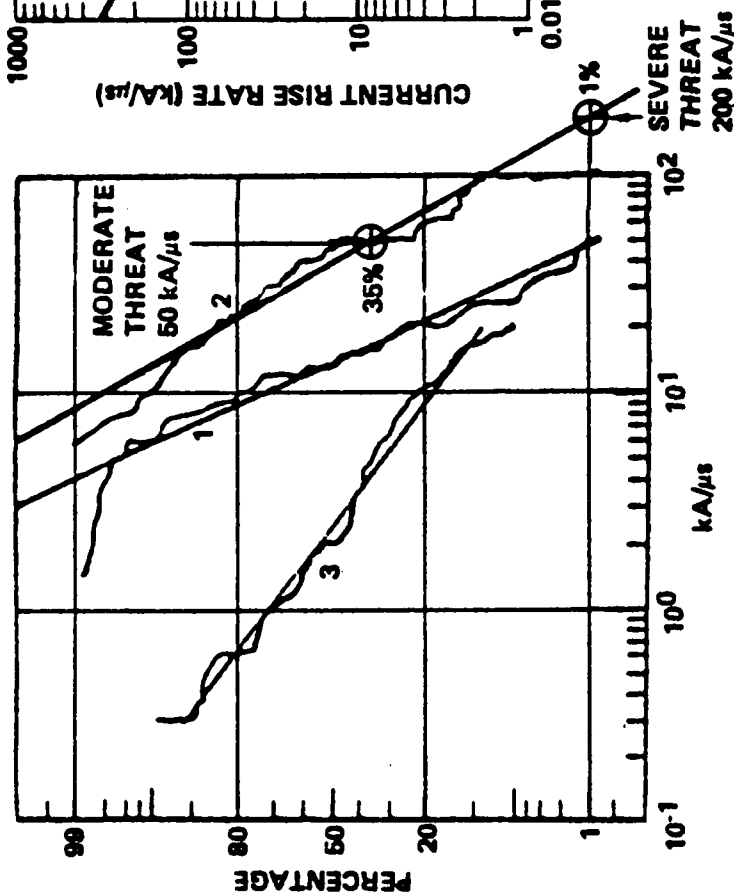
Figure 3.6

**DISTRIBUTION OF MAXIMUM RATE OF CURRENT RISE— FROM BERGER, et al (1975)**

(1) NEGATIVE FIRST STROKES
(2) NEGATIVE FOLLOWING STROKES
(3) POSITIVE STROKES

# Comparison of Initial Threat Current Rise Rate with Available Statistical Data

43
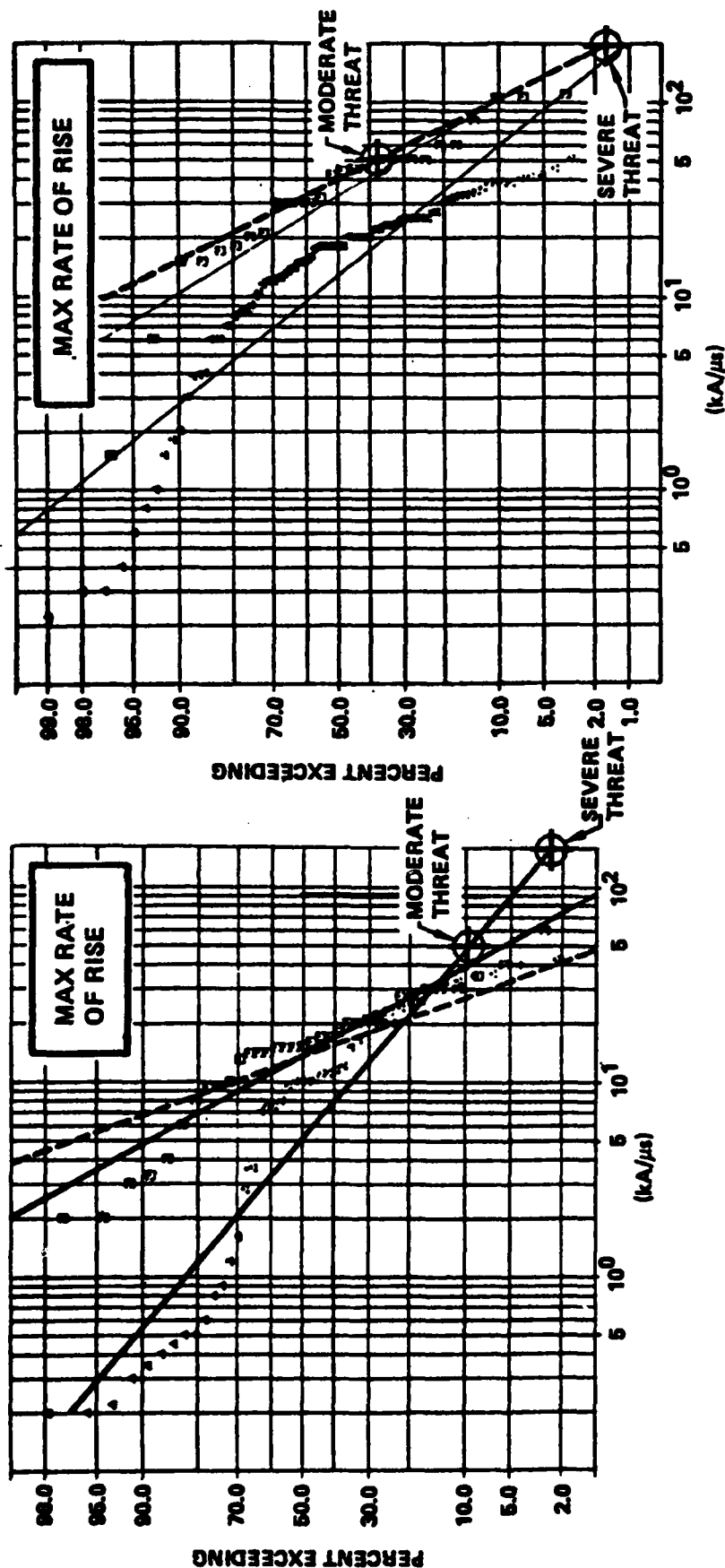
Figure 3.8

Maximum Current Rise Rate
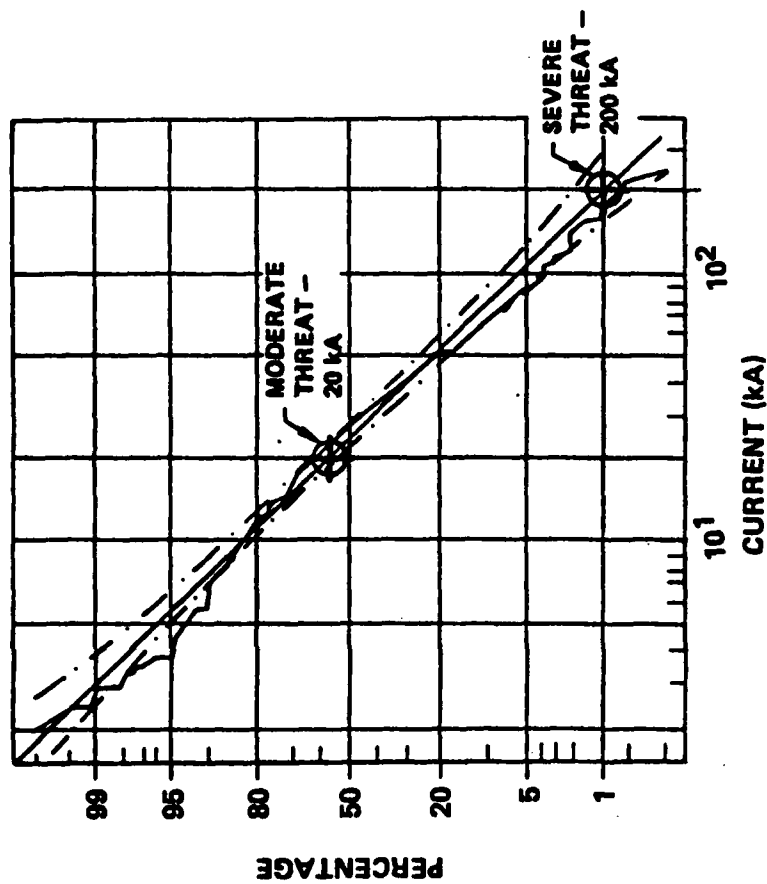
Figure 3.9
Current Amplitude Distributions

Figure 3.10

Current Amplitude Distributions
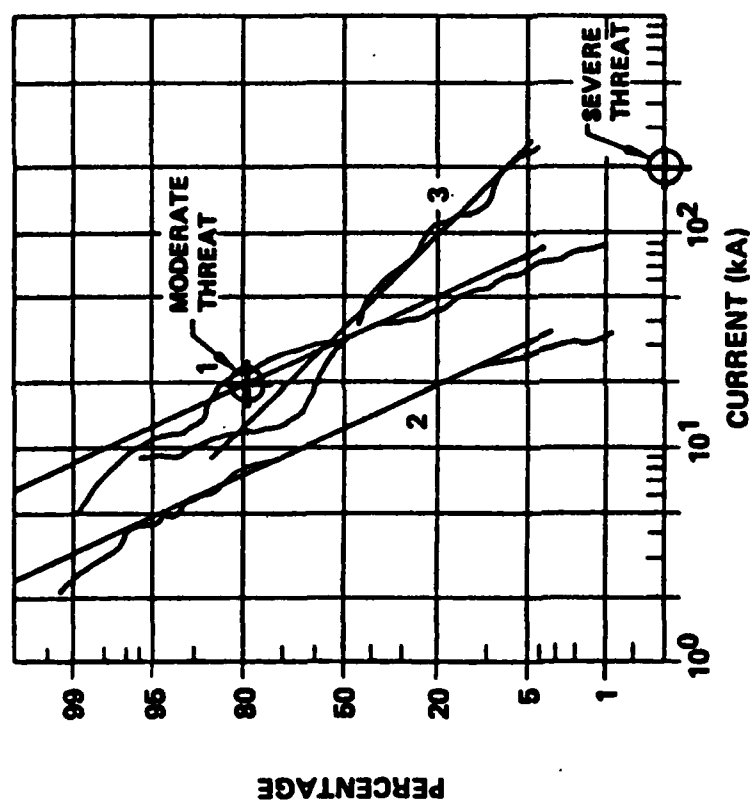
1. Negative first strokes
2. Negative subsequent strokes
3. Positive strokes

Berger, et. al., 1975

46
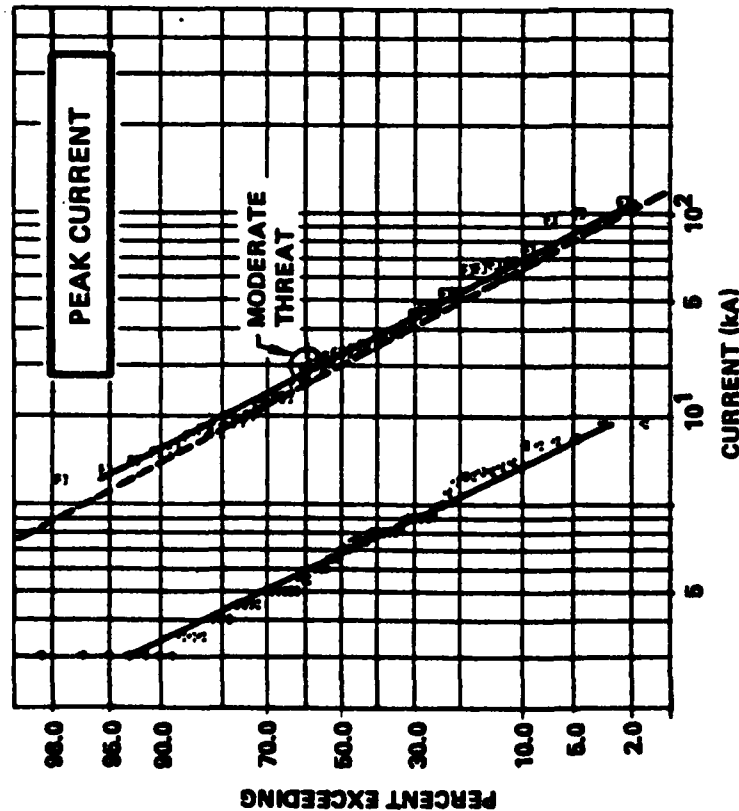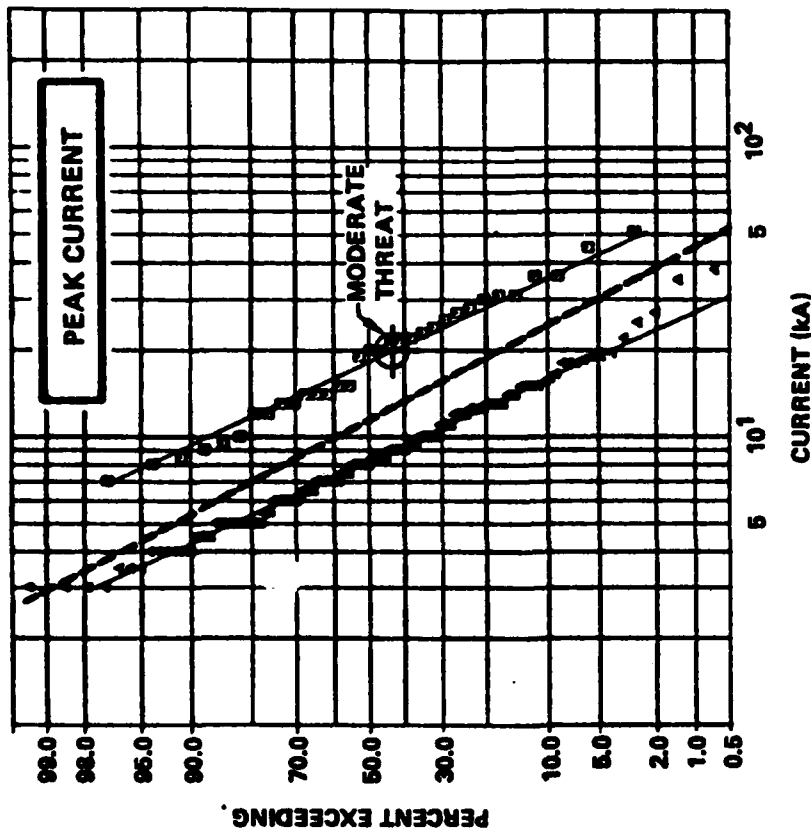
Figure 3.11
Current Amplitude Distributions

Figure 3.12
Energy Input Distribution
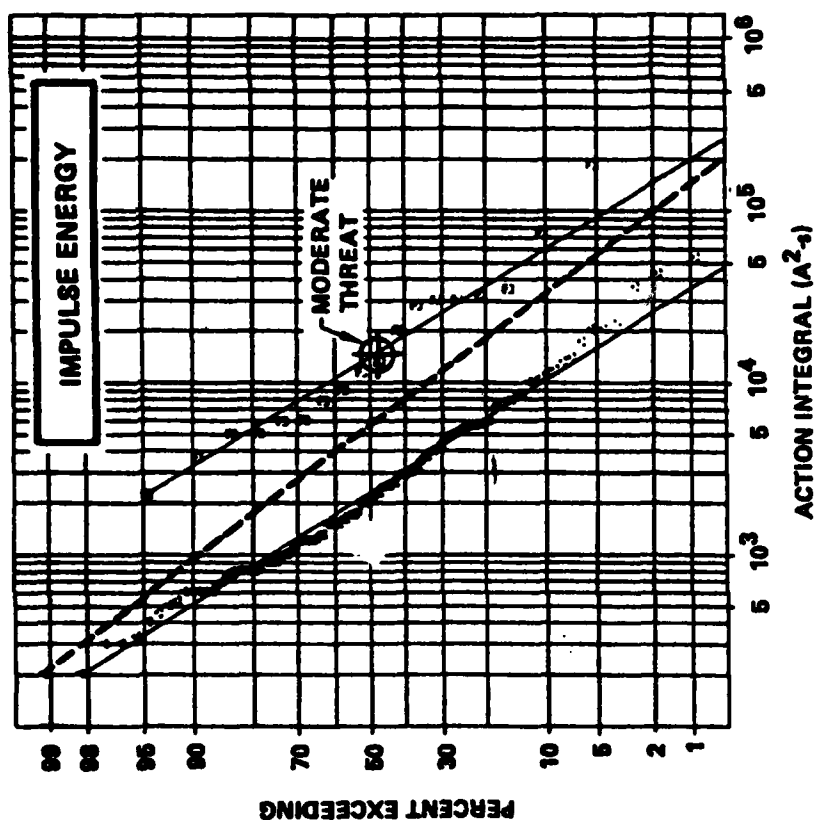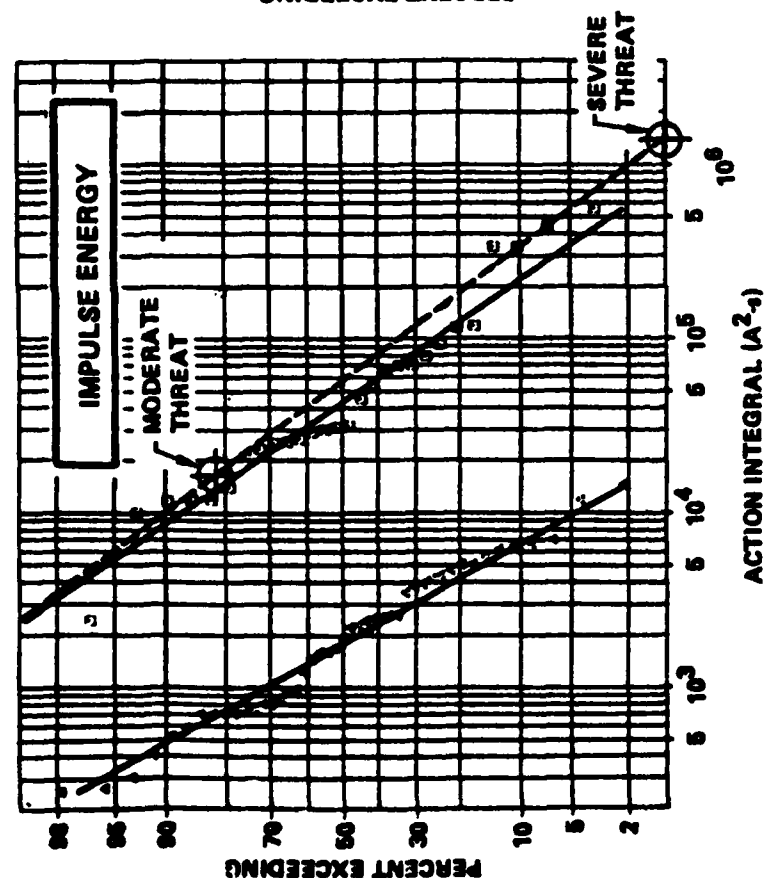
Figure 3.13
Energy Input Distributions

Figure 3.14

Rise Time Distributions
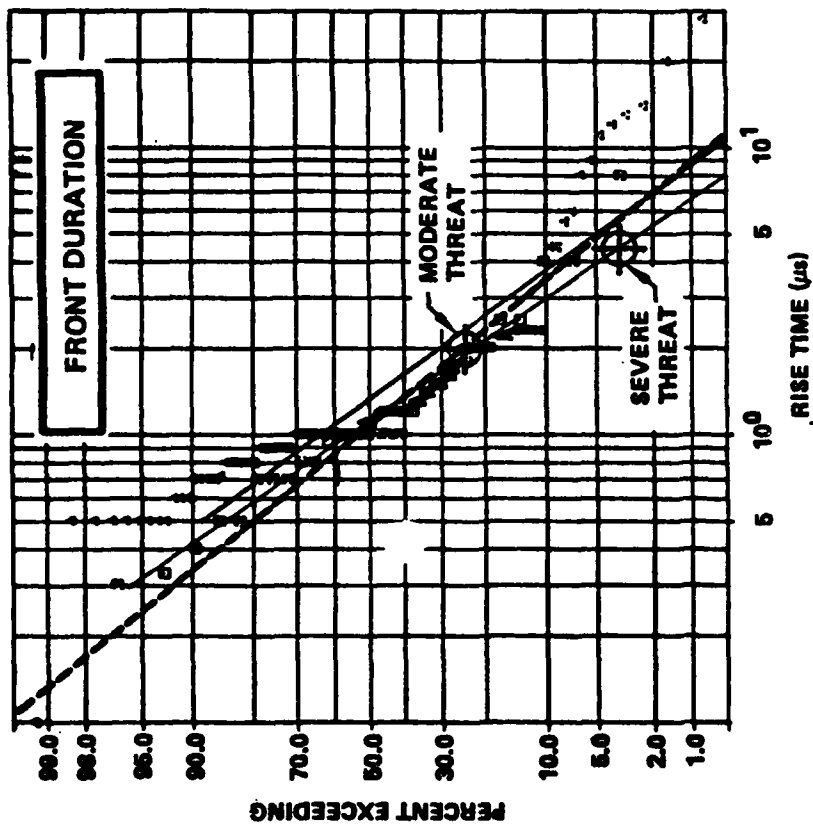
1. Negative first strokes
2. Negative subsequent strokes
3. Positive strokes

Figure 3.15

Rise Time Distributions
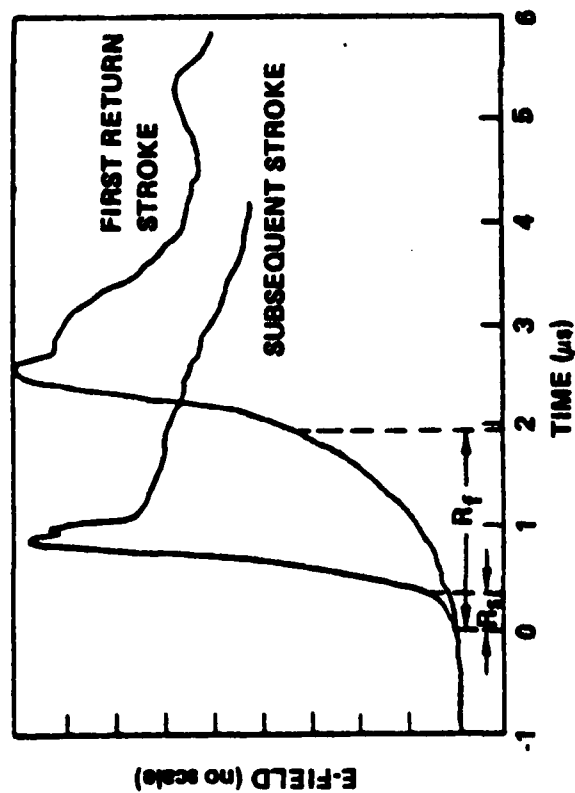
(a) CHARACTERISTIC OF FIRST RETURN STROKE FRONT RAMP ($R_f$) AND SUBSEQUENT STROKE FRONT RAMP ($R_s$) AS MEASURED BY WEIDMAN AND KRIDER (1978) E-FIELD AMPLITUDES ARE NOT TO SCALE. WAVE-FORMS ARE BASED ON MEAN VALUES OF HISTOGRAMS.
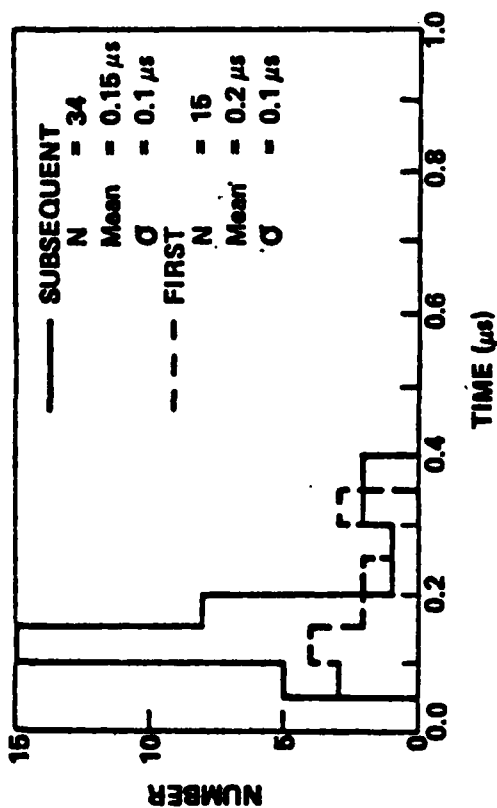
(b) HISTOGRAMS OF THE 10 TO 90% RISETIMES OF THE FAST FIELD TRANSITION IN FIRST AND SUBSEQUENT STROKE FIELDS IN FLORIDA AT A DISTANCE OF 15 TO 30 km OVER SEA WATER.

Figure 3.16

New Data Suggestive of Very Fast Rise Times (<1 μS)

52

Figure 3.17
Fall Time to Half Peak
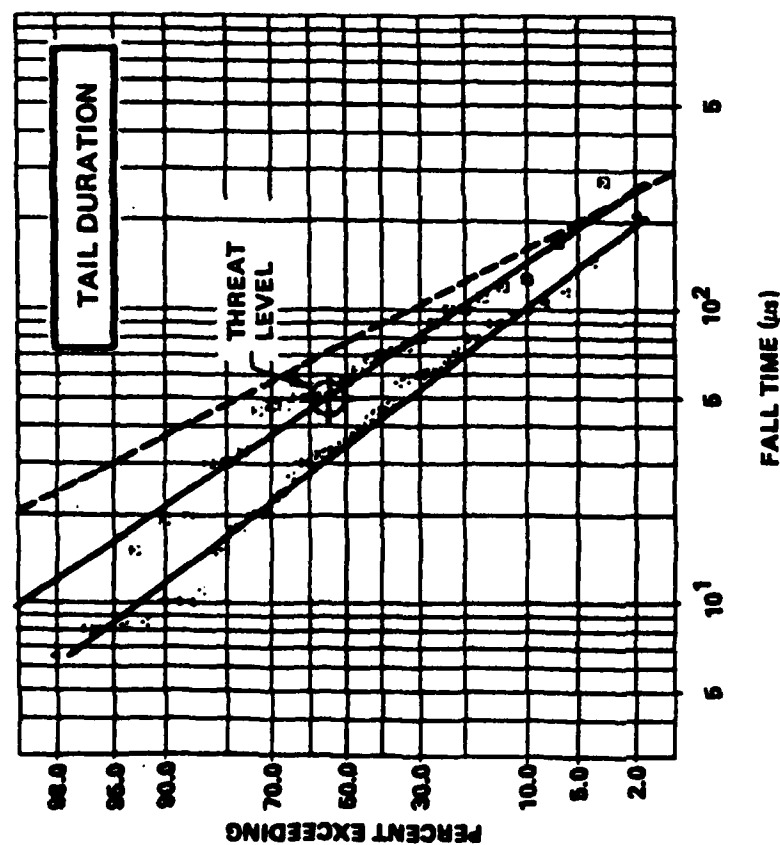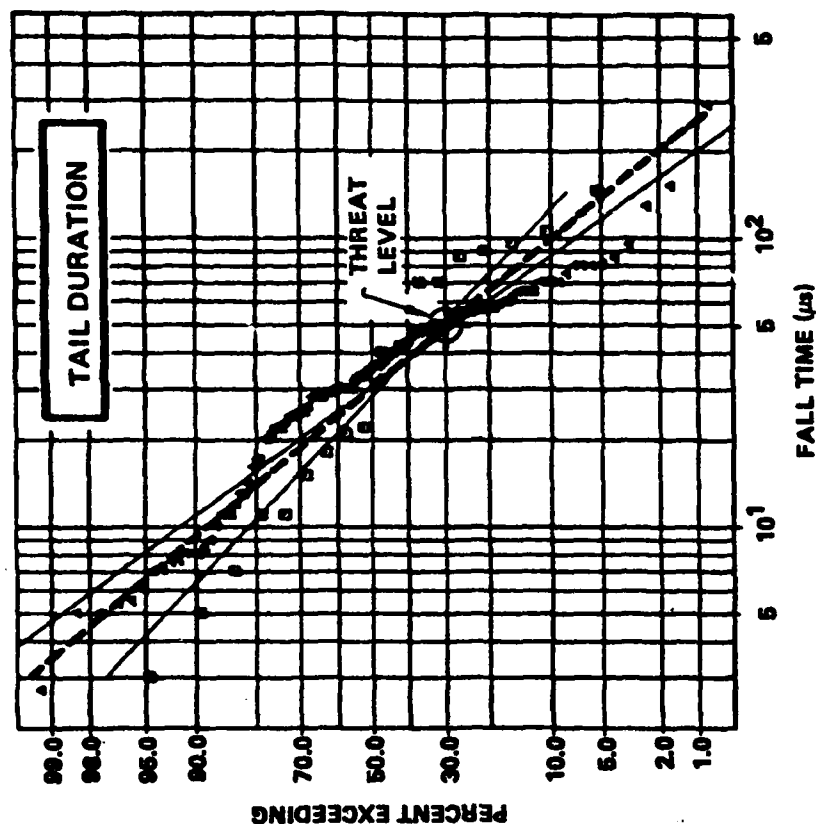
Figure 3.18
Fall Time to Half Peak

54
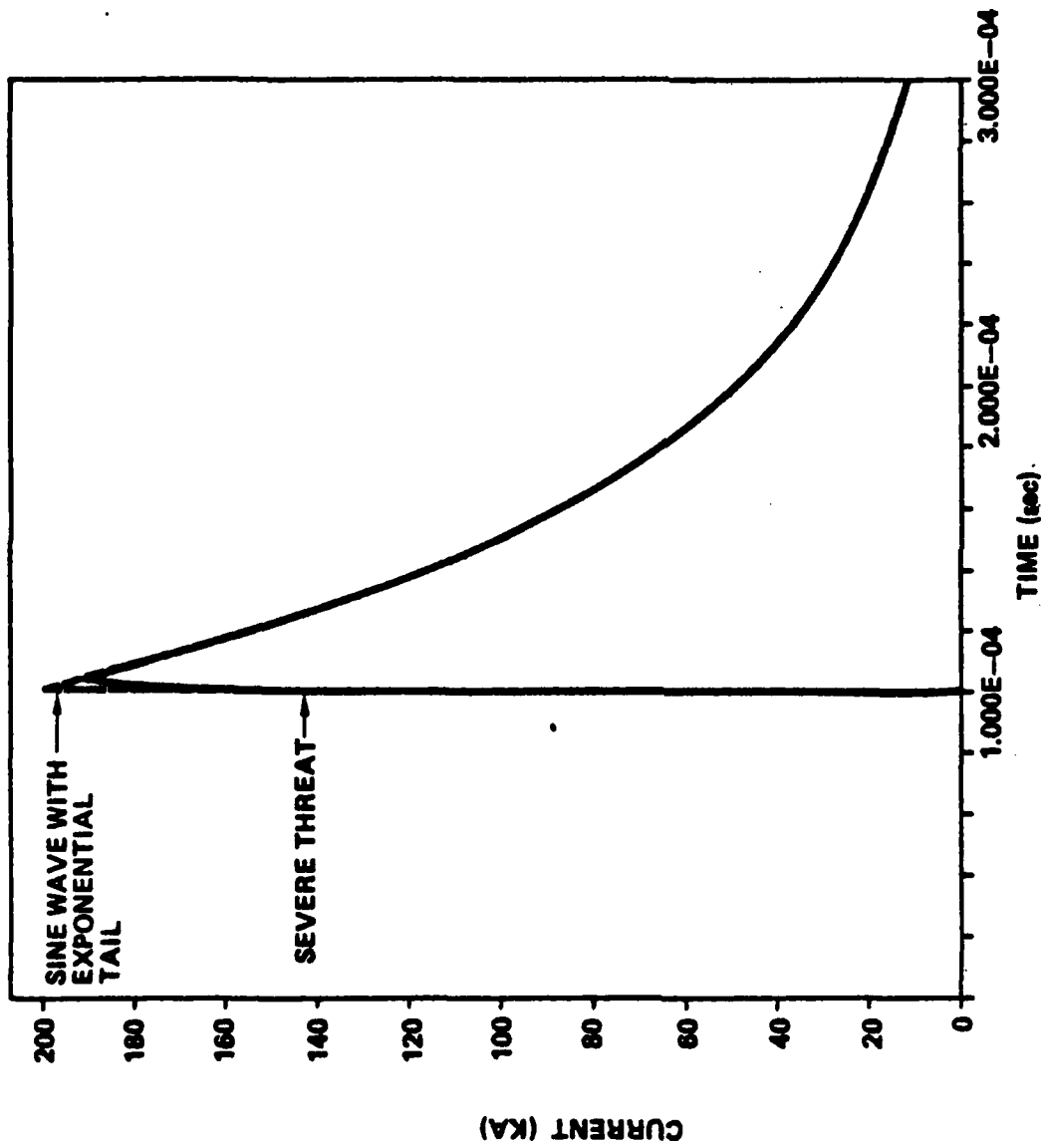
Figure 3.19

Severe AEH Threat Versus "Test-Like" Wave
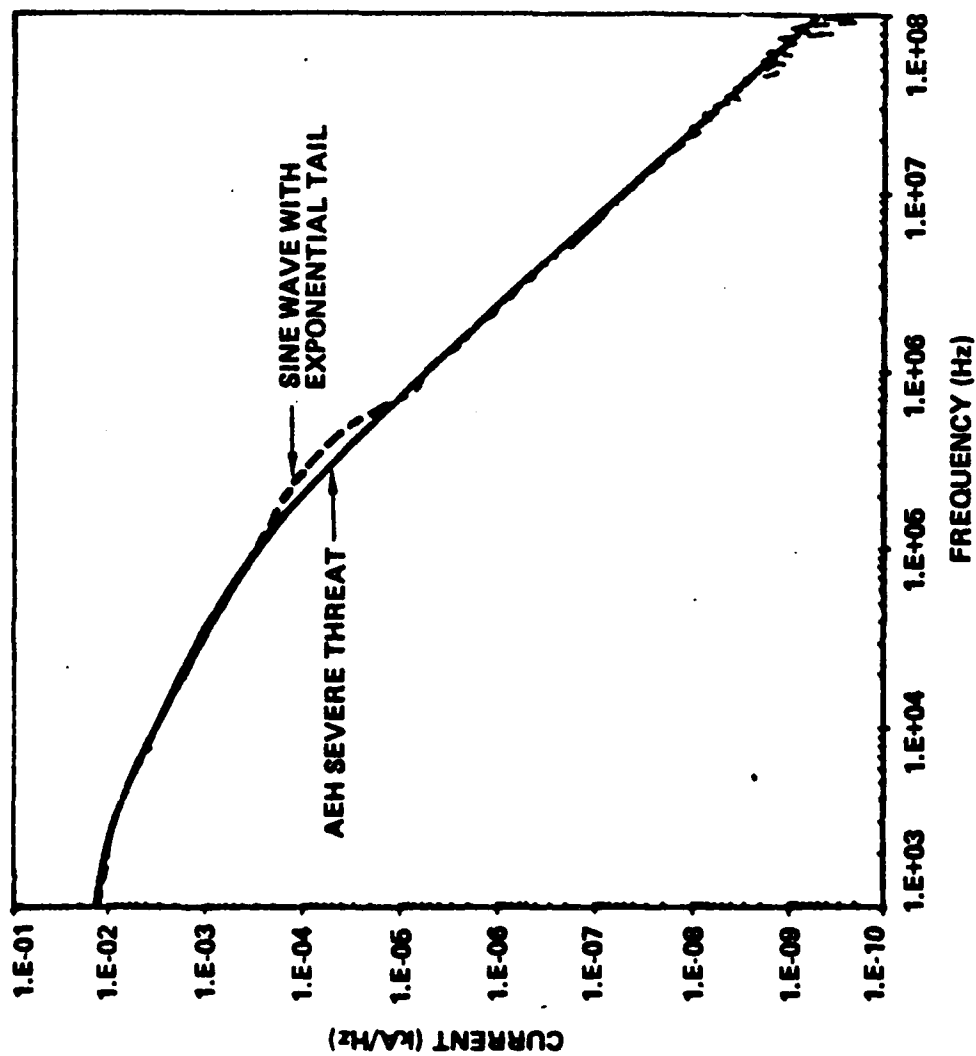
Figure 3.20
Severe AEH Threat Versus Test-Like Wave
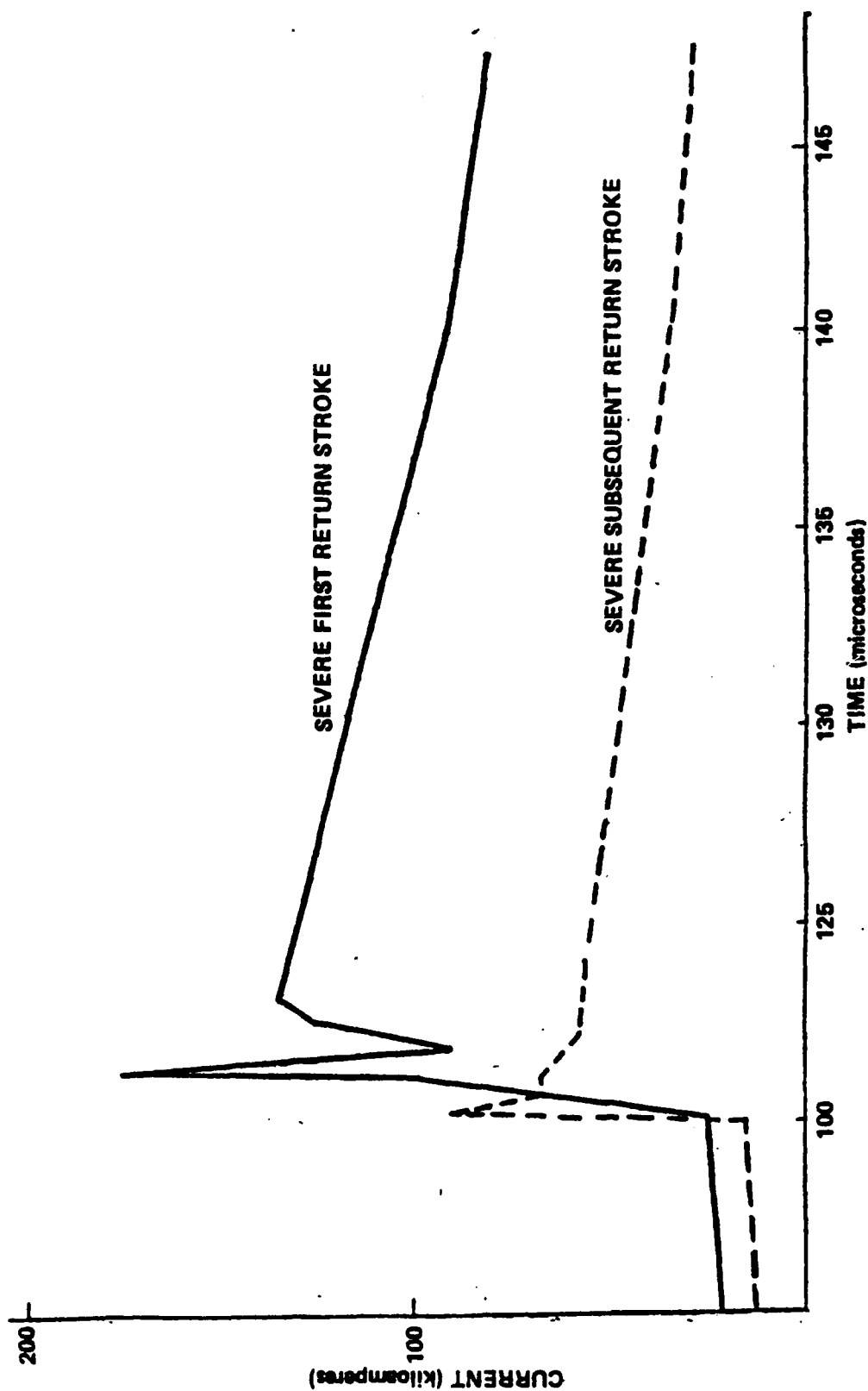
Figure 3.21

Uman's Proposed Lightning Current Test Standards
April 1982
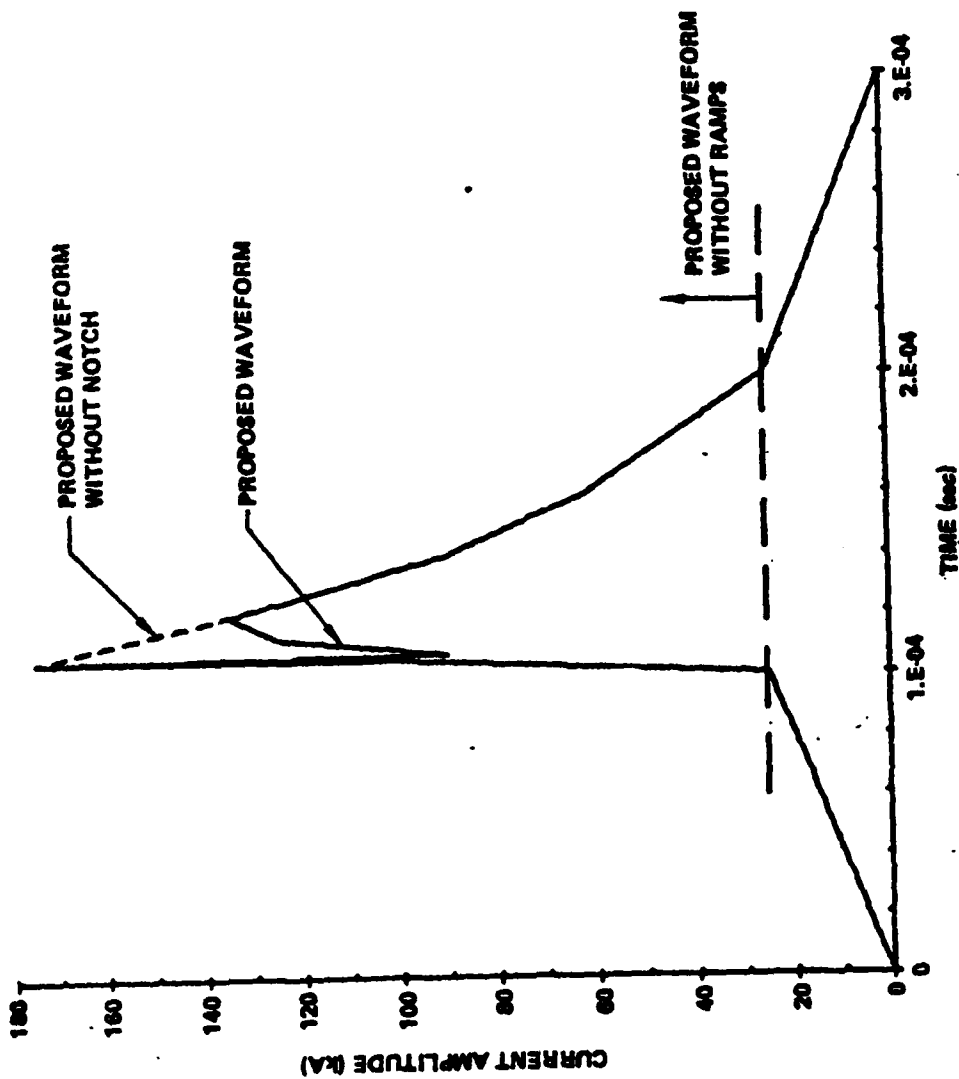
Figure 3.22
Unan's Threat Waveform
— Severe First Return Strokes —
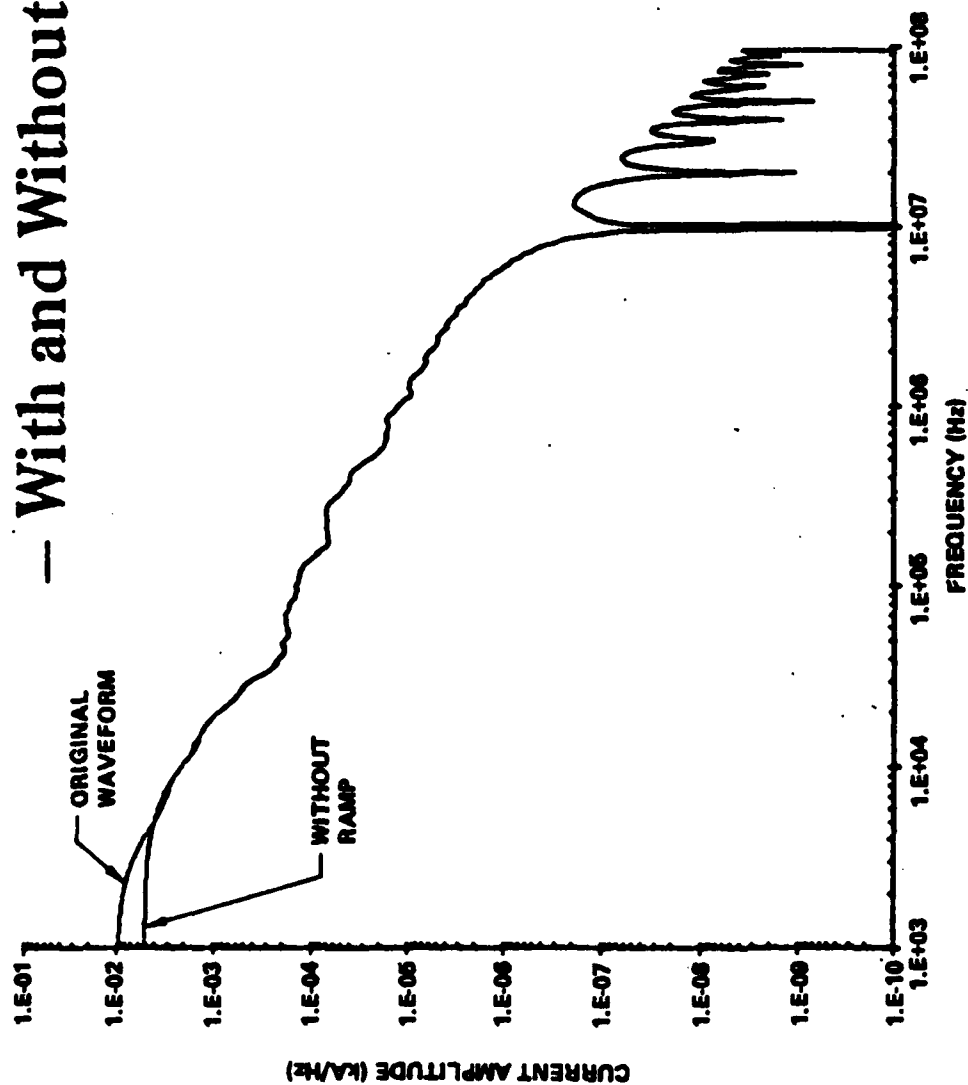
Figure 3.23
Uman's Threat Waveform
— Severe First Return Strokes —

— With and Without Notch —
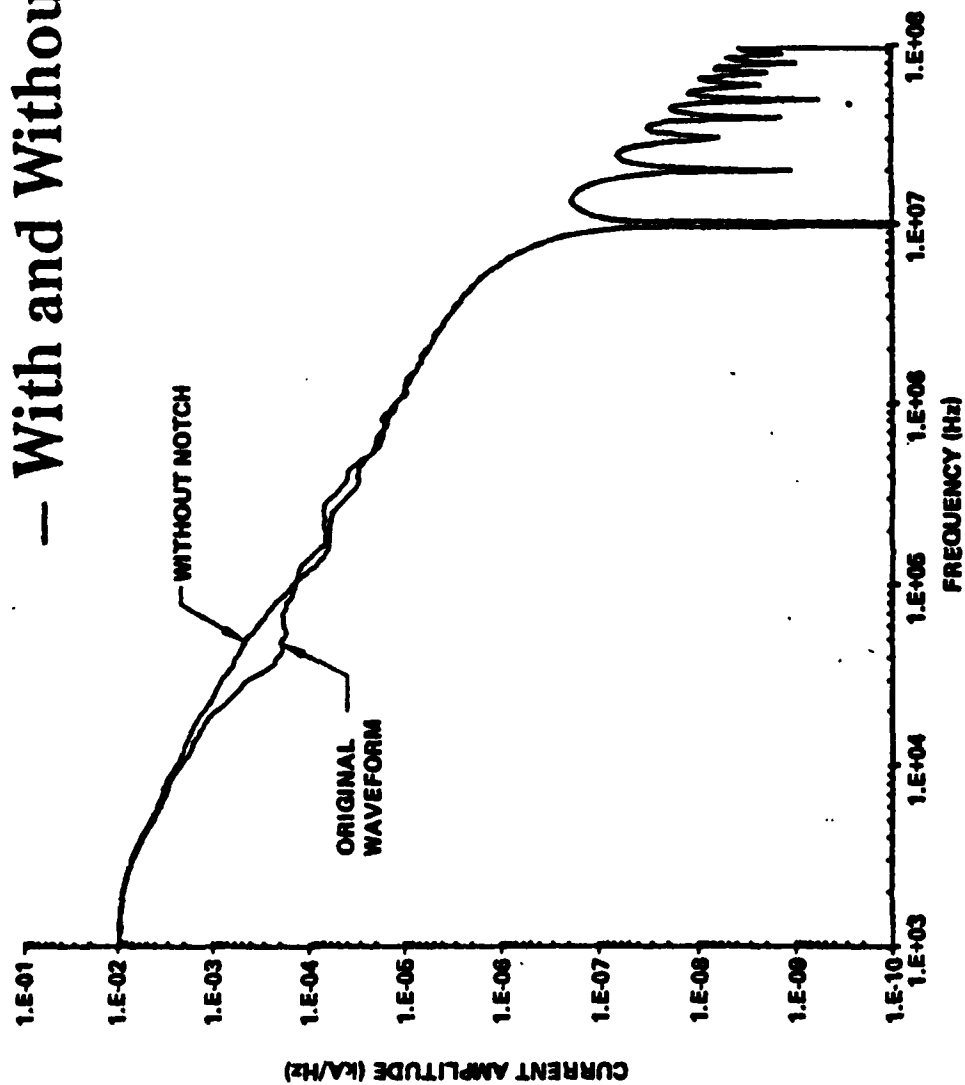
Figure 3.24
Uman's Threat Waveform
— Severe First Return Strokes —
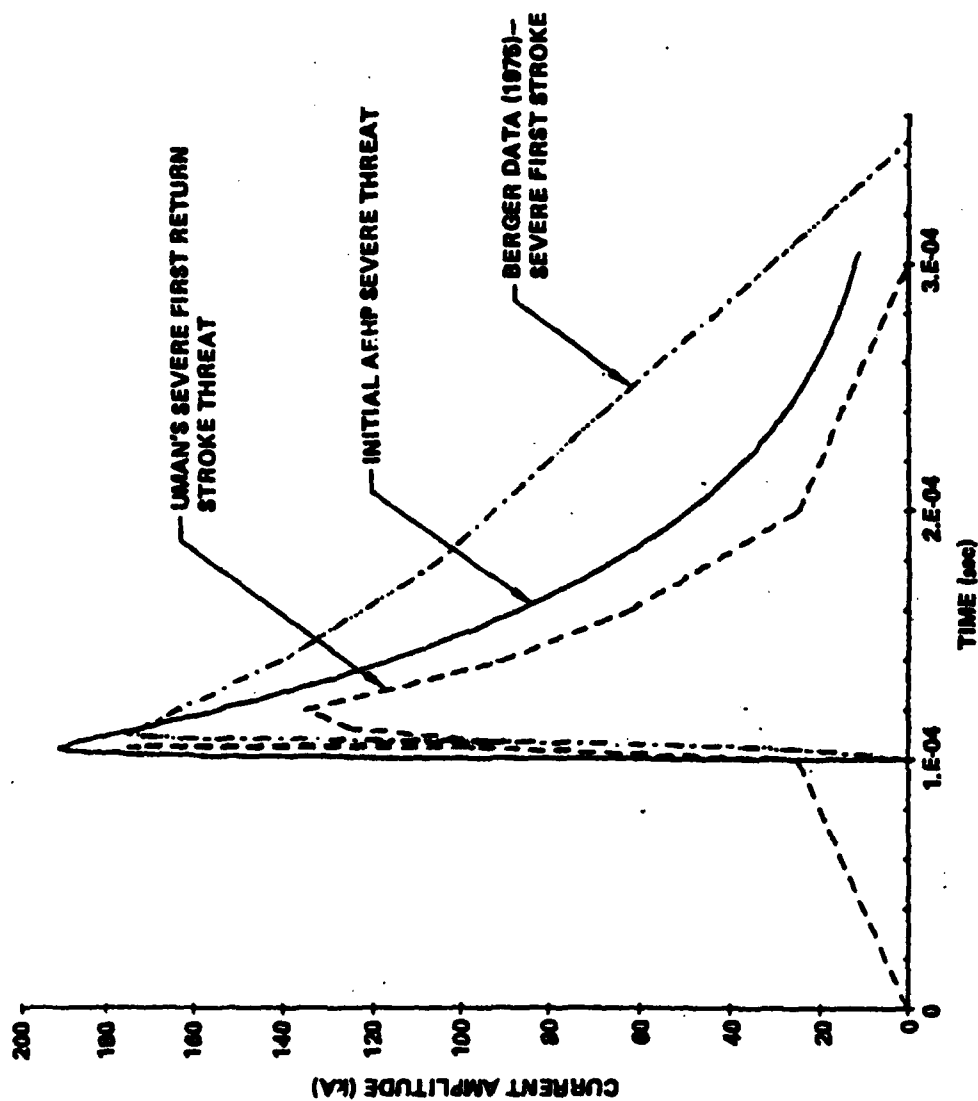
Figure 3.25

Severe First Return Stroke Threat Comparison
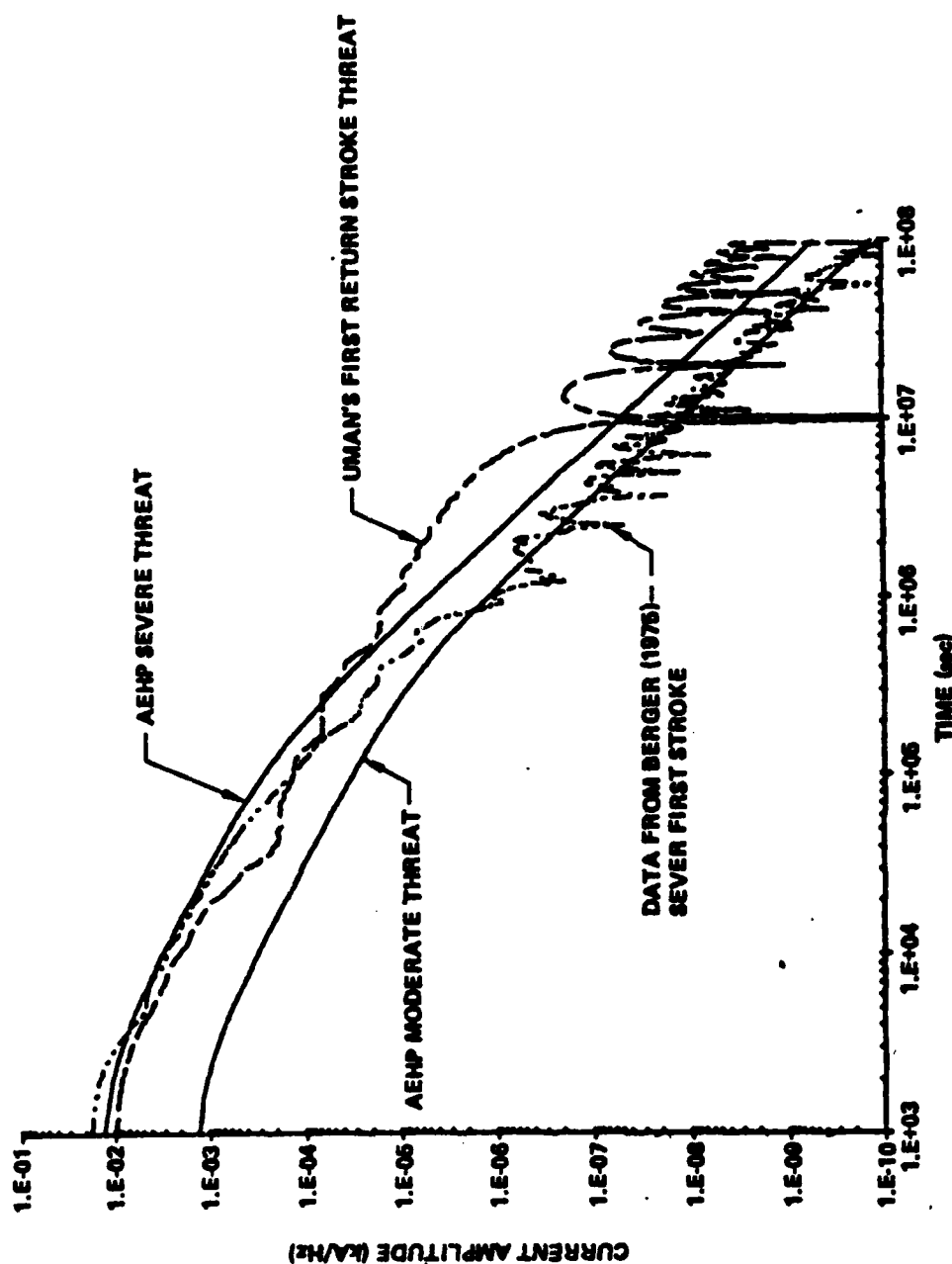
— Time Domain —

Figure 3.26
Severe First Return Stroke Threat Comparison
— Frequency Spectra —
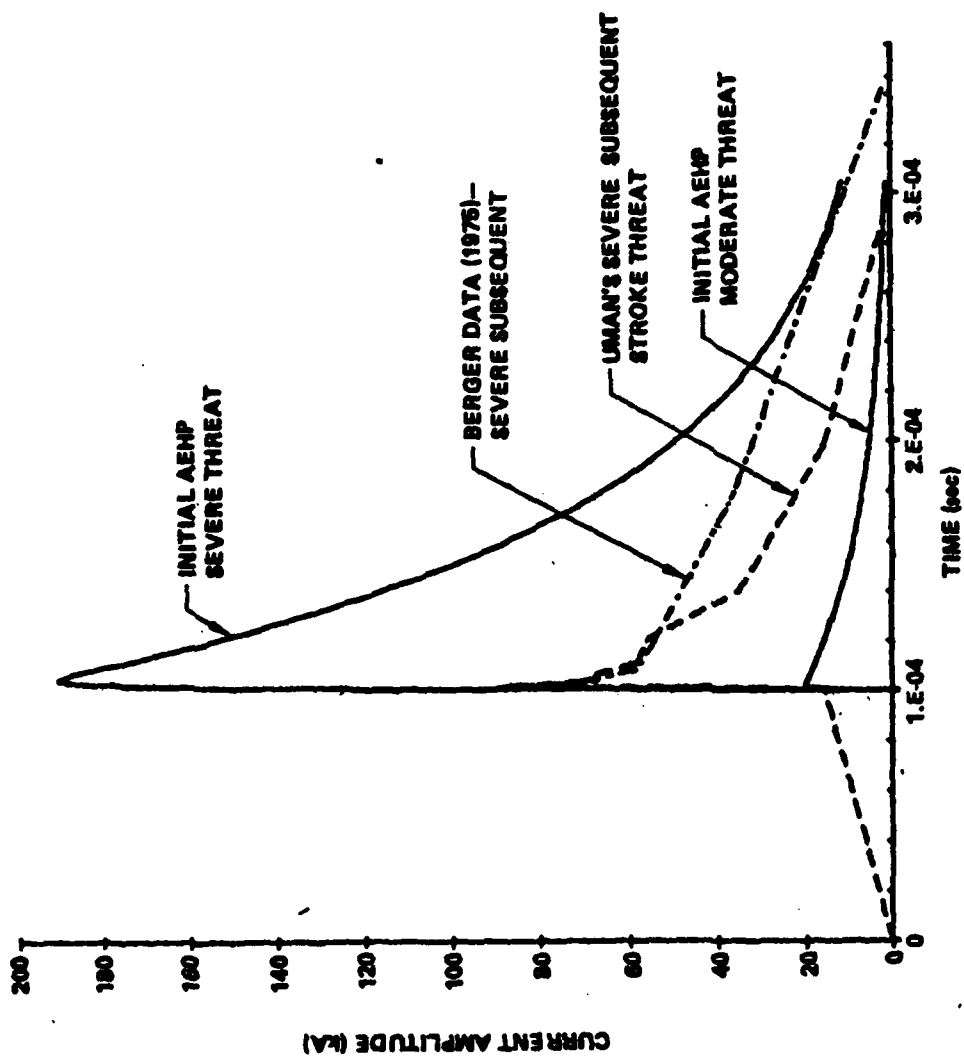
Figure 3.27

Severe Subsequent Stroke Threat Comparison
— Time Domain —
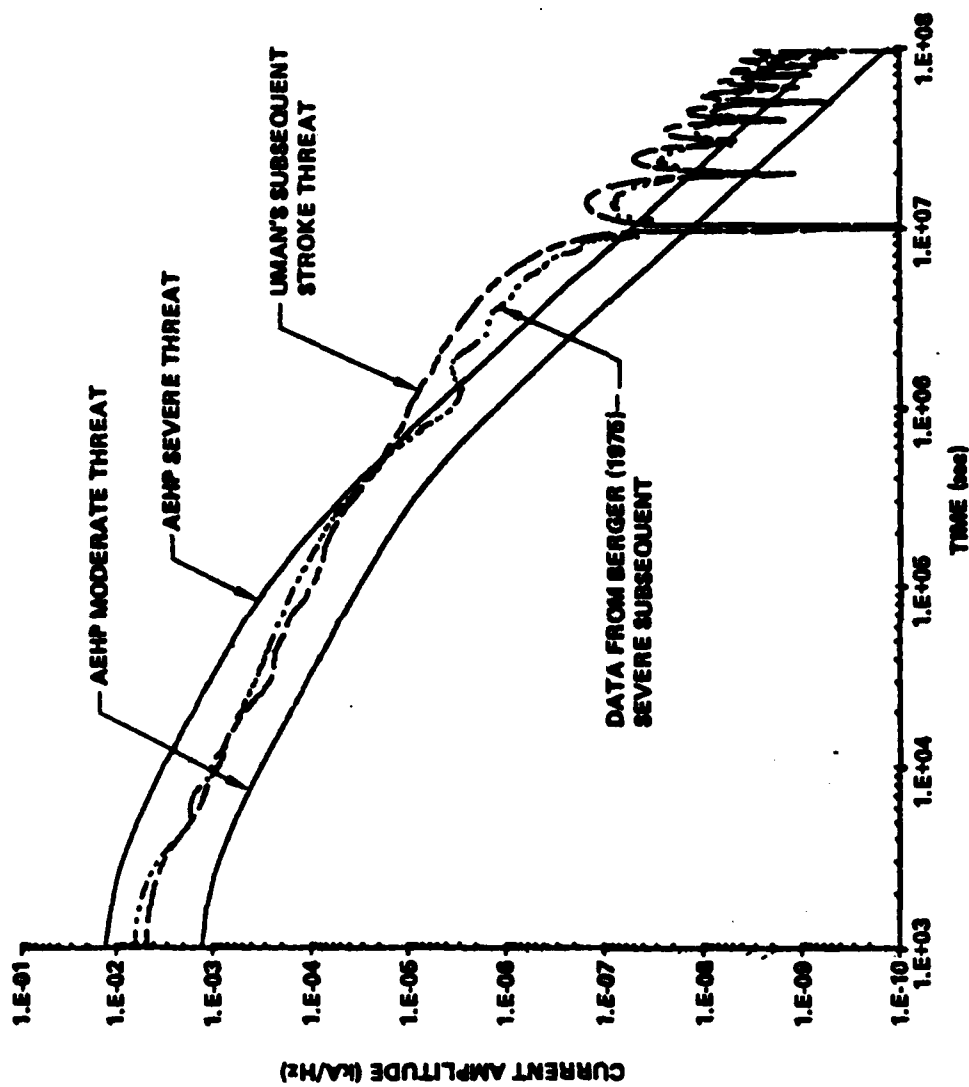
Figure 3.28

Severe Subsequent Stroke Threat Comparison
— Frequency Spectra —
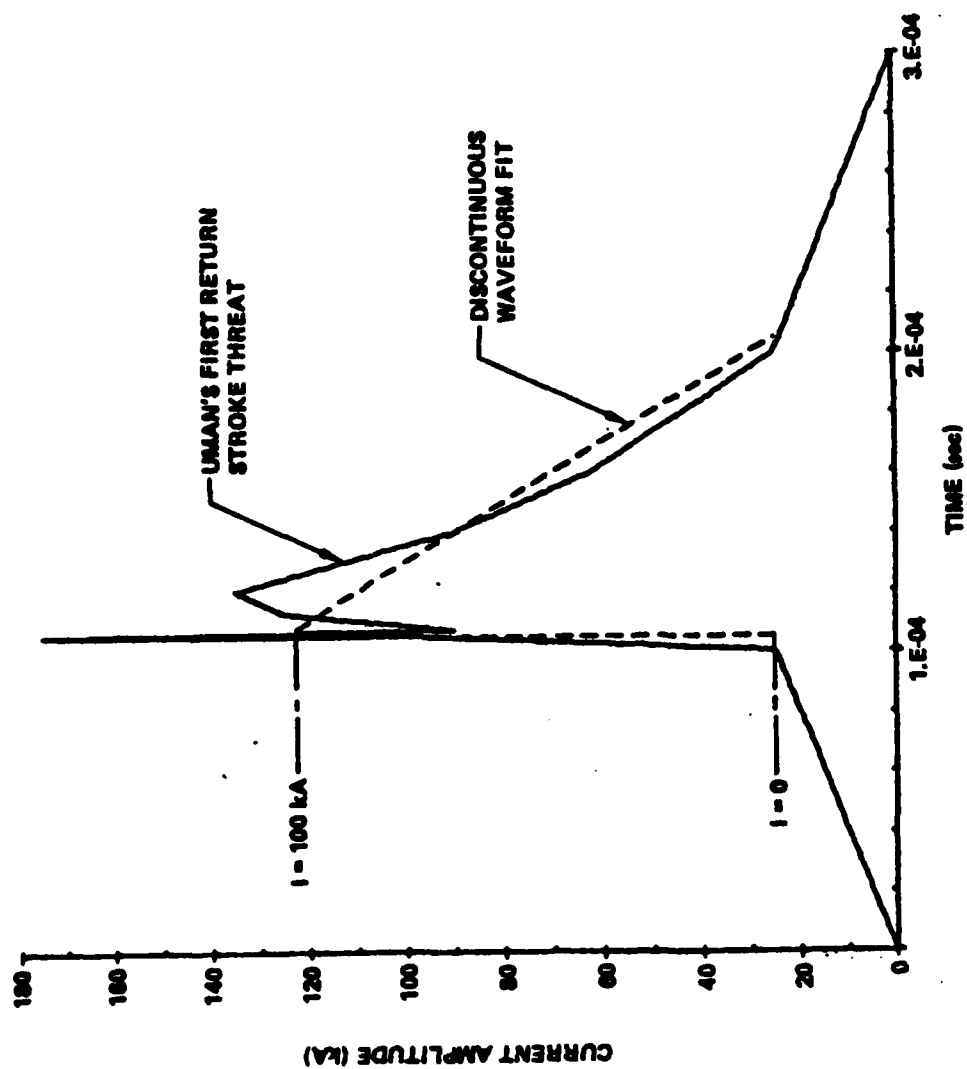
Figure 3.29
Simple Discontinuous Waveform Fit to Uman's
First Return Stroke Threat
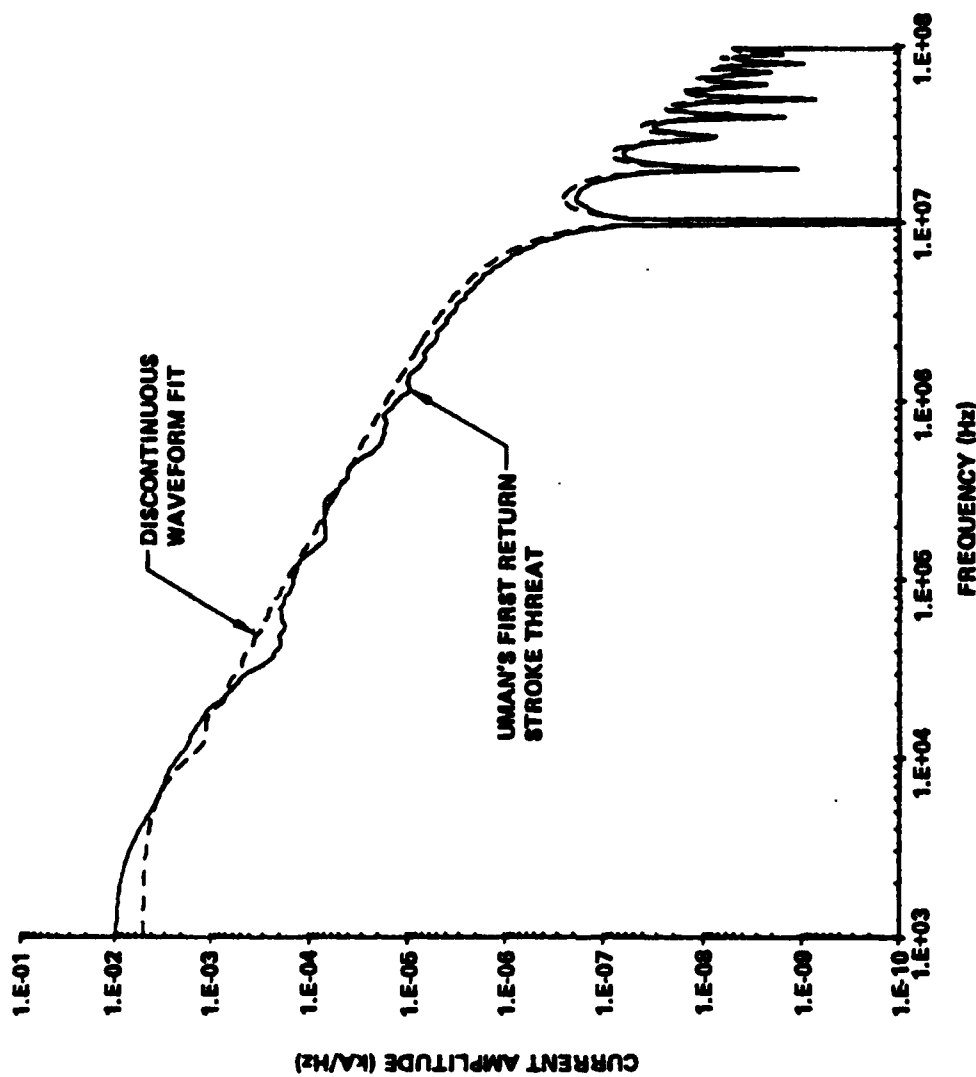
Figure 3.30

Frequency Spectra Comparison of Uman's First
Return Stroke Threat and Discontinuous Waveform Fit
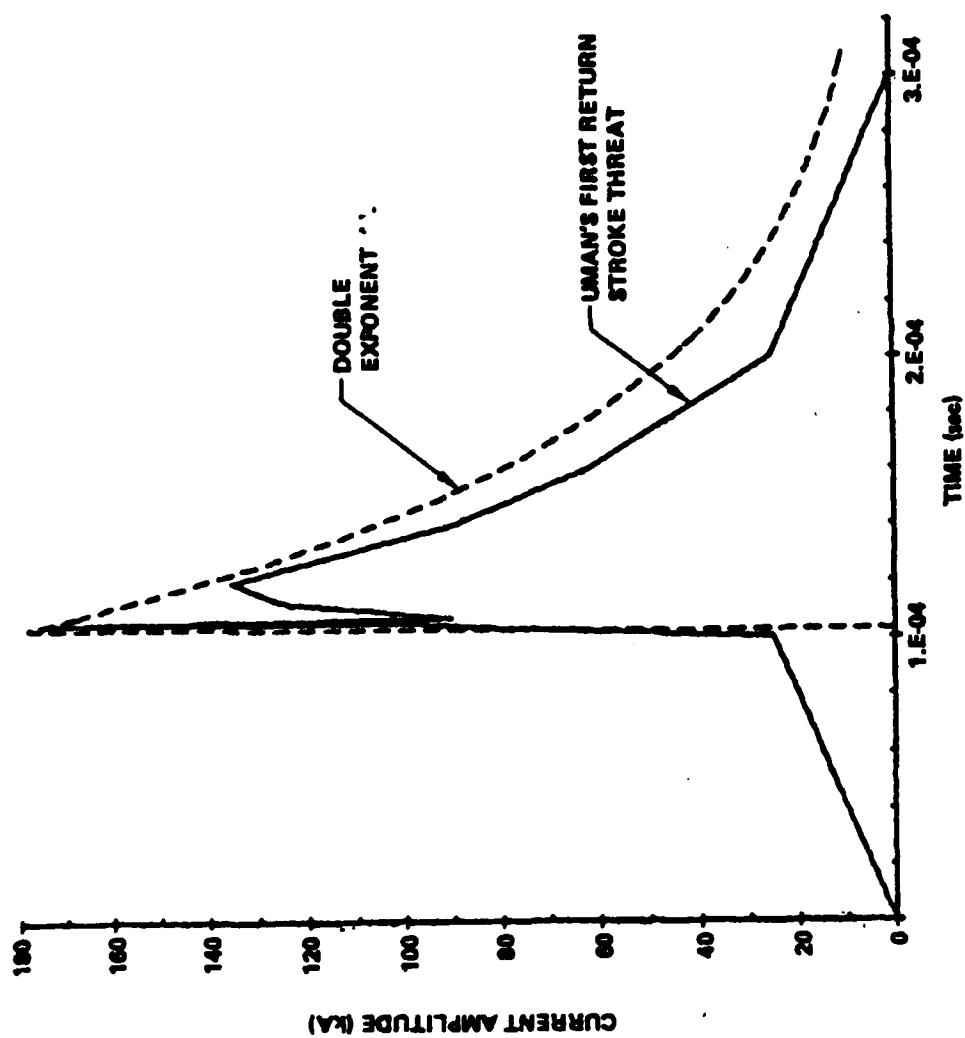
Figure 3.31
Double Exponential Fit to Uman's
First Return Stroke Threat
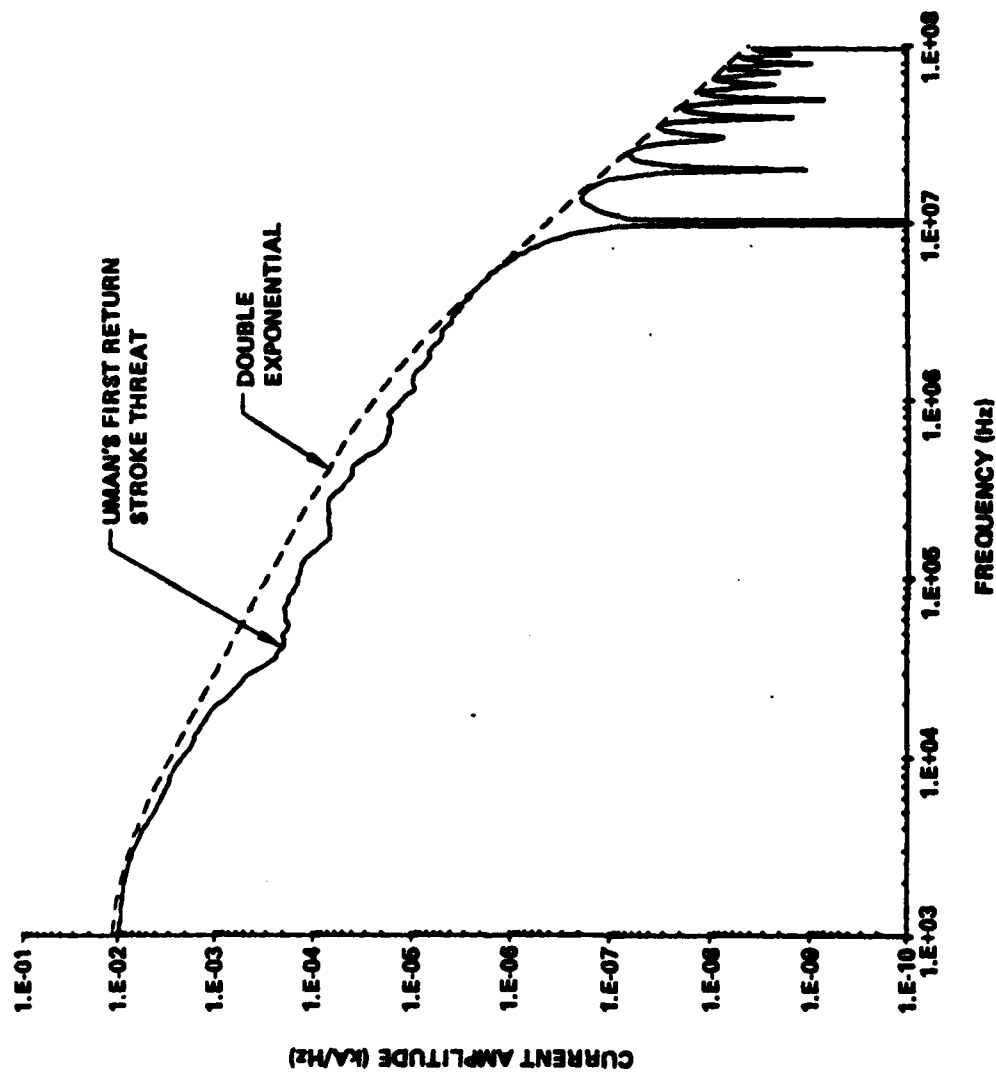
Figure 3.32

Frequency Spectra Comparison of Uman's First Return Stroke Threat and Double Exponential

## 4.0 LIGHTNING MODELING

A model can be defined as a physical or mathematical construct which approximates to various degrees certain observed aspects of natural or man made phenomena. In this section we will be concerned with a evaluation of various mathematical models of lightning processes. The end product required of the lightning modeling will be the prediction of both lightning arc current and EM field values produced by these processes at aircraft altitudes. This model is needed because of the spare data on the statistical variations of lightning currents at altitude. Furthermore this data will require considerable time to obtain. An analytical model will supplement the aircraft inflight measurements by using ground statistics once the extrapolation to altitude is established using a few measurements.

There are basically three levels of detail in current mathematical models for lightning phenomena:

o   Physical analog model including arc, clouds, and electromagnetic propagation
o   Lumped constant electrical transmission line model for arc current
o   Parametric representation matching assumed arc current components to measured EM fields at distant locations

The physical analog model describes the detailed physics of the lightning channel in terms of equations of conservation of mass, momentum, and energy, equations of state, and Maxwell's equations. This type of model requires a detailed knowledge of physical parameters such as the ionization and recombination coefficients and of thermodynamic properties such as the thermal and electrical conductivities. Using this basic approach, one can attempt to predict the channel current as a function of height and time. From a knowledge of the current, the remote electric and magnetic fields can be calculated (e.g., Uman et al., Reference 4-1 and 4-17). Modeling of this type has recently been attempted for lightning return strokes by Strawe (Reference 4-2) and Gardner (Reference 4-3) and holds considerable promise for providing a better understanding of the return stroke. At present, such modeling is limited by assumptions necessary to define the physical parameters.

A less sophisticated level of modeling involves mathematically describing the lightning channel as an R-L-C transmission line with circuit elements that may vary with height and time. The intent of these models is to predict arc channel current as a function of height and time, and to use this current to calculate the EM fields. Price and Pierce (Reference 4-4) and Little (Reference 4-5) have used this approach for return strokes.

In the least sophisticated approach to modeling, and that which has been used extensively for analysis of lightning measurements, a temporal and spatial form for the channel current is assumed and then used to calculate the remote fields. The assumed current is constrained in its characteristics by the properties of lightning currents measured at ground level and by the available data on the measured electric and magnetic fields. Lin et al. (Reference 4-6) have reviewed the literature on this last type of modeling for return strokes and have presented a new return stroke model which is superior to previous models of this type.

In the next sections, particular lightning models of the three types are reviewed and evaluated. A summary of the major models is given in Table 4.1.

The model chosen for the initial analysis is Strawe's model because of simplicity compared to Gardner's model, it is less expensive to run than Gardner's and it includes physics of the lightning channel. Also, the results to date indicate agreement with previous spark modelling and experimental measurements of spark temperatures vs. time and radius vs. time. More complete comparisons with velocity of propagation vs. altitude are being done as well as comparison with EM field measurements.

The Strawe model was chosen for use over Uman's field fitting model because of the desire to predict current profiles at aircraft altitudes. The Uman model does not have this capability.

## 4.1    TRANSMISSION LINE MODELS

The many analytical models for predicting the arc current of lightning return strokes have involved linear charged transmission lines. Models include B vce and Golde (Reference 4-7), Uman and McLain (Reference 4-8), Price and Pierce (Reference 4-4), Rosich (Reference 4-10), and most recently, Little (Reference

4-5). These models predict reasonable peak currents, pulse durations, and propagation velocities provided the proper time independent lightning channel parameters are chosen. However, since the lightning channel expands in diameter by over an order of magnitude during a pulse, constant parameters cannot adequately represent the entire pulse period. More importantly for a threat model, the linear time independent line model produces a step rise in current which contains no information on limits for current rise rate. Rise rate determines the level of induced transients in exposed equipment during a lightning pulse.

The return stroke of a lightning discharge in a cloud-to-ground flash can be represented in a very simple way if the charge on the initiating leader channel is ignored. The capacitance of the cloud then contains all the electrical charge present, and the leader channel is a resistive and inductive element in a simple series LCR circuit. The final step of the leader acts as a switch which completes the circuit. The representation cannot, of course, provide any information about the progress of the return stroke current pulse along the leader channel. The current pulse shape is regarded as identical at all points along the channel.

The leader channel may be treated as a uniform transmission line as a first step. Price and Pierce (Reference 4-4) describe the development of this model (neglecting the cloud capacitance) from the first discussions of a line excited by a source at the base by Bruce and Golde (Reference 4-7). They consider finally a finite, lossy, uniform transmission line terminated in its characteristic impedence and initially charged to a uniform potential. The current at the ground is found to rise instantaneously to a maximum value and then decay, exponentially at first. A similar onset is predicted for current flow at all points of the channel, but the magnitude of the current peak falls as the height above ground increases.

The behavior of the current at ground level is in general accord with observation, though peak values of dI/dt occur at t = 0, whereas there is a delay before this peak occurs in real lightning. At very long times the current falls as $t^{-1/2}$ and this has some correspondence with the intermediate current often observed.

The fact that the line is lossy is important, since a loss-free line produces a current in its terminating resistances that is constant between abrupt step-changes. Such a current waveform is not typical of lightning current pulses. Resistance reduces the importance of reflections, and any model of a lightning channel must include resistance if a realistic current pulse at ground level is to be reproduced. The effective channel resistance per meter is difficult to assess at present. It must be large enough to prevent oscillations in the waveform at ground level, since the natural lightning pulse is unidirectional.

Rosich (Reference 4-9) examines several approximate techniques for determining the effective transmission line characteristic impedance of a lightning return stroke channel. These formulations include (1) the use of a coaxial line model with center conductor dimension equal to that of the central arc core for inductance calculation and of the average positive corona sheath for capacitance, (2) a vertical line segment quasistatic (monopole) model by Berger, (3) a dipole model with sinusoidal current distribution by Schelkunoff, and (4) a 2 dimensional numerical (monopole) solution of Maxwells' equations by Rosich himself. The models are all linear and with constant (in time and position) parameters.

Rosich applies the models to a range of arc and corona radii to obtain a range of effective characteristic impedances $(Z_0)$. $Z_0$ lies in a much more compact range than the radial dimensions since it is essentially logarithmically dependent upon them. The numbers he obtains are typified by a 50 to 500 ohm resistance in series with a few hundred picoFarads. They are typical of the model values commonly assumed in transmission line channel models.

Little (Reference 4-5) determines the transmission line parameters from physical arguments considering only return strokes. To calculate capacitance, the leader channel is regarded as a cylindrical charged conductor of small radius extending almost to the ground with a gap between the end of the leader and the ground. The capacitance is determined by the gap size, dimensions, shape and height of the cloud. The inductance is essentially that of a coaxial line of small radius and is constant throughout the pulse. The resistance is taken large enough to make the current pulse undirectional but

small enough to keep some current oscillations. All parameters are fixed throughout the entire lightning pulse. Comparison of Little's computed current values are compared to data in Table 4.2. The peak current values are high compared to the data.

Lin et al (Reference 4-6) has tested the ability of the Bruce-Golde and transmission line models to predict near and distant electric and magnetic field data for early and late times. Figure 4.1 shows the inability of either model to match the field data at all times. This inability to match the field data throughout the pulse shows the necessity of having time varying parameters to specify lightning characteristics. Also the inability to match both near and far fields simultaneously points out the desirabilty of including self-consistent physics in defining the current channel.

## 4.2 CURRENT MODELS DERIVED FROM FIELD DATA

Modeling attempts using field data to determine lightning current characteristics are discussed in this section. The current is time and height dependent, an improvement on the previous transmission line models discussed in the previous section. Lin, Uman and Standler (Reference 4-6) have defined a fairly complex current distribution. The channel current is decomposed into three components (continuing current, breakdown current and corona current) each dominating a separate time period and having a physically reasonable basis. The continuing or leader current is constant in time and elevation and turns on when the return stroke initiation begins. The breakdown pulse propagates up the channel with a velocity imposed that is based on experimental values. The corona current is caused by the radially inward and then downward movement of the charge stored in the corona. It is initiated at each height as the breakdown pulse front moves by. The current profiles used are shown in Figure 4.2. The fit to near and far field data is quite good in that both close and distant electric and magnetic fields are matched. Two examples are given in Figure 4.3.

Lin et al compares the peak current from the subsequent stroke to measurements. Their mean value of 23 kA is reasonable and agrees with recent results published by Garbagnati (Reference 4-10). No comparison is available with rise time, however, which is one of the most important parameters that the threat model will have to predict.

73

Major limitations of this model include (1) non-uniqueness of the current decomposition, (2) artificially imposed corona current which leads to imposing velocity of propagation as an input parameter to the model, (3) fixed height dependences built in the model and not determined by the physics.

The non-uniqueness of the current decomposition from the EM field values leads to a range of possible current rise rates and maximum amplitude values. This range of values is due to the many parameters introduced in the model and is not yet quantified.

The model assumption of a constant value of velocity of current pulse propagation up the channel also leads to uncertainty in the prediction of current parameters. The velocity values picked to use in the model are averages of experimental observations but the observations themselves show a wide range of values. Also, the height variation of the propagation velocity is not included which leads to further uncertainties.

The artificial height dependences included in the model must be verified by correlation with experimental data or the predictions can not be used for extrapolation purposes to aircraft altitudes.

## 4.3    BASIC PHYSICS MODELS

### 4.3.1    Strawe

Strawe (Reference 4-2) has developed a transmission line model of a cloud-to-ground return stroke in which the non-linear breakdown physics is included. Consistent channel and line parameters are determined from the past current time history using a shock wave (Braginskii type) model of the channel arc. The model determines peak currents, decay times, and scale heights (lengths) similar to linear models. It also provides current rise times and rise rates well in accord with measured data. It indicates that the velocity of propagation of the current wave declines with elevation, as observed photographically, even when the line model is initially uniform in temperature and channel diameter. Most importantly, it predicts a substantial decline in current rise rate with elevation or distance from the discharge initiation.

74

The actual current and the channel arc interact in a lightning discharge to a high degree especially in the early phase when both the current and arc plasma are building. A self consistent model is needed to describe the buildup phase which determines such important current parameters as maximum rate of rise (or rise time) and propagation velocity. Detailed numerical studies (Brode, Reference 4-11; Plooster, Reference 4-12, 4-13; Hill, Reference 4-14) of arc development have been carried out in cylindrical symmetry for assumed current time histories. These analyses have established the time and spatial development of the related plasma parameters, i.e., temperature, pressure, particle densities, conductivity, arc radius, etc., for specified currents but not for natural self consistent ones.

Close agreement between the step excited currents on vertical conducting wires over conducting ground and those on a transmission line has been established (Reference 4-15). This forms a justification for the use of the economical and traditional line model of the return stroke.

In Strawe's model it is assumed that the branched structure of the charged cloud-to-ground leader system can be represented for channel current calculations as a network of transmission line segments. The current so obtained can be used with an assumed channel geometry to calculate the resultant electromagnetic fields.

In the models solved to date only the equivalent line resistance per unit length (R) is considered non-linear and time varying. In principle, since the channel radius changes significantly with time and the channel is geometrically more nearly a vertical monopole than a linear transmission line. The inductance (L) and capacitance (C) per unit length should also be time functions. These involve logarithms of time varying terms and are themselves weak time functions. Initially these time dependences are not included. The channel tortuosity (random path bending) and corona sheath charge storage effects are included as modifications to the L and C values or equivalently as modification to the hot channel $(R = 0)$ velocity factor $(V_f)$ and characteristic impedance $(Z_0)$. Some of the charge stored in the sheath during leader formation is retrievable during the return stroke. This is accounted for by assuming a larger effective conductor radius for capacitance calculation than the sub-centimeter current carrying core.

The resistance models developed for use here are based on the spark channel model of Braginskii (Reference 4-16). This relatively simple model assumes that a conductng channel has been established prior to the initiation of the spark by prebreakdown streamer, and/or leader processes. The resultant arc radius, temperature, pressure, etc. are determined from the spark current time history. The current (i) is assumed to heat ($i^2R$ loss) the initially conducting arc plasma to higher temperatures and tens of atmospheres of pressure. This condition produces a hydrodynamic shock wave in the air surrounding the spark channel resulting in a rapid channel expansion. Braginskii uses the strong shock approximation to simplify the physical picture of the expansion process. This picture produces an essentially uniform electrical conductivity (determined from channel temperature and pressure) which is nearly constant in time. The channel resistance per unit length is determined from the conductivity and the arc radius.

The arc channel geometry is assumed to be axisymmetric or locally of cylindrical symmetry. The channel parameters are described in terms of a deposited energy rate set by the local current time history ($i^2R$ loss). Detailed analyses (References 4-11 to 4-14) have established representative radial contours of these parameters for lightning-like currents. These analyses solve, in cylindrical symmetry, the hydrodynamic equations of continuity of mass, momentum, and energy (transfer) together with two equations or state relating pressure, temperature, mass density, internal energy density, etc. The model was developed to include the lost and reabsorbed thermal radiation from the channel, temporal variation of thermal and electrical conductivity, and low pressure momentum transfer.

In comparison with Uman's EM field current fitting model, the currents components included in Strawe's model are Uman's breakdown current and corona current. To date, the continuing current component is not yet incorporated. This addition would make the late time field values agree more with experimental measurements.

Representative model current time histories are shown in Figure 4.4. The most significant effect shown, from an electrical transient point of view, is the rapid reduction in peak current rise rates with elevation or distance from the discharge initiation point. As expected, the peak amplitude declines slowly and the rise time increases with elevation.

Comparisons of Strawe's model with results given by Plooster (Reference 4-12, Figure 3) on temperature within the core agree well both in magnitude and trend with radius. The results also agree with experimental results on core temperatures given by Orville (see Reference 4-14). Preliminary comparisons of the height dependence of the velocity of propagation up the channel agree in trend with some of Orville's luminosity measurements. Agreement with previous results for both spark modelling and experimental results indicates Strawe's model has incorporated most of the important physics known to date.

### 4.3.2 Gardner

Gardner (Reference 4-3) uses a nonlinear transmission line model of the return stroke channel. It is similar in structure, physics, and mathematical form to that of Strawe except for reduced channel complexity (one dimensional: no branching, bending or network representations of ground connections, etc.) and a more detailed radial treatment of arc development. He uses constant (time and position) L and C line parameters, although this could be generalized to include dependence on local arc and positive corona radii as well as local current time history. The only time varying parameter is the arc channel resistance per unit length R $(z, t)$, as in Strawe's model.

Like Strawe's model the only source of energy input to the arc channel is joule heating $(i^2R)$ due to the channel current. The model represents an extension of the Strawe model in that the 3 region (Braginskii shock model) radial description is replaced by a radial grid of 256 bins allowing for shockwave buildup and decline with a minimum of geometrical restriction or approximation. The 3 region Braginskii radial distribution is a good approximation for early arc channel development. Gardner's approach should be capable of calibrating and improving upon it especially for late time arc development.

Gardner's solution involves the simultaneous solution of the nonlinear telegrapher's equation set describing current propagation on the conducting channel and the nonlinear hydrodynamic equations describing the local pressure p, temperature T, arc radius a, arc conductivity $\sigma$, and ultimately R $(z, t)$ in terms of the local current time history. These are nonlinear partial differential equations requiring numerical solution. Initial conditions involve the values at discharge commencement of leader channel voltage, arc channel radius, temperature, and pressure. The initial current (normally zero) is also required.

Instead of Braginskii's simple equation of state, Gardner uses a more complex set developed by Plooster (Reference 4-13). These equations include more physics and chemistry than does the Braginskii model, although Strawe does include some of the more complex physics by using some curve fits to Plooster's model.

Comparisons of Gardner's results to both Strawe and Plooster agree well in magnitude and radial variation for early times (arc radii < few cm). Shock radii, temperatures and conductivities agree between Gardner and Strawe for early time development of the arc. The later time development does not agree due to different assumptions made in the two models. Gardner's shows the channel developing more slowly with an expanding shock wave propagating away from the channel. Strawe's model continues to have the channel radius defined by the shock radius which for later times implies a rapidly expanding radius.

These comparisons show both Gardner and Strawe to have correct physics for the initial arc development. Strawe's results are good for arc radii out to several centimeters while Gardner's results should be good beyond that.

# CHAPTER 4 REFERENCES

4-1. Uman, M.A., McLain, D.K., Krider, E.P., "The Electromagnetic Radiation from a Finite Antenna," Amer. J. Phys., 43, 33-38, 1975.

4-2. Strawe, D.F., "Non-Linear Modeling of Lightning Return Strokes," Proceeding of the Federal Aviation Administration/Florida Institute of Technology, 6-8 March 1979, Melbourne, Florida, Report FAA-RD-79-6.

4-3. Gardner, R.L., "A Model of the Lightning Return Stroke," Ph.D. Thesis, Universi ' of Colorado, 1980.

4-4. Price, G.H., and Pierce, E.T., "The Modeling of Channel Current in the Lightning Return Stroke," Radio Science, May-June 1977.

4-5. Little, P.F., "Transmission Line Representation of a Lightning Return Stroke," J. Phys. D.: Applied Physics, 11, p. 1893-1910, 1978.

4-6. Lin, Y.T., Uman, M.A., Standler, R.B., "Lightning Return Stroke Models," J.G.R., 85, 1571-1583, March 1980.

4-7. Bruce, C.E.R., and Golde, R.H., "The Lightning Discharge," J. Institute Elec. Eng. Longon, 88, 1941.

4-8. Uman, M.A., and McLain, K.K., "Magnetic Field of LIghtning Return Stroke," J. Geophysical Res., 74, 1969.

4-9. Rosich, R.K., Rymes, M.D., Eriksen, F.J., "Models of Lightning Channel Impedance," IEEE International EMC Symposium, Boulder, CO., 18-20 August, 1981.

4-10. Garbagnati, E., Lopipard, G.B., "Lightning Parameters - Results of 10 Years of Systematic Investigation in Italy," Proceedings of International Conference on Lightning and Static Electricity, Oxford, England, March 1982.

4-11. Brode, H.L., "Review of Nuclear Weapons Effects," Ann. Rev. Nucl. Sci., 18, 153, 1968.

4-12. Plooster, M.N., "Numercial Simulation of Spark Discharges in Air," Phys. Fluids, 14, 2111, 1971.

4-13. Plooster, M.N., "Numerical Model of the Return Stroke of the Lightning Dischrage," Physics of Fluids, 14, 2124, 1971.

4-14. Hill, R.D., "Channel Heating in Return Stroke Lightning," J. Geophysical Res., 76, 637, 1971.

4-15. Strawe, D.F., "Lightning Source Model Development Program," Boeing Document D180-22936-1, January 1978.

4-16. Braginskii, S.I., "Theory of the Development of a Spark Channel," Soviet Physics, JETP, 7, 1068, 1958.

4-17. Uman, M. A. and E. P. Krider, "A Review of Natural Lightning: Experimental Data and Modeling", IEEE Transactions on Electromagnetic Compatibility, May 1982.

4-18. Frese, M. H., and R. L. Gardner, "A Comparison of Calculated Lightning Channel Characteristics as Computed by a Simple Physical Solution and a Detailed Finite Difference Calculation", MRC Report to BMAC under Contract CM9221, Report No. AMRC-R-417.

# Table 4.1
## Lightning Channel Models

| Investigator | Approach | Evaluation |
|---|---|---|
| R. L. Gardner MRC | Electrical Transmission Line Model and Hydrodynamic Model Coupled into Partial Differential Equations for Channel, Leader, and Leader Formation | Parameter Needing Data to Define Accurately. Contains all Relevant Arc Physics. More Accurate but Higher Cost than Strawe Model. |
| R. K. Rosich EMA | Determines Arc Channel Impedance From Idealized Linear Constant Coefficient Models. | Predictions Limited to Impedance of Arc Channel Over a Range of Radial Dimensions. Impedance Expected to be 50 to 500 Ohms in Series With Small Reactive Part. |
| D. F. Strawe Boeing | Electrical Transmission Line Model Having Time-Varying Parameters. Parameters Determined From Plasma Physics—Physical Limitations of Hot Arc Channel. | Predictions Limited by Assumed Parameters That Need Data to Define Accurately. Model Contains All Relevant Physics of Arc (Branching, Tortuosity, Plasma). |
| M. A. Uman U of Florida | Reconstruct Major Features of Arc Discharge (Four Current Terms) Using Measured Electromagnetic Fields at Ground. | Predictions Limited by Simplifications to Obtain Gross Features. Decomposition of Measurements is Not Unique (Two Stations/Four Currents) and Rate of Rise Not Predicted. |
| Phil Little | Lossy Transmission Line Model for Channel | Linear Model Which Does Not Simulate Arc Development |

81

## Table 4.2

## Transmission Line Model Comparison to Ground Current Data

| Example no. | Peak current $I_{max}$ (kA) | Observed % above† | Peak d$I$/d$t$ $i_{max}$ (kA μs⁻¹) | Observed % above† | Rise time $\tau$ (μs) | Observed % above† | Impulse charge $Q$ (C) (<40 μs) | Observed % above† | Action integral $G$ (10⁴ A² s) (<40 μs) | Observed % above† |
|---|---|---|---|---|---|---|---|---|---|---|
| 1 | 92 | (0.9) | 64 | (1) | 2.0 | 92 | 1.6 | 88 | 6.2 | 52 |
| 2 | 83 | 1 | 95 | (0.95) | 1.6 | 97 | 1.6 | 88 | 5.9 | 52 |
| 3 | 95 | (1) | 54 | (1) | 2.0 | 92 | 1.5 | 89 | 7.0 | 45 |
| 4 | 83 | 1 | 91 | (0.95) | 1.6 | 97 | 1.5 | 89 | 6.8 | 52 |
| 5 | 74 | 4 | 66 | (1) | 2.3 | 85 | 1.4 | 89 | 5.3 | 58 |
| 6 | 54 | 10 | 48 | 1 | 3.5 | 70 | 1.2 | 92 | 4.2 | 65 |
| 7 | 79 | 2 | 11 | 75 | 1.3 | 98 | 1.3 | 90 | 5.6 | 55 |
| 8 | 95 | (1) | 54 | (1) | 2.0 | 92 | 1.6 | 88 | 7.8 | 40 |

† Percentage of observed values above computed value: bracketed figures are estimates.
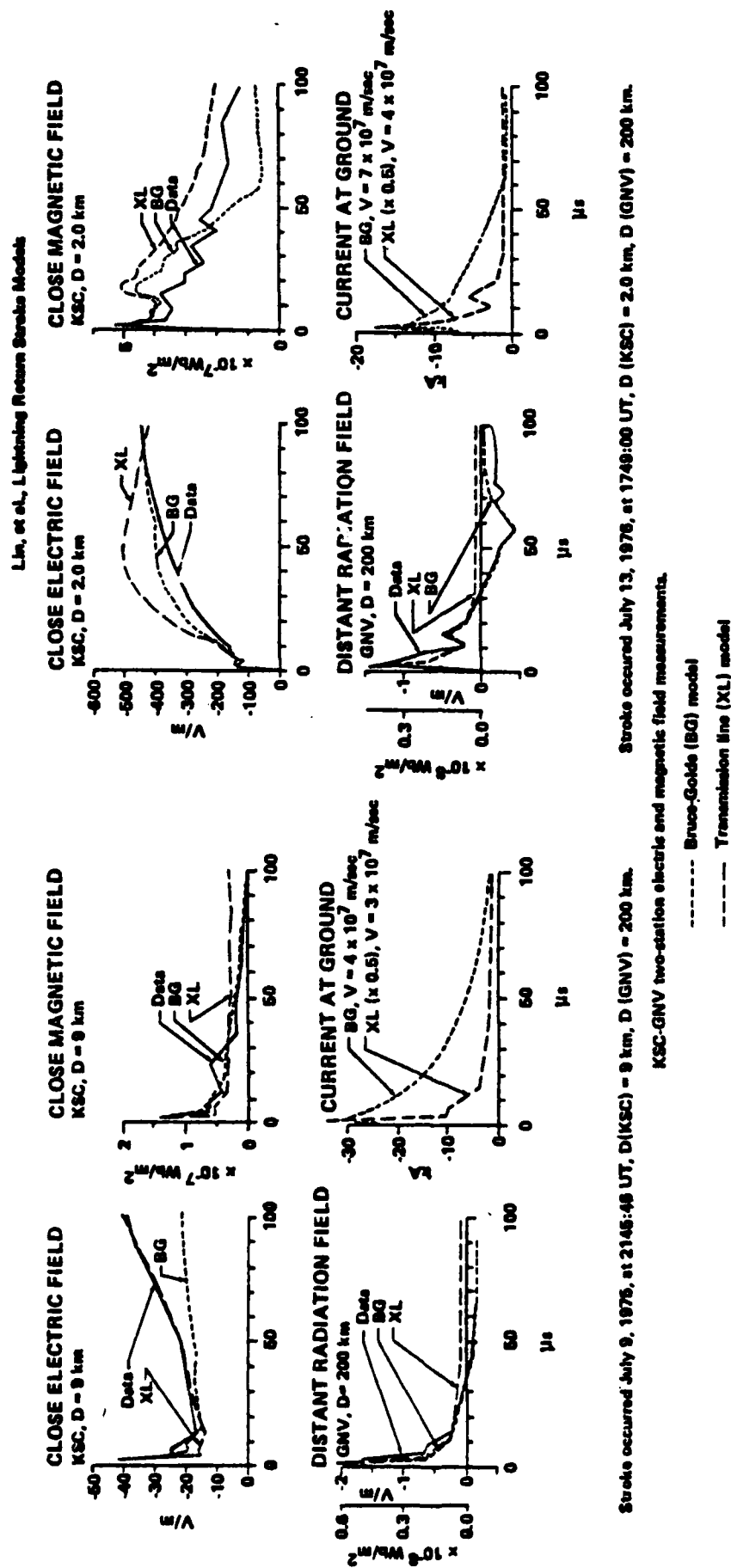
82

Figure 4.1

Comparison of Bruce-Golde and Transmission
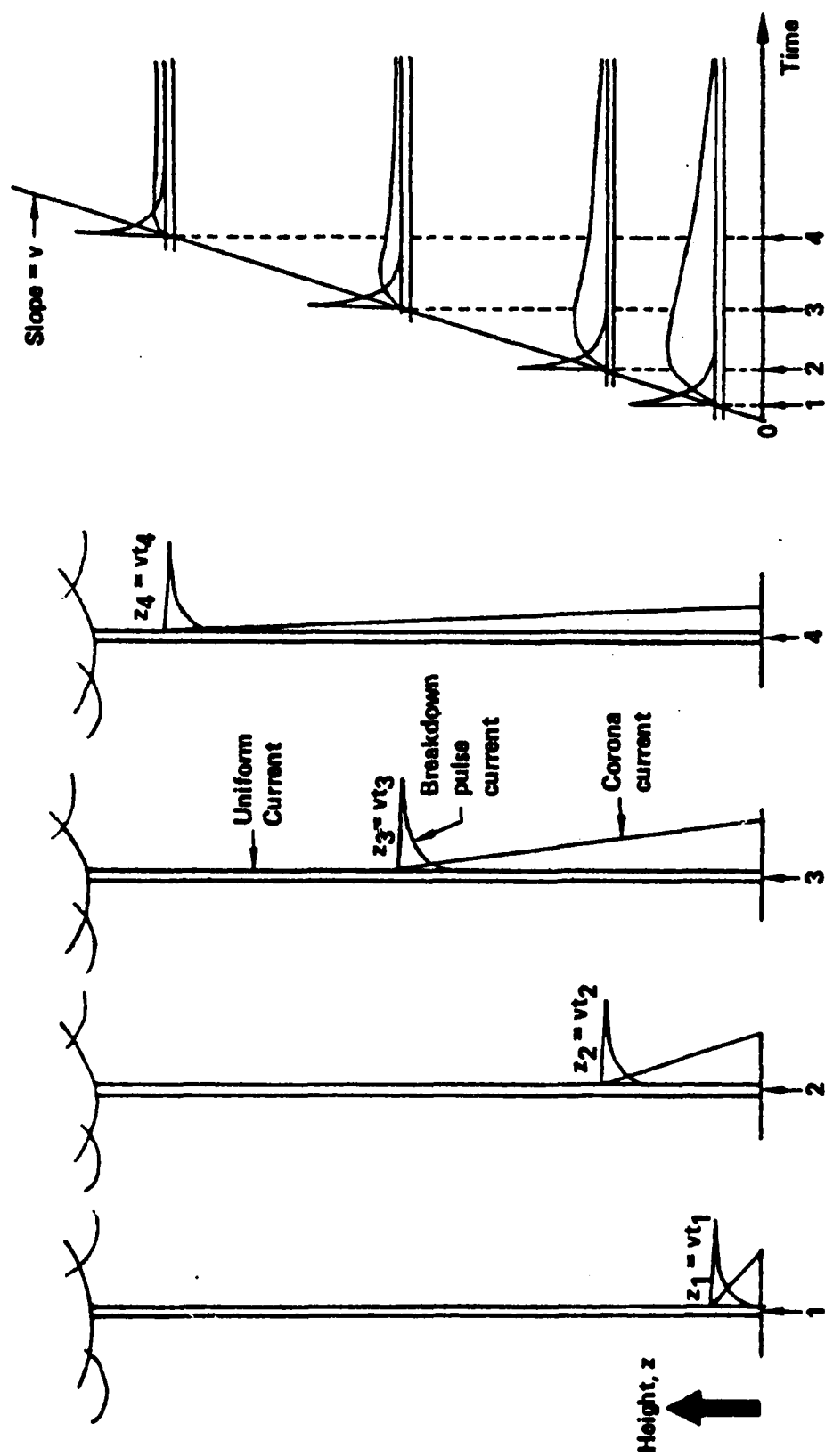Line Models to Data

83

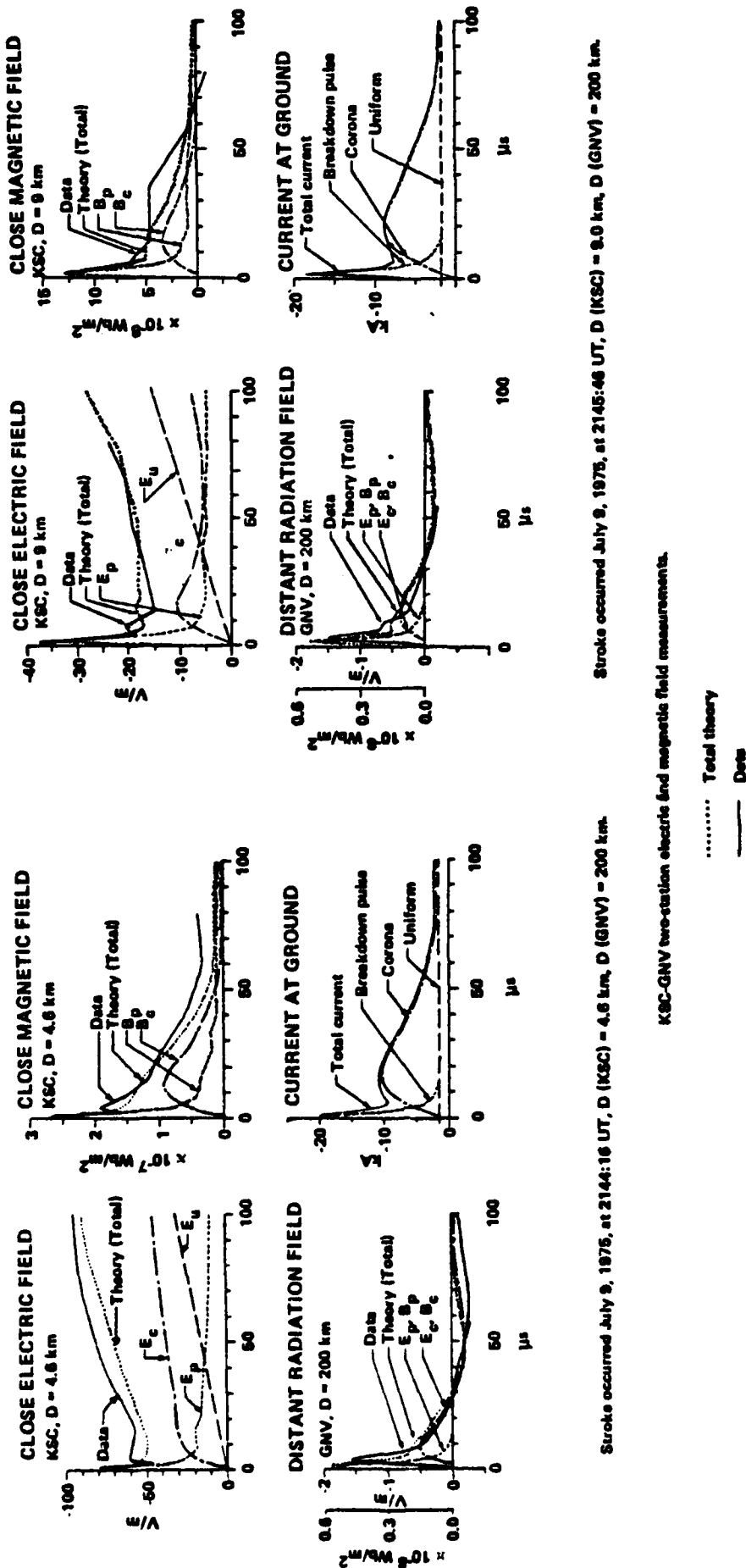Figure 4.2

Current Distribution for Model of Lin, et al.

Figure 4.3

Comparison of Lin, et al. Model to Data
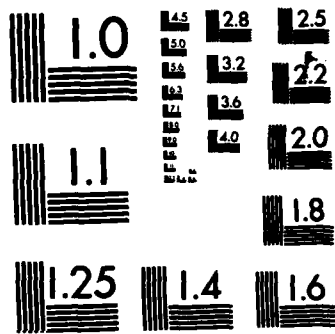
MICROCOPY RESOLUTION TEST CHART
NATIONAL BUREAU OF STANDARDS-1963-A
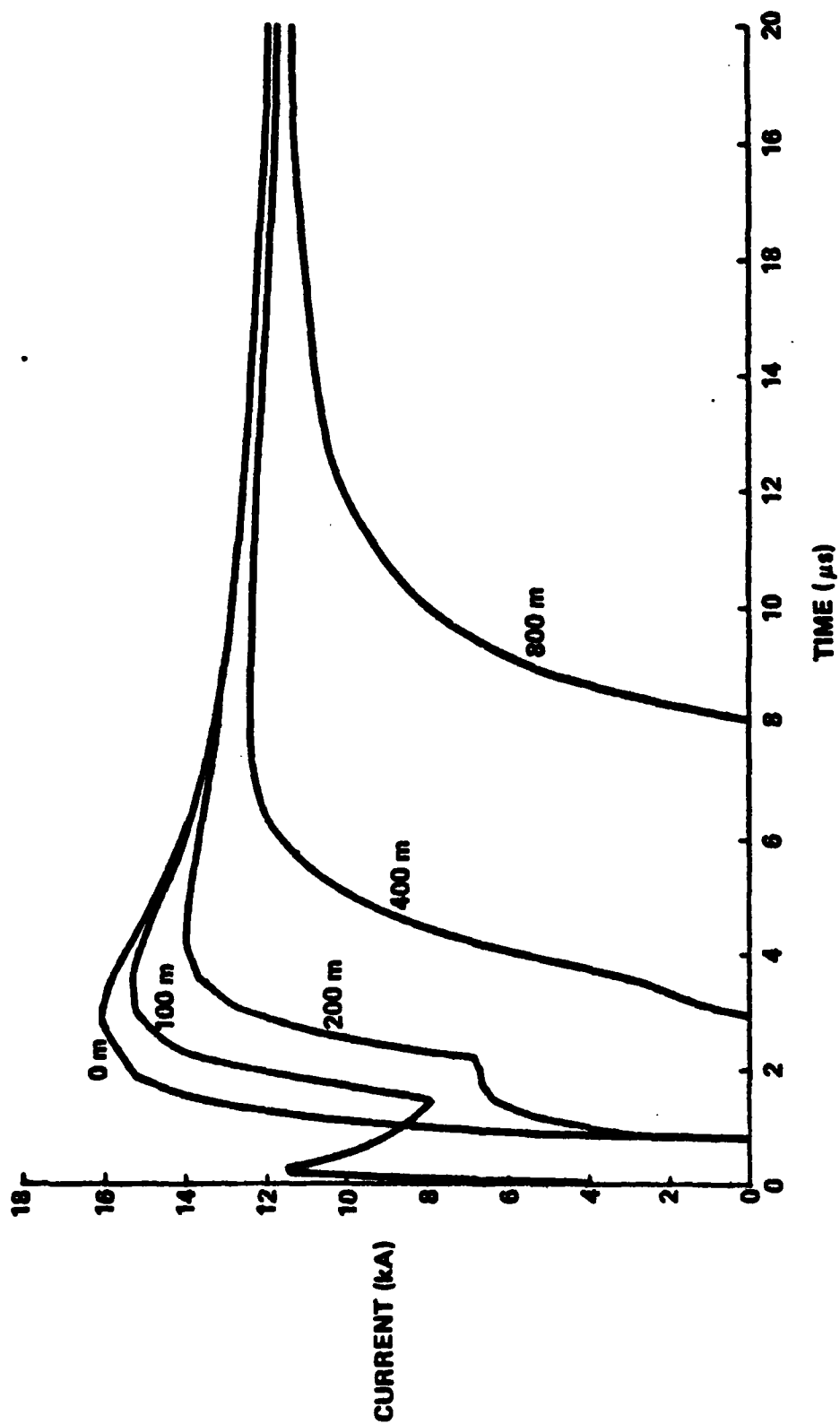
Figure 4.4
Model II, Configuration 1

86

# 5.0 STATIC ELECTRIFICATION

Static electrification of a conventional aircraft can occur in various ways as illustrated in Figure 5.1. Figure 5.1(a) illustrates frictional electrification; as uncharged precipitation particles strike the aircraft, they acquire a positive charge, leaving an equal and opposite negative charge on the aircraft and raising its potential to tens or hundred of thousands of volts. Charging occurs both on the metal structure of the aircraft and on dielectric surfaces such as the windshield. Dielectric surfaces can thus become charged with respect to the airframe. Engine charging, illustrated in Figure 5.1(b), occurs when flight vehicles are operated at low altitudes. Processes as yc incompletely understood occur within the engine combustion chamber and cause a predominantly positive charge to be expelled with the engine exhaust. This causes an equal and opposite (negative) charge to be imparted to the aircraft charging it to potentials of tens or hundreds of thousands of volts. Exogenous charging, illustrated in Figure 5.1(c), occurs when the vehicle flies in a region of electric field, such as that generated between oppositely charged regions of clouds; this field can cause discharges to occur from the extremities of the vehicle.

The operational conditions under which static electrification can occur depend somewhat on the class of vehicle. Since airplanes encounter severe charging during operation in clouds in horizontal flight, electrification can continue for considerable periods of time on all-weather missions. On jet aircraft operating at low altitude, engine charging can be an additional source of long-term electrification. Helicopters become charged while flying through naturally occurring clouds. In addition, a hovering helicopter can stir up snow or dust thereby generating its own cloud of particles to produce frictional electrification. Thus, helicopters encounter static problems in regions where conventional aircraft do not.

The charging process itself produces virtually no difficulty, but vehicle voltage and electric fields can become so high after a period of time that electrical discharges occur. It is the discharge of the accumulated static electricity that generally produces the most harmful effects.

## 5.1    NOISE SOURCES

An important consequence of static electrification is electrical noise. The various noise mechanisms that have been identified are shown in Figure 5.2. As the airplane becomes charged, the electric fields at the extremities of the vehicle become sufficiently high to cause corona breakdown of the air. At the operating altitude of airplanes, this breakdown occurs as a series of very short pulses containing energy in the radio frequency spectrum. These noise pulses can couple into communication, navigation, or digital circuitry to produce interference.

Another source of noise occurs when dielectric surfaces on the front of the airplane, such as the windshield and radome, are exposed to frictional charging, as illustrated in Figure 5.2. These surfaces can be charged by impinging particles. Since these materials are insulators, the charge is bound at the place where it was deposited and cannot be discharged until sufficient electric charge has accumulated to produce a streamer (a spark-like discharge) across the dielectric surface to the metal airframe. Streamer discharges are slow in duration, and involve the transport of charge over a large distance. They therefore produce radio frequency interference which can couple into susceptible systems on the aircraft. In some cases, the streamering on a square inch of surface in a critical location is sufficient to disable systems.

A third source of interference that often occurs inadvertently on airplanes is associated with sparking between unbonded adjacent metal sections of the aircraft. For example, consider Figure 5.2, which shows a break in the wing; charging processes on the airframe will raise the potential of the inboard section with respect to the outboard section until a spark occurs in the gap. This spark produces a short current pulse, which is also a source of noise. In flight, the current required for corona discharge from the isolated wing tip is supplied from the remainder of the airplane.

Finally, slowly varying induction pulses can be produced in antennas by the passage of charged particles. This noise is of importance only at VLF or ELF and does not pose much of a problem to conventional communication and navigation equipment. With the advent of systems operating at frequencies of the order of 10 kHz, however, induction noise should be considered.

## 5.2 CHARGING PARAMETERS

The interference problem due to any of these noise sources depends on the charging rate of the plane. The most important process as measured in flight tests is frictional charging. Examples of both frictional and engine charging are shown in Figure 5.3 (Reference 5-1).

The precipitation charging current to a vehicle is given by (Reference 5-2)

$$i = q_p c v A_{eff}$$

(3)

where

$q_p$ = Charge per particle

$c$ = Particle concentration

$v$ = Aircraft velocity

$A_{eff}$ = Effective intercepting area of aircraft.

The various parameters in the equation and their interdependencies have been studied analytically, in the laboratory and in flight, and are generally understood for the operating regimes of current aircraft. Typical values of particle parameters for an aircraft operating in the subsonic flight regime are given in Table 5.4 for two cloud types.

Table 5.4 Precipitation Particle Parameters (Reference 5-3)

| Cloud Type | $q_p$ pico Coulomb | $\frac{c}{m^3}$ |
|---|---|---|
| Cirrus | 1 - 10 | $2 \times 10^4$ |
| Thunderstorm Anvil | 1 - 35 | $5 \times 10^4$ |

Laboratory experiments involving the charging of projectiles fired through ice crystal clouds were conducted to determine the relationship between the charge acquired and the impact velocity. The results of these experiments indicate that the projectile charge decreases with increasing velocity as shown in Figure 5.4 (Reference 5-4). These results were further verified by flight tests. It was noted that the observed effect might be caused by the melting of the ice crystals by the energy of the impact, since flight-test experience indicates that clouds composed of water droplets tend to charge an aircraft at

a much lower rate than do clouds containing ice crystals. Thus, if an ice crystal is completely melted upon impact, greatly reduced charging would result. Thus, the charging should follow value of the unmelted ice mass as it does in Figure 5.4.

The effective intercepting area, $A_{eff}$, as been found to be affected by aircraft speed as well as body shape. The results of studies of water droplet impingement on airfoils indicate that the effective intercepting area of a typical aircraft would vary with speed as shown in Figure 5.5 (Reference 5-2). Combining the results of Figures 5.4 and 5.5 yields the curve of Figure 5.6 (Reference 5-2) which indicates the predicted charging current behavior as a function of speed. It is noted that because of ice-crystal melting, the charging rate decreases rapidly at speeds above 1500 mph. The maximum charging current occurs at about 1400 mph and is only 2.6 times the charging current at 600 mph. This result is highly significant in that it indicates that precipitation static problems on highly supersonic aircraft are not appreciably more severe than they are on subsonic aircraft.

## 5.3 CORONA

As the static charging increases, the electric potential of regions of the aircraft can be increased to the point that corona discharge take place. These discharges are in the form of a series of short pulses. The individual pulses associated with these discharges can be modeled as (Reference 5-4)

$$f(t) = Ae^{-\alpha t}$$ (4)

where A is the pulse amplitude and $\alpha$ is the pulse decay constant. Both A and $\alpha$ are functions of atmospheric pressure, and hence of altitude. The number of such pulses per minute, denoted by $\nu$, is also a function of atmospheric pressure. A good fit to observed values of A, $\alpha$ and $\nu$ can be obtained by using:

$$A = 7.90569 \times 10^5 \, p^{0.25}$$
$$\alpha = 2.777 \times 10^{-2} \, p$$ (5)
$$\nu = 3.83767 \times 10^3 \, p^{0.48}$$

where p is atmospheric pressure, measured in torrs.

Pressure and altitude can be related by

$$P = 760 \exp - \left(\frac{h + 0.002\ h^2}{25}\right) \qquad (6)$$

where h is altitude given in kilofeet and p is again in torrs. The noise spectrum produced by $\nu$ pulses per second is given by (Reference 5-4)

$$P = A \left(\frac{\nu}{\pi}\right)^{1/2} (\omega^2 + \alpha^2)^{-1/2} \qquad (7)$$

Figure 5.7 (Reference 5-5) shows some characteristics of this spectrum.

Note that the low frequencies are a larger threat for high altitudes. This trend with altitude changes for higher frequencies. Above about 10 MHz, higher noise levels are present for lower altitudes.

## 5.4 STREAMERS

When charge is deposited on dielectric surfaces such as radomes, windshields or composite material structures, it cannot flow freely to other parts of the aircraft because of the insulating character of these surfaces. If the potential between these surfaces and the main body of the aircraft becomes too great, a surface streamer discharge will occur.

The current flow from a single pulse of a streamer discharge can be approximated by (Reference 5-4)

$$I(t) = I_{max} (ae^{-\alpha t} + be^{-\beta t})$$

where, for a typical streamer,

$$
\begin{aligned}
a &= 0.597 & \alpha &= 1.67 \times 10^7 \text{ Hz} \\
b &= 0.403 & \beta &= 3.47 \times 10^6 \text{ Hz} \\
I_{max} &= 0.01 \text{ A}
\end{aligned}
$$

$(8)$

Clearly, this current is many orders of magnitude smaller than that due to lightning.

This waveform has been used with a typical coupling factor of $\psi = 3$ m$^{-1}$ for several streamer lengths to compute the induced current with a wire located immediately below the streamer. The results of these calculations are shown in Figure 5.8 (Reference 5-3).

The charge transferred by a single streamer discharge is 1 to 1.5 x $10^{-9}$ Coulomb. This is roughly the same as the charge transfer in a corona pulse. The difference in pulseforms produced by the two mechanisms results from the difference in the lengths of the two discharges. The corona discharge extends to only one tip radius from the burr or other imperfection from which it occurs. A streamer on the other hand extends many inches out on to the dielectric. This long discharge length causes the streamer to contain substantial low frequency energy.

Streamer noise spectra are given in Figure 5.9 (Reference 5-5) and a function of sample area. The noise spectra is proportional to area since the total charge stored and thus the discharge current is proportional to area.

## 5.5    COUPLING OF NOISE TO AIRCRAFT SYSTEMS

In general, noise sources on an aircraft are located in one place, and the affected antenna or system are located somewhere else. To calculate the interference to a system by a noise source, it is necessary to define the coupling between the source and problem system. Measurements have been made, for example, for a Boeing 707 and a helicopter. Using the measured coupling values, noise source spectra can be calculated and measured. Examples are shown in Figure 5.10 (Reference 5-3) for given source current levels. Note that both coronal and streamer noise levels are much larger than either daytiome or nighttime atmospheric noise levels. Note also that for the helicopter spectra, the low frequency streamer noise is a factor of two higher than the coronal noise.

## CHAPTER 5 REFERENCES

5-1.   Nanevicz, J. E., "Static Charging Effects on Avionic Systems", AGARD Lecture Series No. 110, 1980.

5-2.   Nanevicz, J. E.; Vance, E. F., "Studies of Supersonic Vehicle Electrification", Lightning and Static Electricity Conference, 1970.

5-3.   Nanevicz, J. E., "Static Electricity Phenomena: Theory and Problems", Conference on Certification of Aircraft for Lightning ad Atmospheric Electricity Hazards, ONERA - Chatillon, France, September 1978.

5-4.   Wallenberg, et. al., "Advanced Composite Aircraft Electromagnetic Design and Synthesis", Interim Report, Syracuse Research Corp., April 1980.

5-5.   Oh, L., G. C. Huang, R. Goldman, "Natural and Induced Electrical Effects on Integrated Antennas and Circuits at Frequencies to 10 GHz", AFAL-TR-69-210, September 1969.

PRECIPITATION PARTICLES

(a) FRICTIONAL

(b) ENGINE

(c) EXOGENOUS
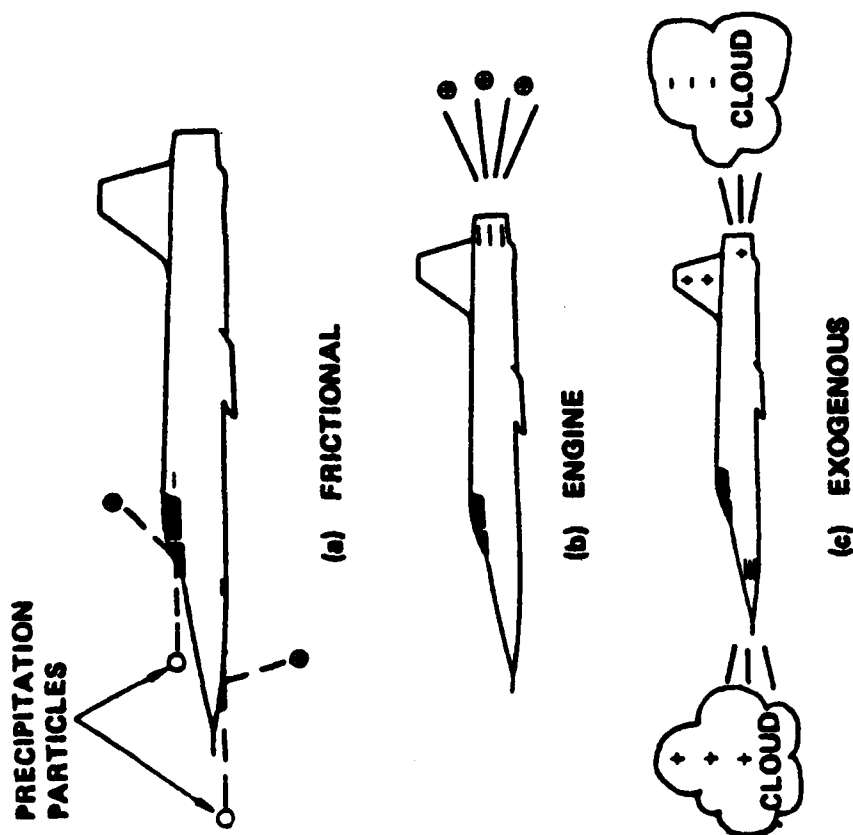
CLOUD

CLOUD

Figure 5.1

Charging Processes

INDUCTION PULSES
PRODUCED BY
CHARGED PARTICLES
PASSING ANTENNA

CORONA
DISCHARGES
FROM
EXTREMITIES

STREAMERS ON
INSULATING
SURFACES

SPARKS BETWEEN
UNBONDED METAL
SECTIONS
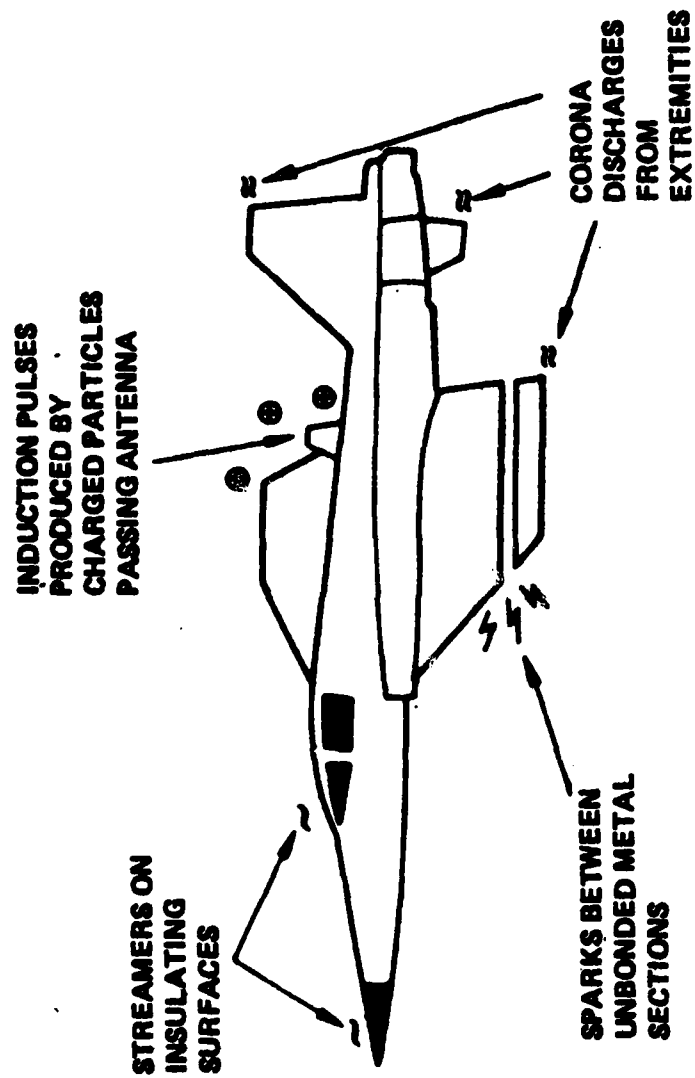
Figure 5.2
Noise Generation Sources
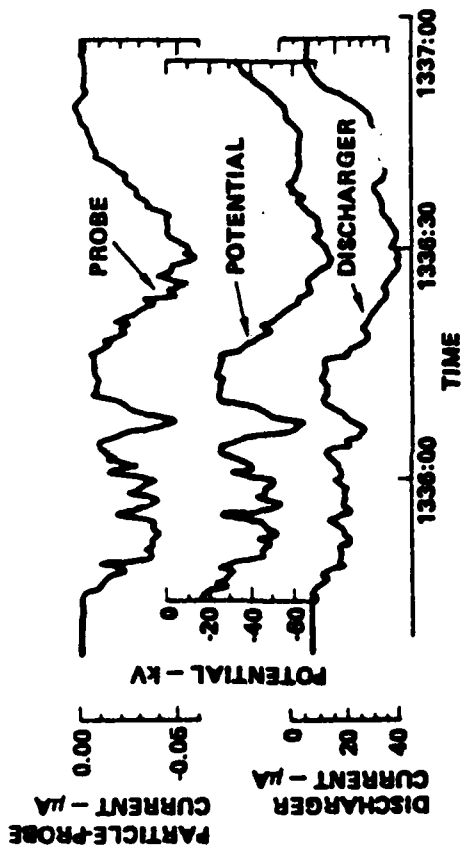
PRECIPITATION-CHARGING OF JET FIGHTER
AIRCRAFT IN FLIGHT THROUGH CIRRUS CLOUD
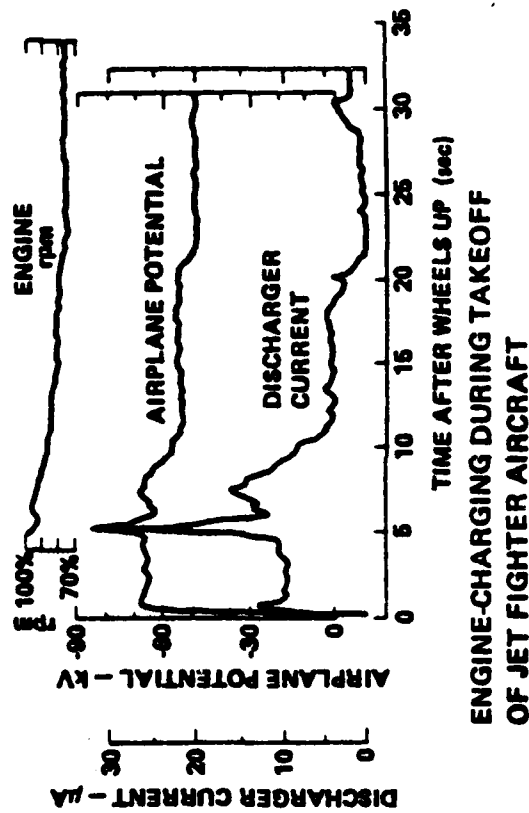
ENGINE-CHARGING DURING TAKEOFF
OF JET FIGHTER AIRCRAFT

Figure 5.3

P-Static Charging

96
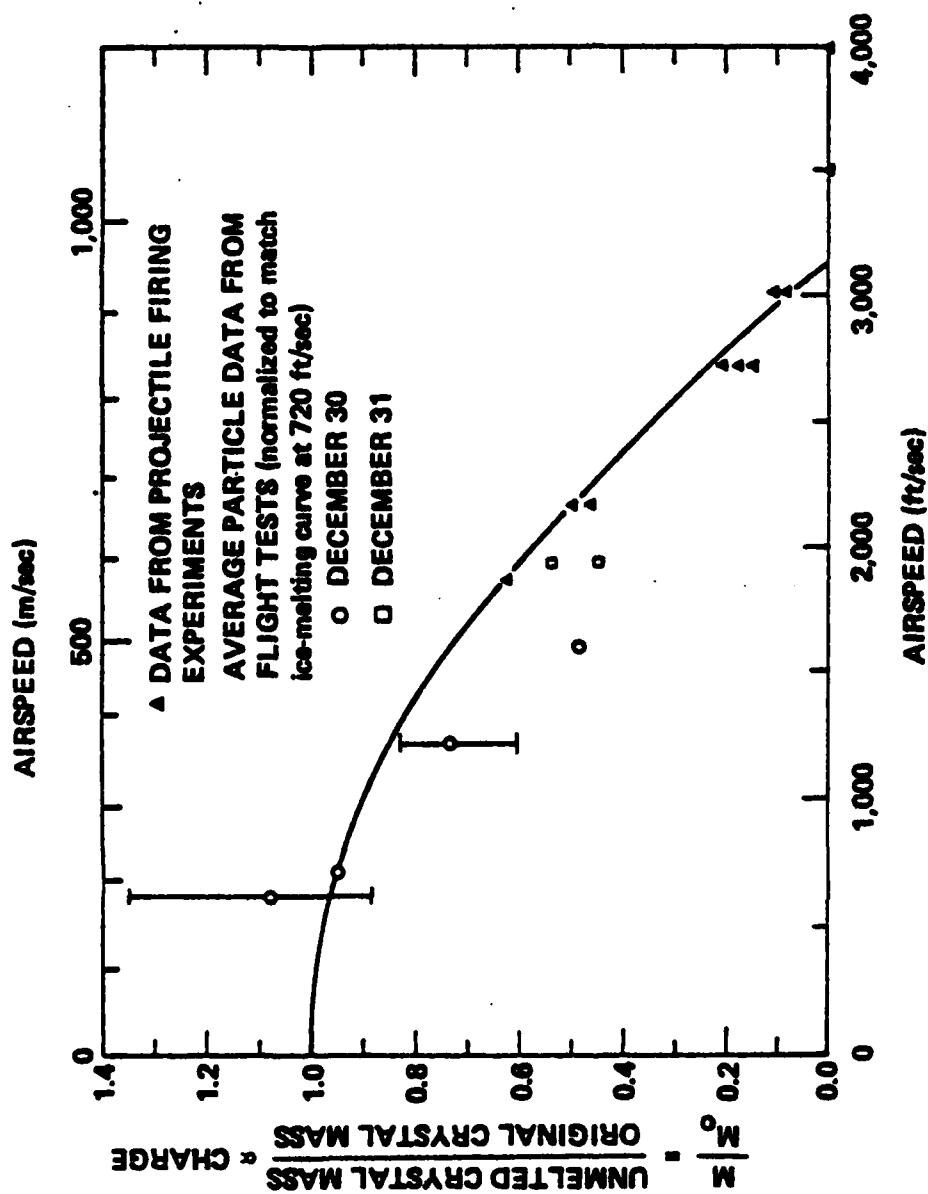
Figure 5.4

Variation of Particle Charge with Speed
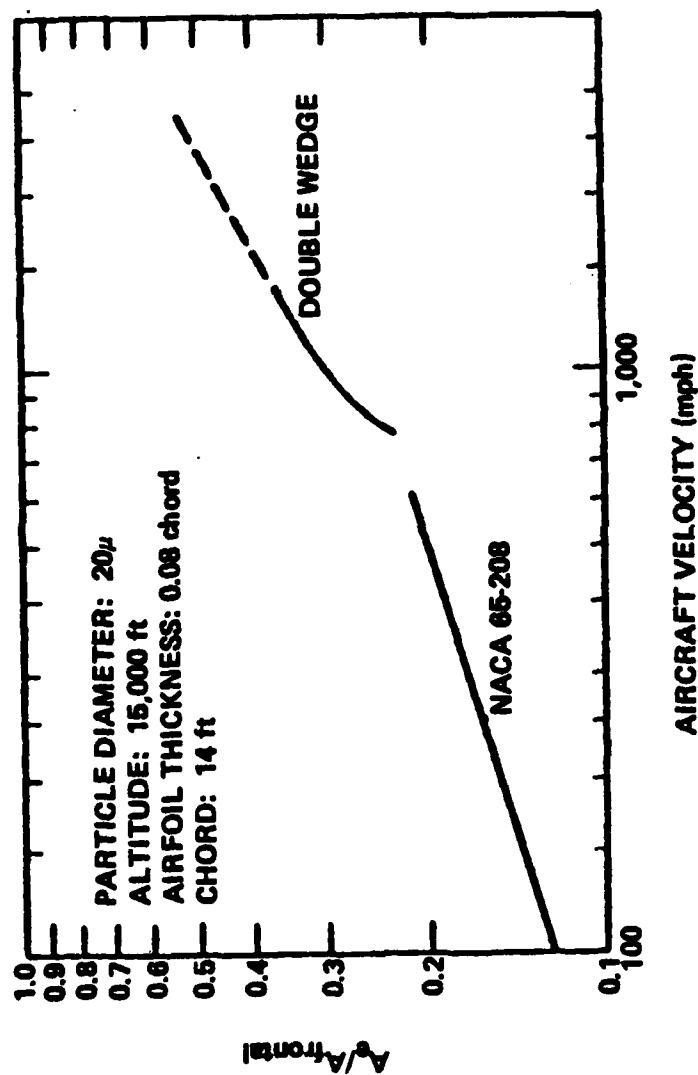
Figure 5.5

Advanced Aircraft Effect Intercepting Area
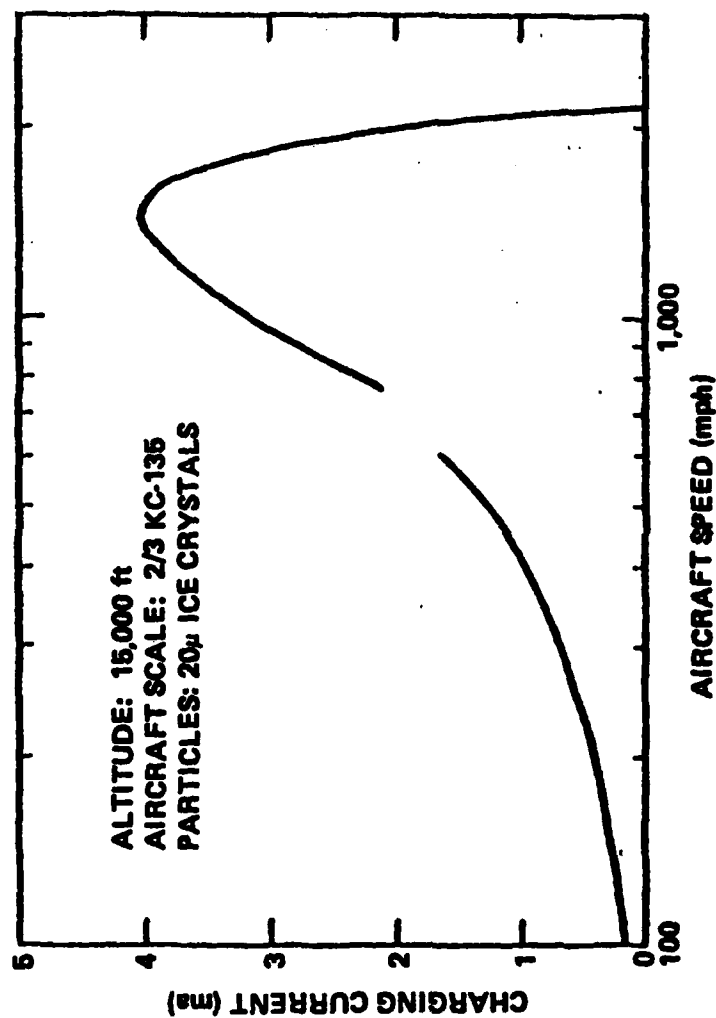
Figure 5.6

Predicted Charging Current for Advanced Aircraft
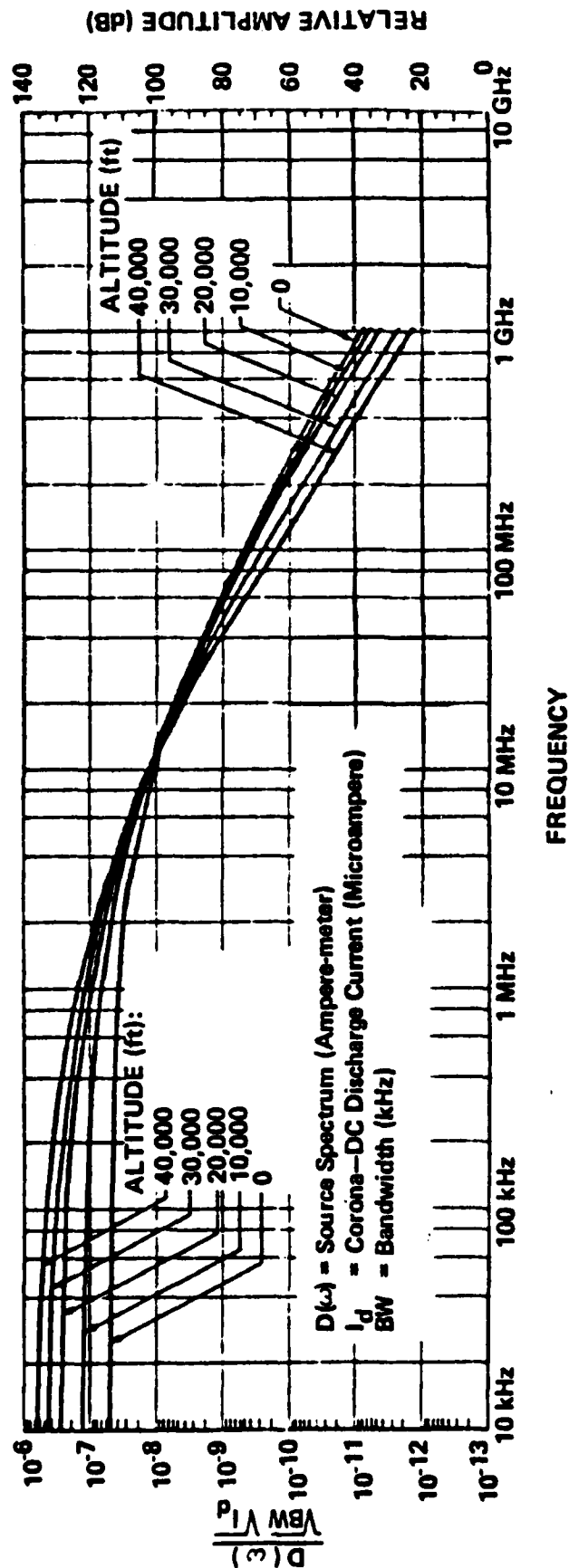
Figure 5.7

Measured Corona Noise Spectra
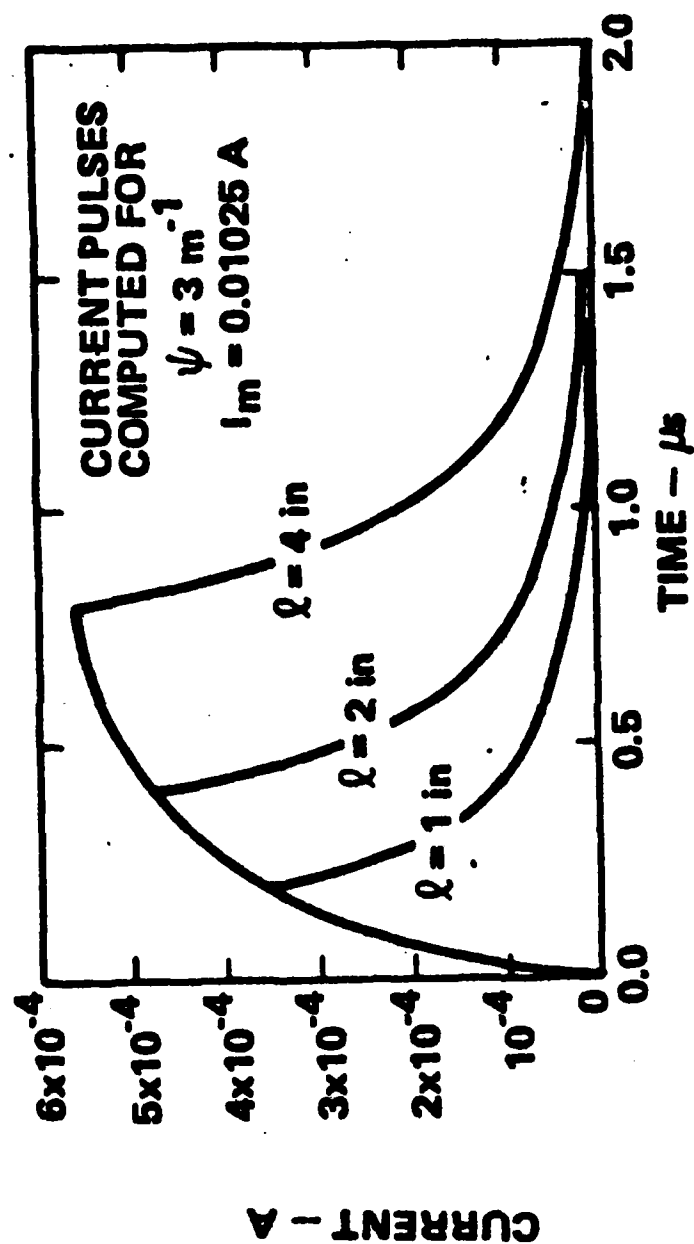
Figure 5.8

Typical Current Pulses Induced by Streamer Discharges
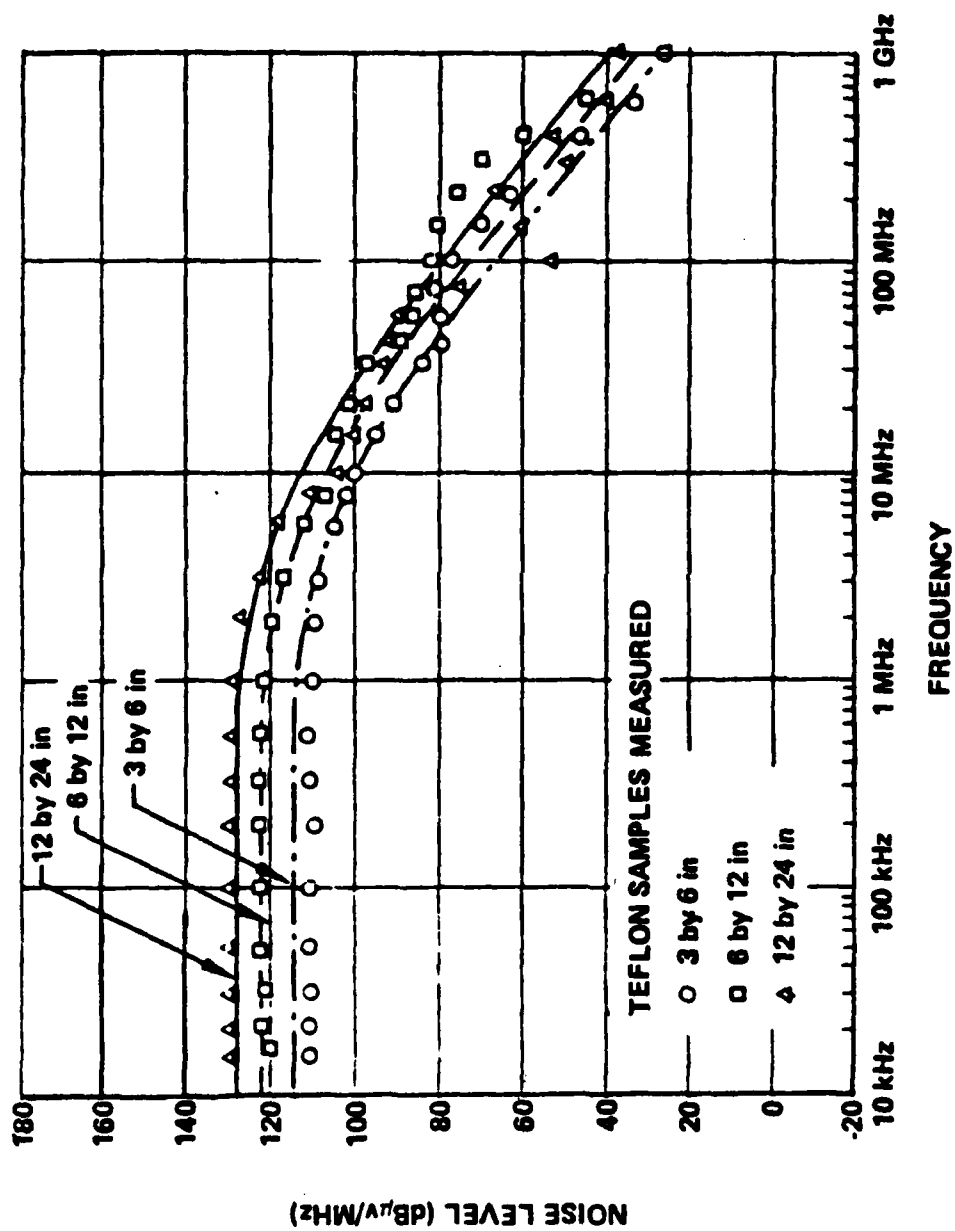
Figure 5.9

Streamer Noise Spectra – Measured and Calculated
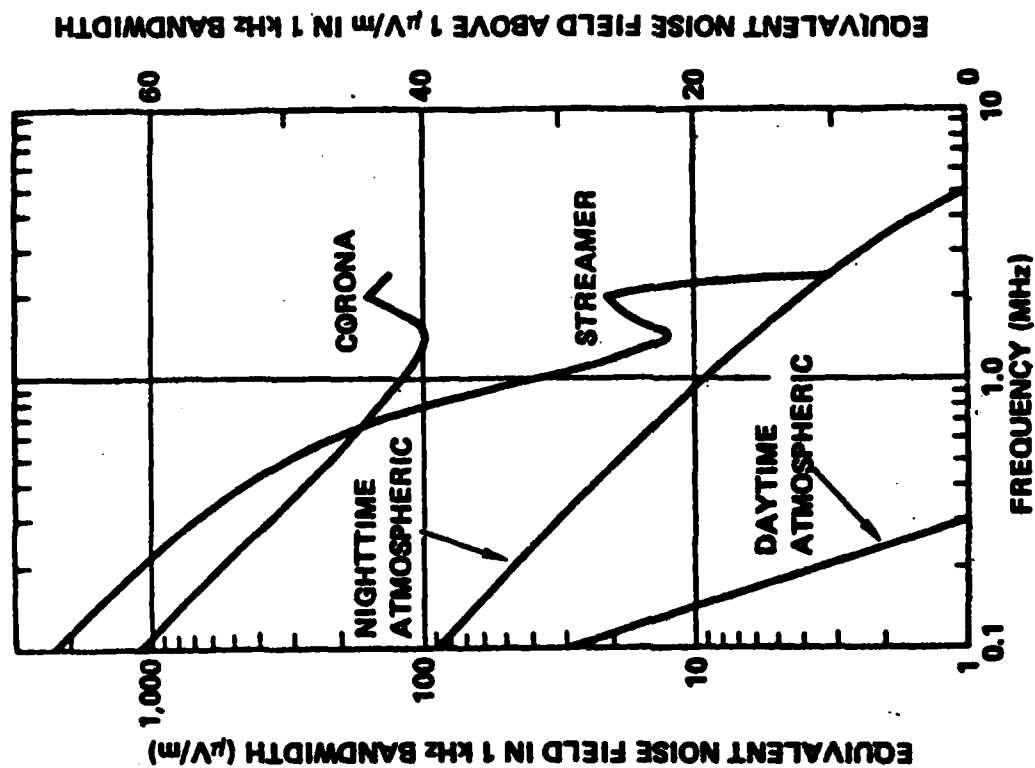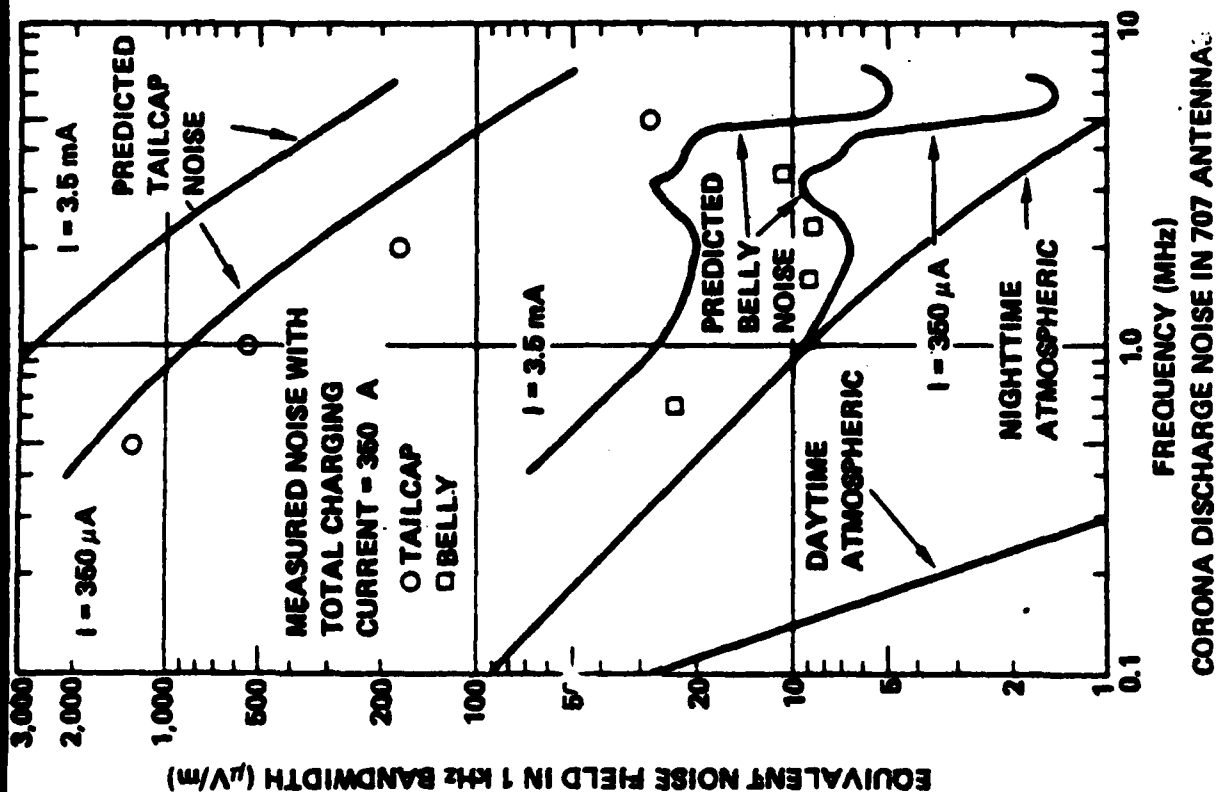
Figure 5.10

Measured Coronal and Streamer Noise

# 6.0 PARAMETRIC THREAT LEVELS

The threat levels presented to aircraft by both lightning and static electricity are presented here. The lightning threat levels are presented for both attached and nearby strokes from statistical ground based current measurements. Static electricity threat levels include corona and streamer time waveforms and frequency spectra. The threat variation with altitude, velocity, etc. is also presented.

## 6.1 LIGHTNING

Lightning may be a single or multiple stroke event either cloud to cloud or cloud to ground. Cloud to ground statistics are used to parameterize the ground lightning threat. Multiple stroke threat characteristics are shown in Figure 6.1. The number of strokes and the total length of an event determines how long a system may be inoperable. The magnitude of the strokes determine whether a system can recover.

Current measurements on single strokes were accumulated by Berger (Reference 6-1) and Garbagnati (Reference 6-2). Statistical results are shown in Tables 6.1 and 6.2. The results show mean values (50%) and upper and lower 1% levels for all parameters listed. The results are almost identical. Both results were obtained on nearby mountain tops so the correlation is a good check on the consistency of the measurements. Debate about whether this data represents "typical" lightning is still ongoing.

### TABLE 6.1
### BERGER (NEGATIVE STROKES)

|                              | 99%            | 50%          | 1%              |
|------------------------------|----------------|--------------|-----------------|
| MAXIMUM RISE RATE (KA/$\mu$s) | 8              | 40           | 200             |
| MAXIMUM AMPLITUDE (KA)        | 9              | 30           | 120             |
| RISE TIME ($\mu$s)            | 0.11           | 1.1          | 9               |
| FALL TIME TO HALF PEAK ($\mu$s) | 20           | 80           | 300             |
| ACTION INTEGRAL ($A^2$-s)     | $2.2 \times 10^3$ | $6 \times 10^4$ | $1.5 \times 10^6$ |

## TABLE 6.2
## GARBAGNATI (NEGATIVE STROKES)

| | 99% | 50% | 1% |
|---|---|---|---|
| MAXIMUM RISE RATE (kA/$\mu$s) | 6 | 40 | 220 |
| MAXIMUM AMPLITUDE (kA) | 9 | 22 | 120 |
| RISE TIME ($\mu$s) | 0.13 | 1.2 | 7 |
| FALL TIME TO HALF PEAK ($\mu$s) | 20 | 95 | 300 |
| ACTION INTEGRAL (A$^2$-S) | $2.4 \times 10^3$ | $6 \times 10^4$ | $1.5E \times 10^6$ |

To obtain statistical bounds on the frequency spectra from this data, a double exponential waveform was fit to Berger's 1%, 50%, 99% levels. The fit was made to match maximum rise rate, maximum amplitude and action integrals. The parameters chosen and the resulting values for the remaining parameters (rise time and fall time) are shown in Table 6.3. The resulting current waveforms are plotted in Figure 6.2. The associated spectra are shown in Figure 6.3. Both the current levels for a direct attached lightning stroke and the associated magnetic field values are given. The threat of nearby lightning strokes comes from the EM fields. The magnetic field threat level for a nearby stroke (range = 50m) is shown in Figure 6.4 for the same waveforms given in Figure 6.2.

## TABLE 6.3
## DOUBLE EXPONENTIAL FIT TO BERGER'S (1975) STATISTICS

| PARAMETERS | LOWER 99% | 50% MEAN | UPPER 1% |
|---|---|---|---|
| $\alpha$ (sec$^{-1}$) | $2.3 \times 10^4$ | $7.9 \times 10^3$ | $5.2 \times 10^3$ |
| $\beta$ (sec$^{-1}$) | $8 \times 10^5$ | $1.3 \times 10^6$ | $1.6 \times 10^6$ |
| $I_0$ (kA) | 10. | 30.8 | 125. |
| MAXIMUM RISE RATE (kA/$\mu$s) | 8. | 40. | 200. |
| MAXIMUM AMPLITUDE (kA) | 9. | 30. | 122. |
| ACTION INTEGRAL (A$^2$-s) | $2.2 \times 10^3$ | $6 \times 10^4$ | $1.5 \times 10^6$ |
| RISE TIME ($\mu$s) | 4.4 | 3.9 | 3.6 |
| FALL TIME TO HALF PEAK ($\mu$s) | 37. | 90. | 140. |

The parametric range of the cloud to ground lightning threat is established by Figures 6.3 and 6.4. These give the statistical range of expected values between upper and lower 1% values and the mean values for both attached and nearby lightning.

## 6.2    STATIC ELECTRIFICATION

The parametric variation of corona and streamer noise threat levels depends on a wide range of variables. The threat levels depend on charging rates which in turn depend on surface area exposed on an aircraft, speed, altitude, and weather conditions. The exposure of an aircraft to this type of threat depends on the specific aircraft and its mission profile. Each aircraft's threat level will be different (References 6-3, 6-4).

Coronal threat levels are established by modeling individual pulses in a string of pulse discharges to obtain a noise spectrum normalized to charging rate (Figure 6.5) as a function of altitude (Reference 6-5).

Streamer threat levels depend on dielectric surface area over which charge is stored. Noise threat levels are presented as of function of surface area in Figure 6.6 (Reference 6-5).

# CHAPTER 6 REFERENCES

6-1.    Berger, K., Anderson, R. B., Kroninger, H., "Parameters of Lightning Flashes", Electra, 80, 23-37, 1975.

6-2.    Garbagnati, E., Lopipard, G. B., "Lightning Parameters - Results of 10 Years of Systematic Investigation in Italy", Proceedings of International Conference on Lightning and Static Electricity, Oxford, England, March 1982.

6-3.    Nanevicz, J. E., "Static Electricity Phenomena: Theory and Problems", Conference on Certification of Aircraft for Lightning and Atmospheric Electricity Hazards, ONERA - Chatillon, France, September 1978.

6-4.    Nanevicz, J. E., "Static Charging Effects on Avionic Systems", AGARD Lecture Series No. 110, 1980.

6-5.    Oh, L., G. C. Huang, R. Goldman, "Natural and Induced Electrical Effects on Integrated Antennas and Circuits at Frequencies to 10 GHz", AFAL-TR-69-210, September 1969.

| Variables | Range |
|-----------|-------|
| • Duration of induced transient | 50 - 500 μs |
| • Inter-stroke time interval | 10 - 100 ms |
| • Time duration of lightning event | 0.01 - 2 sec |
| • Number of strokes | 1 - 24 |

Figure 6.1
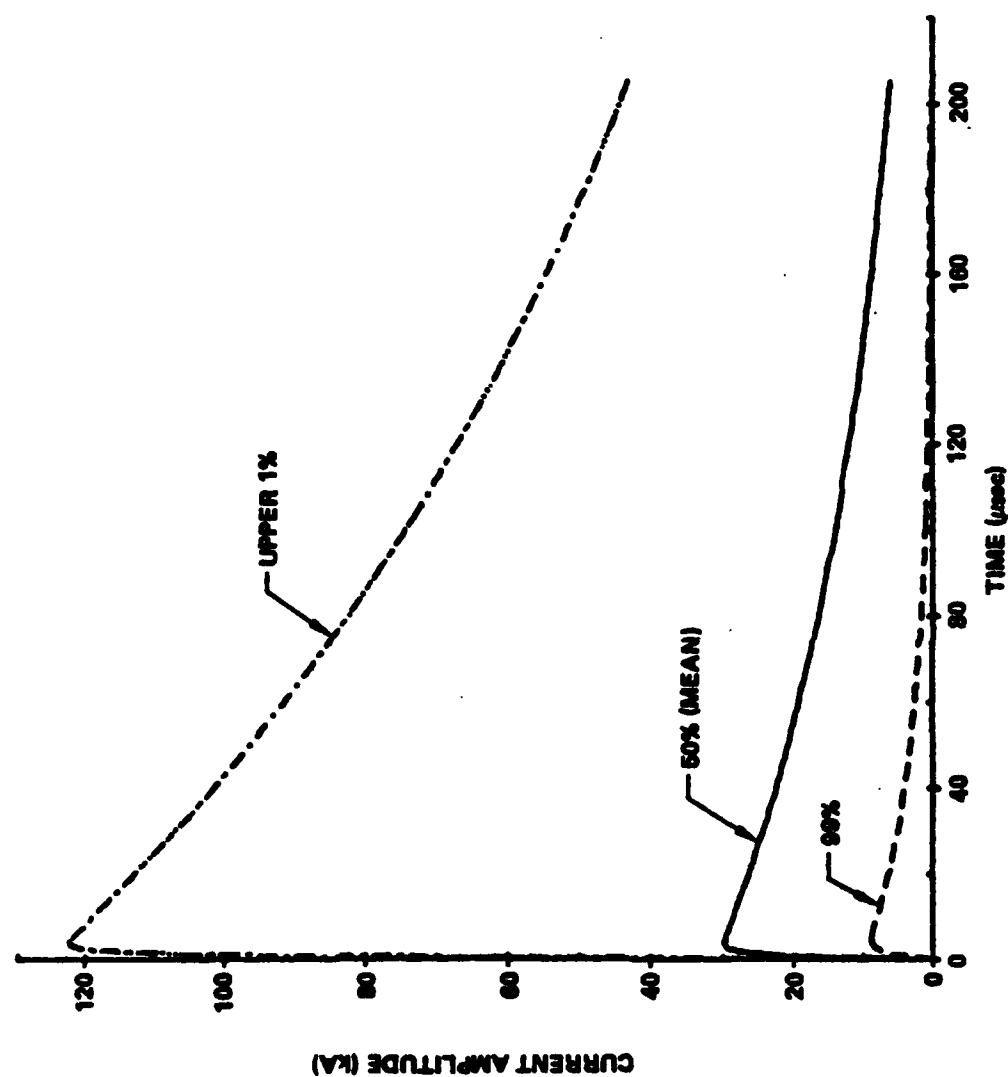Multi-Stroke Threat
(Non-Damage Effects)

Figure 6.2

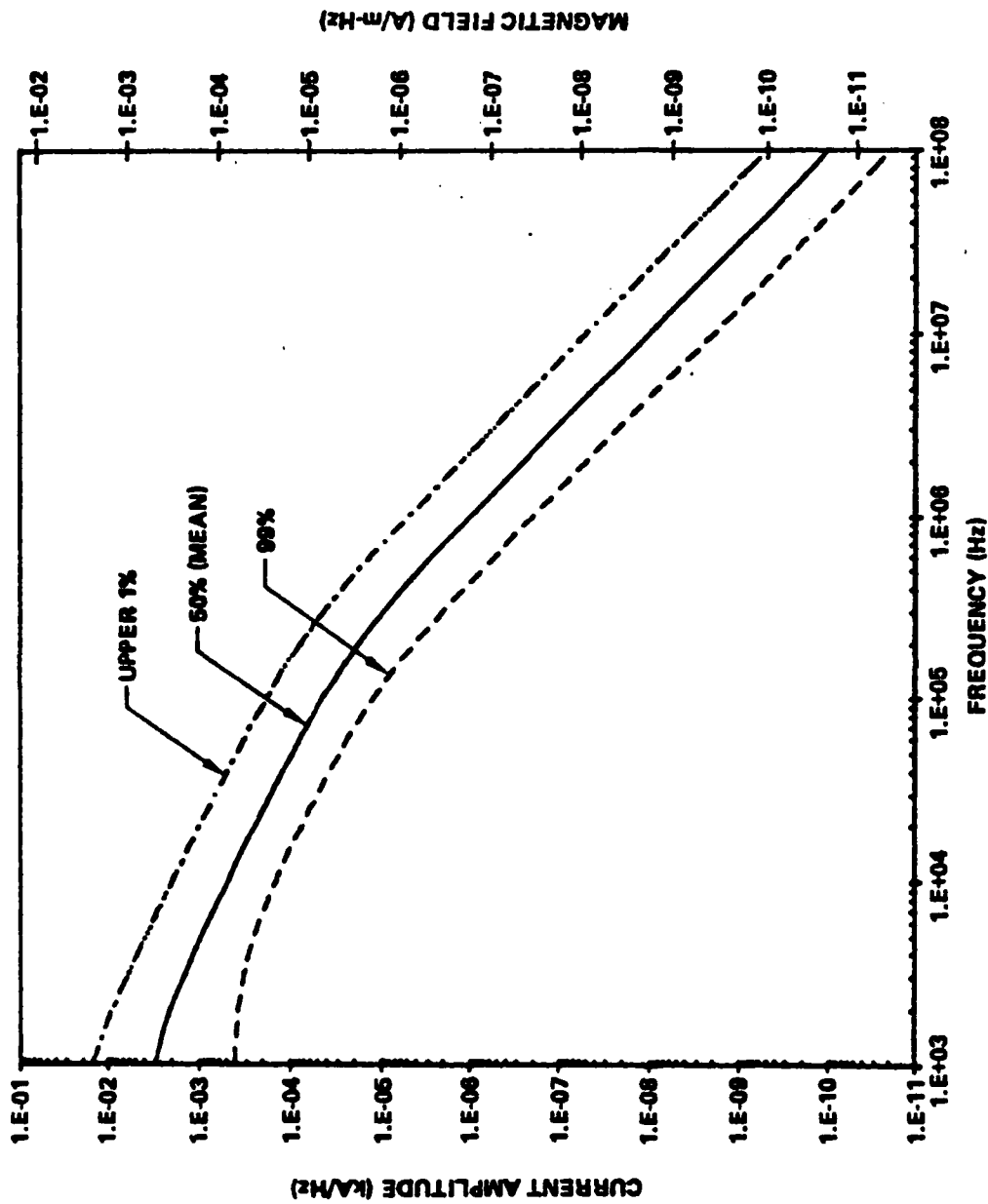Lightning Current Waveforms
– Mean and Upper and Lower 1% Values –

Figure 6.3

Attached Lightning Frequency Spectral Bounds
— Current Amplitude and Magnetic Fields —
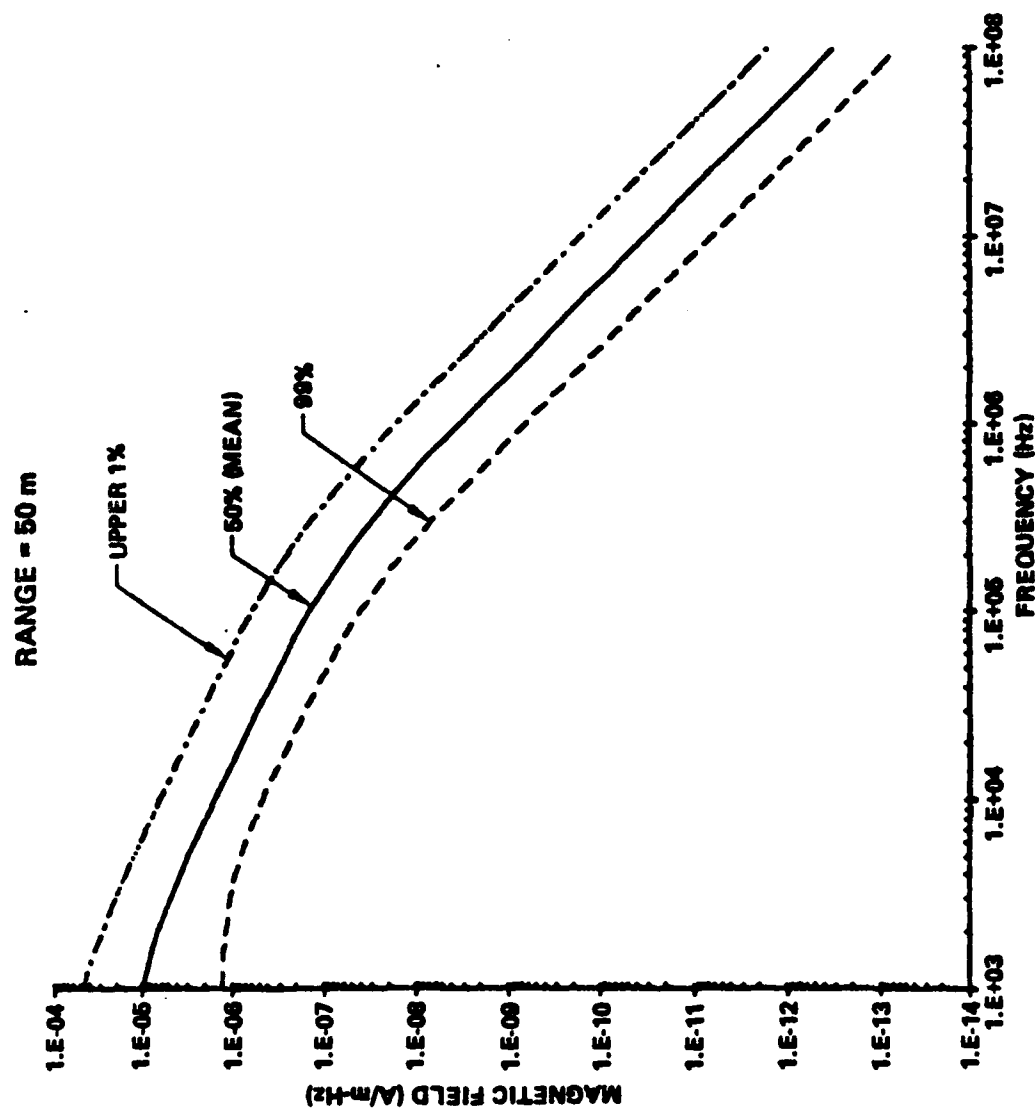
Figure 6.4
Nearby Lightning Magnetic Field
— Frequency Spectral Bounds —
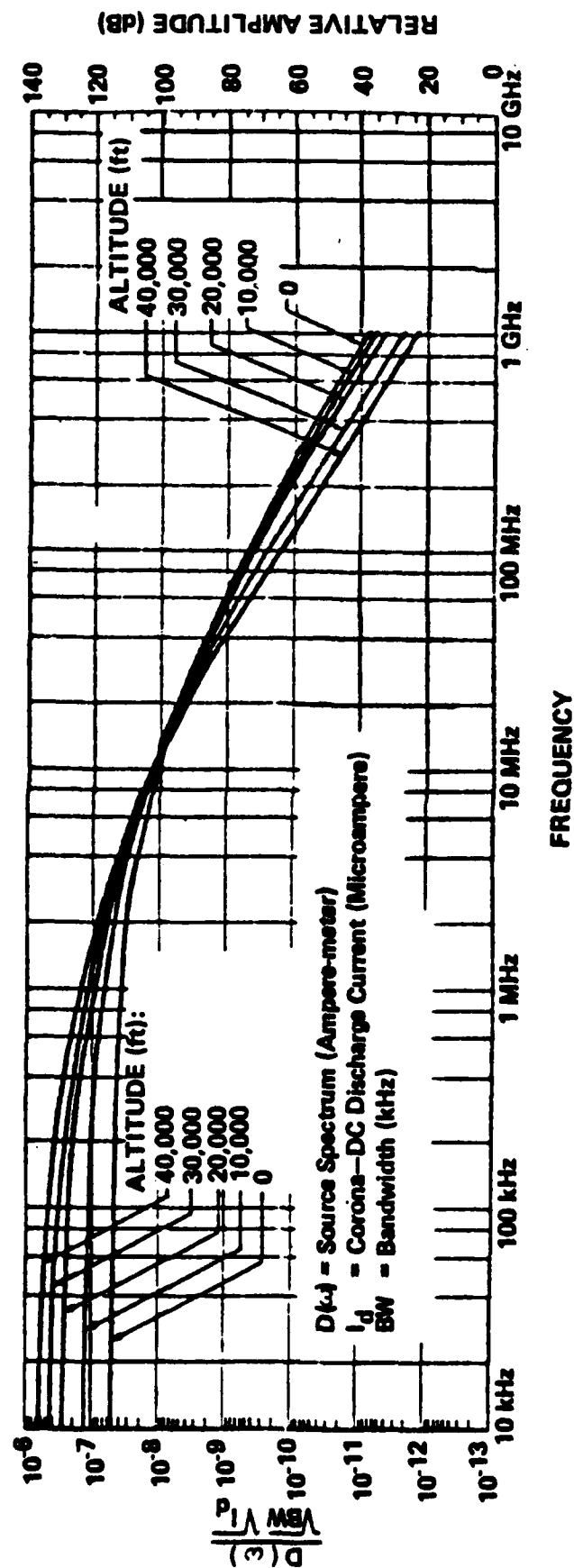
Figure 6.5
Measured Corona Noise Spectra
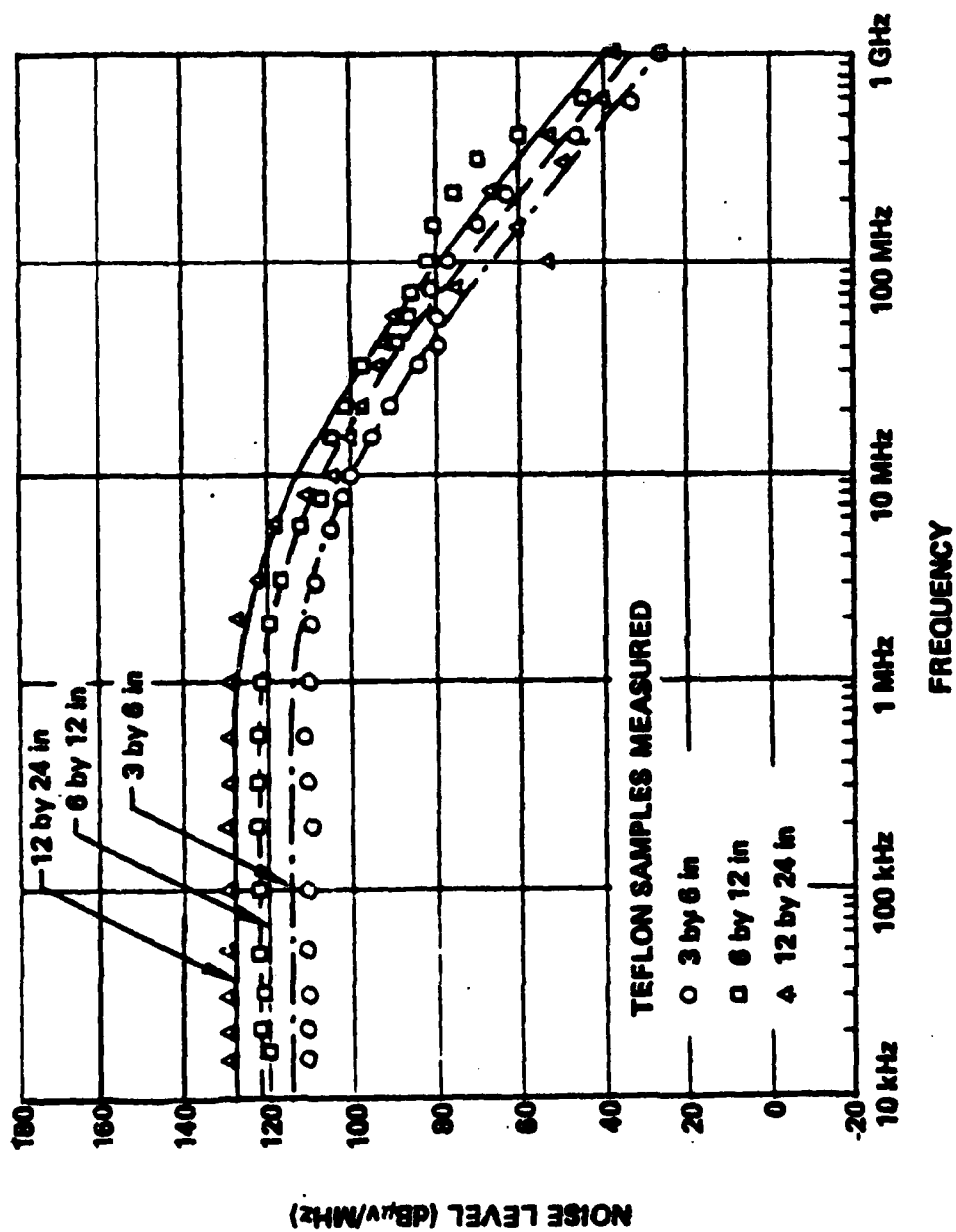
Figure 6.6

Streamer Noise Spectra – Measured and Calculated

113

# 7.0 METEROLOGICAL PHENOMENON

Operating an aircraft in all kind of weather exposes it to atmospheric electricity (AE) threats. Probability of aircraft exposure to AE threats must be calculated for various segments of a mission (e.g. climb, cruise, descent). The probability of exposure coupled with the probability of the severity of exposure determine the protection level necessary for individual vehicles.

Probability of a lightning strike to an aircraft is dependent on many variables. Included are such items as geographic, monthly, daily and height variations in the lightning flash density per area per unit of time. Also important is the aircraft's effective cross section in attracting lightning strikes. The probability of a strike can be calculated by using the type of formula as follows

$$P_s = (F) (N) (A\alpha) (f_{diurnal}) (f_{month}) (f_{altitude}) (f_{geographic}) \qquad (9)$$

$P_s$ = lightning strike probability per hour of flight time
$F$ = lightning flash rate density (flashes/hr/km$^2$)
$N$ = Number of strokes per flash
$A$ = effective cross section of aircraft in attracting lightning (km$^2$)
$f_{month}$ = monthly dependence of flash rate
$f_{diurnal}$ = daily dependence
$f_{altitude}$ = altitude variation
$f_{geographic}$ = geographic effect.

Each factor determining $P_s$ will be discussed separately in the sections below.

## 7.1 LIGHTNING FLASH RATE DENSITY

The historically and internationally accepted parameter of lightning incidence is the thunderstorm day (i.e. a day on which thunder is heard at a recording station) (Reference 7.1). Isobront maps (e.g. Figure 7.1) show areas of differing levels of thunderstorm incidence. Generally the highest incidence

of thunderstorms is near the equator and lowest near the pole. However, Figure 7.1 of the United States shows that large regional variations exist. Limitations of thunderstorm day data are that neither storm duration or severity is taken into account. These factors influence the flash rate which is the parameter of principle interest in any threat scenario. Information on the frequency of lightning flash occurrence only exists in regions where thunderstorm research programs exist. Relating discharge frequency to thunderstorm days has been done for various regions. Results are given in Table 7.1.

Examples of ground flash rate densities are given in Tables 7.2-4 for various measurement techniques. The highest density rate from any of these tables is 12 flashes/km$^2$/yr seen in Table 7.3 in Singapore and in Table 7.4 in the U.S. Recently, Maier and Piotrowitz (Reference 7.2) report maximum annual ground flash densities of 18 flashes/km$^2$ in western Florida. Other regions of the U.S. were reported to have smaller flash rate densities.

Cloud flash incidence must also be quantified. Cloud flashes are generally harder to see visually or photographically. Also, a large number of flashes cannot be classified as cloud or cloud-to-ground from visual observations. Table 7.5 shows various measurements of cloud to cloud-to-ground flashes (last column). The data ranges from 0.9 to 9.5. The scatter is due largely, to the problems cited above. Prentice and Mackerras (Ref. 7.3) have developed rough mean values for various latitude ranges taken from twenty-nine sources. Table 7.6 shows the calculated values.

## TABLE 7.6

| Latitude Range | Average ratio of cloud to cloud-to-ground flashes |
|---|---|
| $2^0$-$19^0$ | 5.7 |
| $27^0$-$37^0$ | 3.6 |
| $43^0$-$50^0$ | 2.9 |
| $52^0$-$69^0$ | 1.8 |

The values have a wide scatter and are from relatively few measurement

115

stations.  More recent data from the National Severe Storm Laboratory in Oklahoma (Reference 7.9) has shown ratios as high as 40:1 for cloud vs cloud-to-ground.  Additional data on relative occurence of cloud to cloud-to-ground flashes is needed to more accurately define this ratio.

Each flash is made up of a number of strokes which occur very close together in time.  For cloud-to-ground flashes, interstroke time intervals range from 10 to 100 ms (Reference 7.4).  Cloud flashes can have much shorter interstroke time intevals of 0.1 to 1.0 ms.  Thomson (Reference 7.4) has statistically analyzed ground flashes from a large number of workers worldwide.  The maximum number of strokes per ground flash is about 4.2 at the 50% level and up to 16 strokes/flash at the upper 1% level.  This is compared to an upper flash rate for cloud events seen on aircraft of $10^3$ strokes/flash (Reference 7.5) and $10^4$ strokes/flash (Reference 7.6).

## 7.2 MONTHLY VARIATION

Variation of monthly lightning activity is dependent on latitude.  In temperate climates, the maximum occurs in mid-summer with some activity occasionally in mid-winter (Reference 7.1).  In subtropical thunderstorms, large activity is seen only in summer.  Large summer activity is seen in Table 7.6 of data taken at Kennedy Space Center in Florida and in Table 7.7 from Brisbane, Australia.  In the tropics several patterns have been observed, non consistent.  Since large variations in lightning incidence exist year to year, long term averages of these parameters must be developed to obtain reliable statistics on risk factors.

## 7.3 DIURNAL CHANGES

Diurnal variations in lightning flashes are fairly well established.  The maximum flashing rate occurs in the late afternoon and evening with a minimum about 10 hours earlier.  The peak hours of activity and amplitude of variation vary with location and month.  Examples taken from Reference 7.7 are shown in Figure 7.3.  A ten year study in Brisbane by Mackerras (Ref. 7.8) concluded a maximum activity ocurred between 1900 and 2000 hours with the hours earlier in the winter and later in the summer.

## 7.4 ALTITUDE STATISTICS

Aircraft lightning strike incidents plotted as a functions of altitude were published in 1977 (Ref 7-9). The strike rate plotted in Figure 7.4 for routine aircraft operations show a peak rate near 3-4 km altitude. This was the only data available until recently.

During the last several years research from the National Severe Storms Laboratory (Reference 7.10) has shown two centers of lightning activity from VHF studies of thunderstorms that are separated in altitude. The lower maximum is about 5 km in altitude which agrees with the previous data while the upper center is about 12 km. Altitude distributions for one set of storms is shown in Figure 7.5. Major flashes are defined in this study as those with greater than 30 VHF signals at each station. All minor flashes (those with less than 30 VHF signals) were thought to be cloud flashes.

The upper altitude maximum of lightning activity is consistent with the findings of NASA's F106-B flight program (Reference 7.11). Flying at lower altitudes resulted in few direct strikes to the aircraft. Strikes were only obtained by flying higher, from 8 to 12 km with a maximum number of strikes per thunderstorm penetration at 11 km seen in Figure 7.6.

The reason behind NASA's difficulty in getting struck at lower altitudes while being hit often higher up is not well understood. One strong possibility is that at lower altitudes the aircraft must be near developing leaders or run into a developed channel. At upper altitudes the aircraft may be closer to the charge centers in the clouds and actually trigger a direct lightning strike.

## 7.5    GEOGRAPHIC EFFECTS

Lightning flash rates have been observed to vary greatly between various regions of the world. An example of the great variation in thunderstorm days across the U.S. is seen in Figure 7.1. High frequencies of thunderstorms are seen in Florida and in Wyoming and Colorado. Low incidence rate is seen on the west coast, for example. Worldwide, the trend is generally a decrease in thunderstorm activity away from the equator.

117

Attempts have been made to correlate lightnings flash rate parameters with latitude. Pierce (Reference 7.12) has represented the latitudinal variation of the proportion of discharges that go to ground (p) as

$$P = \frac{N_g}{N_c} = 0.1 \left[1 + (\lambda/30)^2\right] \tag{10}$$

Where $N_g$ = number of discharges to ground, $N_c$ = number of cloud discharges. More recently Prentice and Mackerras (Ref 7.3) have developed the following empirical relation from data from 13 countries.

$$\frac{N_c}{N_g} = 4.11 + 2.11 \text{ COS } 3\,\lambda \quad (0<\lambda<60^o) \tag{11}$$

Thomson (Ref 7.4) has recently studied interstroke time intervals and the number of strokes per flash to discover any systematic latitudinal variations. His conclusions were that only interstrokes times showed any latitude dependencies but only at tropical latitudes.

Generally the regional variations in thunderstorm severity seem to be much more evident than global trends, at least for thunderstorm parameters measured to date.

7.6 OTHER PARAMETERS

The problem of aircraft avoiding lightning is dependent on the knowledge of all variables that correlate with lightning activity. Not all of these parameters are known. Studies by the NASA F106B and NSSL show much more needs to be understood to predict lightning strikes to aircraft. NASA's experience with the F106B showed that the highest strike rate occurred for temperatures of $-40^o$ to $-50^oC$ as seen in Figure 7.6 (Ref 7.11). They also occurred near 11 km in altitude (Figure 7.7). Strikes tended to occur for all turbulence and precipitation intensities but generally more strikes were seen in low turbulence and low precipitation areas (see Figure 7.8).

NSSL in coordination with the NASA F106 also compiled parameters related to direct strikes using the UHF radar at Wallops Island (Reference 7.13). Their data also showed high correlation of direct strikes to the F106 at low temperatures ($-40^{\circ}$C or less) (Figure 7.9), low turbulence levels (Figure 7.10), some correlation to light precipitation (Figure 7.11), and to low lightning flash rates (Figure 7.12). This last correlation is very unexpected. The reason for low numbers of direct hits with high flash rates nearby is unknown. Speculation is that it is related somehow to the triggering mechanism of cloud-aircraft lightning.

Other parameters may also be important in studying direct strikes to aircraft. One parameter not mentioned yet is aircraft size, shape and material. The effects of these parameters is not known. A volume effect is suspected i.e. larger aircraft are assumed to "attract" lightning from a larger volume of space. Shape factors may assume a role in triggered lightning. Certainly attachment points are effected by shape. Material effects are also unknown. Tests by Grumman (Ref 7-14) and McDonnell Douglas (Ref 7-15) on graphite composite have shown little difference in attachment points relative to aluminum. However, the effect on lightning strikes is unknown.

Our knowledge of the mechanism of lightning occurring within storm systems is still in its infancy and must progress much further before we can be reasonably certain of all the parameters effecting direct strikes to aircraft.

## 7.7 STRIKE PROBABILITY TO AIRCRAFT

The probability of lightning striking an aircraft depends on the type of aircraft and its mission profile. For example, a fighter may climb quickly to high altitudes, cruise for several hundred miles, then descend to low altitude near its destination. The total strike probability is governed by the time the aircraft spends at different altitudes and weather conditions. The probability is also effected by the aircraft size, the time of year at which the aircraft is flying, the time of day and the regional area through which it is moving. These parameters were discussed in sections 7.2-6.

The total probability of a strike to an aircraft can be calculated from the following equation:

$$P_{Total} = \frac{\sum_i p_i t_i}{\sum_i t_i} \qquad (12)$$

where $P_{Total}$ = total probability of direct strike

   $P_i$ = probability of strike under different conditions
       (weather, region, time of day etc.)

   $t_i$ = time spent under above conditions

Considering only altitude variations, the aircraft is considered under the cloud-to-ground lightning threat below 20,000 feet and under the cloud lightning threat above that level. Therefore, equation 12 becomes simply

$$P_{Total} = \frac{Pc\text{-}g \, t_{low} + Pc\text{-}c \, t_{high}}{t_{low} + t_{high}} \qquad (13)$$

where     $Pc\text{-}g$ = probability of cloud-to-ground lightning strike

   $Pc\text{-}c$ = probability of cloud-to-ground lightning strike

   $t_{low}$ = time spent at low altitud. (<20,000 ft)

   $t_{high}$ = time spent at high altitude (>2000 ft)

Missiles and helecopters spend all their time at low altitude and so are only effected by cloud-to-ground lightning. Fighters and transports which spend most of their time at high altitude are effected mostly by cloud-to-cloud lightning. This is reinterated in Table 7.9.

TABLE 7.9

Approximate Strike Probability

| Fighter | Missile | Transport | Helicopter |
|---------|---------|-----------|------------|
| Pc-c | Pc-g | Pc-c | Pc-g |

Note that Pc-g and Pc-c are assumed to include all the factors listed in equation 9 , i.e statistics on the type of lightning, aircraft size, monthly, daily, altitude and geographic dependences for that specific type of lightning.

# CHAPTER 7 REFERENCES

7-1.    Golde, R. H.; ed; "Lightning, Vol I: Physics of Lightning", Academic Press, 1977.

7-2.    Maier,, M.W., Piotrowicz, J. M.; "Improved Estimates of the Area Density of Cloud-to-Ground Lightning Over the United States"; Int. Conf. on Lightning and Static Electricity, Fort Worth, Texas, June 1983.

7-3.    Prentice, S.A.; Mackerras, D., "The Ratio of Cloud-to-Ground Lightning Flashes in Thunderstorms", J. of Ap. Met; 16, 545-550, May 1977.

7-4.    Thomson, E.M.; "The Dependence of Lightning Return Stroke Characteristics on Latitude", JGR, 85, 1050-1056, Feb. 1980.

7-5.    Trost, T.F.; Pitts, F.L.; "Analysis of Electromagnetic Fields on an F106B Aircraft During Lightning Studies"; Int. Conf on Lightning and Static E' ctricity, Oxford, England, March 1982.

7-6.    Rustan, P.L.; Kuhlman, B.; Showalter, J.; Reazer, J.; "Electromagnetic Measurements of Lightning Attachment to Aircraft"; Int. Conf. on Lightning and Static Electricity; Fort Worth, Texas, June 1983.

7-7.    Cianos, N.; Pierce, E.T.; "A Ground Lightning Environment for Engineering Usage", SRI Tech. Report No. 1, Project 1834, August 1972.

7-8.    Mackerras, D.; "Lightning Occurence in a Subtropical Area", in "Proceedings of the Garmisch Conference", H. Dolezalek, R. Reiter, eds; Dietrich Steinkopff Verlag, Darmstadt, 1976.

7-9.    Fisher, F.A.; Plumer, J.A.; "Lightning Protection of Aircraft"; NASA RP-1008, 1977.

7-10    Rust, W.D.; MacGorman, D.R.; Brandes, E.S.; Mazur, V.; Arnold, R.; Marshall, T.; Christian, H.; Goodman, S.J.; "Lightning and Related Phenomena in Thunderstorms and Squall Lines", AIAA 22nd Aerospace Science Meeting, Reno, Nevada, Jan 1984.

7-11    Fisher, B.D.; Plumer, J.A.; "Lightning Attachment Patterns and Flight Conditions Experienced by the NASA F-106B Airplane from 1980-1983", AIAA 22nd Aerospace Science Meeting, Reno, Nevada, Jan 1984.

7-12    Pierce, E.T.; "Latitudinal Variation of Lightning Parameters", Vol 9, 194-195, 1970.

7-13    Mazur, V.; Fisher, B.D.; Gerlach, J.C.; "Conditions for Lightning Strikes to an Airplane in a Thunderstorm"; AIAA 22nd Aerospace Science Meeting, Reno, Nevada, Jan. 1984.

7-14    Craft, W.L., "Protection Optimization for Advanced Composite Structures," Grumman Aerospace Corporation, February 1981.

7-15    McBrayer, P.R., Shouby, C.D., Weinstock, G.L., "Lightning Attachment Characteristics for Metal/Composite Materials," IEEE EMC Conf., 1977.

# Table 7.1
# Empirical Relationships Between Lightning Flash Density and Annual Thunderdays

| Country | Ground-flash density $(km^{-2} yr^{-1})$ | Reference |
|---|---|---|
| India | 0.1T | Aiya (1968) |
| Rhodesia | 0.14T | Anderson and Jenner (1954) |
| Sweden | $0.004T^2$ (approx) | Müller-Hillebrand (1964) |
| U.K. | $\alpha T^b$ | Stringfellow (1974) $[\alpha = 2.6 \pm 0.2) \times 10^{-3}; b = 1.9 \pm 0.1]$ |
| U.S.A. (North) | 0.11T | Horn and Ramsey (1951) |
| U.S.A. (South) | 0.17T | Horn and Ramsey (1951) |
| U.S.A. | 0.1T | Anderson et al. (1968) |
| U.S.A. | 0.15T | Brown and Whitehead (1969) |
| U.S.S.R. | $0.036T^{1.3}$ | Kolokolov and Pavlova (1972) |
|  | $0.1T^{1.3*}$ | Kolokolov and Pavlova (1972) |
| World (temperate climate) | 0.19T | Brooks (1950) |
| World (temperate climate) | 0.15T | Golde (1966) |
| World (tropical climate) | 0.13T | Brooks (1950) |
| World | 0.25.* | Pierce (1966) |

*Total flash density

Ref: from Golde, 1977.

123

## Table 7.2
## Frequency of Occurrence of Ground Flashes (Visual/Optical Methods)

| Country | Regional annual thunderdays | Observations | | Ground-flash density ($km^{-2} yr^{-1}$) | Reference |
|---|---|---|---|---|---|
| | | Number of years | Radius (km) | | |
| Australia | 30 | 10 | 20 | 1.2 | Mackerras (1976) |
| East Germany | 21 | 11 | – | 0.8 (min) | Fritsch (1943) |
| South Africa | 55 | – | – | 7.7 | Schonland (1964) |
| Switzerland | 51 | 10 | 2.5 | 4 (approx) | Berger (1967) |
| U.K. | 12 | 17 | 0.03 | 2.3 | Golde (1945a) |
| U.K. | – | 9 | 2 | 0.1 | Ashmore (1945) |
| U.S.A. | 33 | 2 | 4.8 | 1.4 | Hagenguth (1947)* |
| U.S.A. | 11 to 40 | 9 to 19 | 30 | 0.4 to 2.3 | Fuquay (private communication) |
| U.S.S.R. | 20 | 7 | 5.0 | 2.8 | Kuliev (1968) |
| West Germany | 19 | 20 | – | 0.7 (min) | Walter (1933) |

*With data from Golde (1961).

Ref: from Golde, 1977.

## Table 7.3

## Frequency of Occurrence of Ground Flashes (Recordings)

| Country | Regional annual thunder-days | Observations | | | Ground-flash density ($km^{-2}\ yr^{-1}$) | Reference |
|---|---|---|---|---|---|---|
| | | Method | Number of years | Radius (km) | | |
| Australia | 5 to 107 | C | 3 to 5 | 30 | 0.2 to 3.9 | Prentice (1974) |
| Canada | 26 | C | 5 | 19 | 1 (min) | Ellis and Linck (1958) |
| Central Africa | 79 | C | 6 | 30 | 3.4 | Jenner (private communication) |
| Finland | 17 | C | 14 | 17[a] | 1.5 | Laitinen (private communication) |
| Norway | 8 | C | 4 | 12.5 | 0.4 | Müller-Hillebrand et al. (1965) |
| Singapore | 171 | C | – | 30 | 12 | Horner (private communication) |
| South Africa | 73 | C | 7 | 36 | 6.5 | Anderson et al. (1975) |
| Sweden | 13 | C | 5 | 12.5 | 0.9 | Müller-Hillebrand et al (1965) |
| Thailand | 100 | C | – | – | 9 (approx) | Pierce (1968a) |
| U.K. | 14 | PD | 3 | 4 | 1.8 | Whipple and Scrase (1936)[b] |
| U.K. | 17 | FC | 11 | 4 | 0.6 | Wormell (1939)[b] |
| U.K. | 16 | C | – | 30 | 1.0 | Horner (private communication) |
| U.K. | 16 | C | 4 | 30 | 0.5 | Stringfellow (1974) |
| U.S.A. | 30[c] | FC | 2 | 16 | 3.3 | Trueblood and Sunde (1949) |
| U.S.A. | 50[c] | FC | 2 | 16 | 7.2 | Trueblood and Sunde (1949) |
| West Germany | 15 to 25 | C | 3 | 17.5 | 1.0 to 4.7 | VDE (1968) |
| West Germany | 23 to 35 | C | 3 | 17.5 | 3.0 to 5.5 | VDE (1968) |

Legend:
C    counter
PD   point discharge
FC   field change

a   Assumed in reference.
b   With data from Golde (1945a).
c   From Golde (1973).

Ref: from Golde, 1977.

125

# Table 7.4
# Frequency of Occurrence of Ground Flashes
## (Power Transmission-Line Studies)

| Country | Regional annual thunderdays | Number of years | Ground-flash density $(km^{-2} yr^{-1})$ | Reference |
|---|---|---|---|---|
| Czechoslovakia | 30 | 6 | 6.3 | Popolansky (1960)* |
| Japan | 30 | — | 4 | Owa (1964) |
| Netherlands | 30 | — | 4 to 6 | Provoost (1970) |
| Sweden | 10 | — | 1.3 | Lundholm (1957) |
| U.K. | — | 10 | 0.5 (min) | Forrest (1945) |
| U.K. | — | 5 | 2 | Davis (1963) |
| U.S.A. | 39 to 62 | 7 to 8 | 7.4 to 12.1 | Golde (1945b) |
| U.S.A. | 30 | 5 | 6.2 | Griscom et al. (1965) |
| U.S.A. | 30 | — | 5.3 | Young et al. (1963) |
| West Germany | 20 to 24 | 4 to 8 | 2.3 to 6.2 | Baatz (1951)* |

*With data from Golde (1961).

Ref: from Golde, 1977.

# Table 7.5

## Ratio of Cloud Flashes to Cloud-Ground Flashes

| Item | Location of observation | Country | Height above sea level (m) | Latitude (λ) | Longitude | Source | Method (1) | Period | Number of flashes | Number of storms | Annual thunderdays T — During period of observations | Annual thunderdays T — Long period average (a) | Ratio (a) C to C-G flashes |
|---|---|---|---|---|---|---|---|---|---|---|---|---|---|
| 1 | Singapore | Singapore | 11 | 2°N | 104°E | Wang (1963) | FC | 1960-61 | 1340 | 37 | – | 171 | 5.9** |
| 2 | Zeta | Nigeria | 608 | 11°N | 8°E | Perry* | – | – | – | – | – | 81 | 7.0 |
| 3 | Bangalore | India | 908 | 13°N | 78°E | Aiyar and Sonde (1953) | FC+LFC +V | 1962-63 | – | – | – | 44 | 0.0 |
| 4 | Salisbury | Rhodesia | 1500 | 18°S | 31°E | Anderson** | FC | 1962-63 | 1062 | – | – | 65 | 2.2 |
| 5 | New Salisbury | Rhodesia | 1300 | 18°S | 30°E | Anderson and Jenner (1954) | LFC | 1953-54 | – | 72 | – | 65 | 5.5 |
| 6 | Brisbane | Australia | 0 | 27°S | 153°E | Prentice and Mackerras (1969) | V+LFC | 1960-69 | 10000 | – | – | 39 | 3.5 |
| 7 | Bulawayo East | S. Africa | 749 | 33°S | 26°E | Schonland and Craib (1927) | FC | 1926 | 749 | 15 | – | – | 5.0*** |
| 8 | Bulawayo East | S. Africa | 749 | 33°S | 26°E | Schonland (1928) | V | 1926-27 | 2125 | – | – | 26 | 2.4 |
| 9 | Dayr | Japan | – | 35°N | 131°E | Tamura (1944) | FC | 1938 | 2457 | – | – | 29 | 2.1 |
| 10 | Kyoto | Japan | 43 | 35°N | 135°E | Tamura (1944) | FC | 1933 | 4034 | – | – | 47 | 1.6 |
| 11 | New Mexico | U.S.A. | – | ~35°N | – | Fuquay (1962b) | V | 1961 | – | 13 | – | 28 | 1.6 |
| 12 | Montblel | Japan | – | 35°N | 139°E | Takeuti (1965) | FC | 1963 | – | 13 | – | 28 | 2.0 |
| 13 | Gunma Ken | Japan | 113 | 37°N | 139°E | Ishikawa (1960) | FC | – | 1245 | – | – | 30 | 3.0 |
| 14 | Auckland | New Zealand | 26 | 37°S | 174°E | Kreielsheimer and Ledge-Osborn (1971) | FC | 1968-69 | 577 | – | – | 15 | 2.7 |
| 15 | Washington Oregon | U.S.A. | – | 43°N | 123°W | Morris (1934) | V | .025-31 | 4690 | – | 25 | 28 | 1.6 |
| 16 | Turin | Switzerland | – | 46°N | 8°E | Muller-Hillebrand (1965) | FC | 1960-61 | 4781 | 24 | 47 | – | 2.2 |
| 17 | Missoula† | U.S.A. | 2000-2500 | 47°N | 116°W | Barnes (1963) | V+FC | 1958-59 | – | – | – | 29 | 2.0 |
| 18 | Missoula† | U.S.A. | 2000-2500 | 47°N | 116°W | Fuquay (1962b) | FC | Pre-1962 | – | – | – | 29 | 1.5 |
| 19 | Missoula† | U.S.A. | 2000-2500 | 47°N | 116°W | Fuquay (1962b) | FC | 1960-61 | 5200 | – | – | 29 | 1.55 |
| 20 | Missoula† | U.S.A. | 2000-2500 | 47°N | 116°W | Fuquay and Baughman (1969) | FC | 1965-67 | 12850 | – | – | 29 | 2.2 |
| 21 | Rivo | U.S.S.R. | 77 | 47°N | 40°E | Serploov (1967) | V | 1964-65 | 1729 | 23 | 26 | – | 2.7 |
| 22 | Kiev | U.S.S.R. | 178 | 50°N | 30°E | Serploov (1967) | V | 1964-65 | 684 | 22 | 30 | – | 5.3 |
| 23 | Cambridge | U.K. | 86 | 52°N | 0° | Pierce (1955) | – | – | – | – | – | 14 | 1.6 |
| 24 | Cambridge | U.K. | 85 | 52°N | 0° | Wormell (1939) | FC | Pre-1939 | 500 | – | – | 14 | 1.7 |
| 25 | L. Delat | U.S.S.R. | 1000 | 54°N | 102°E | Filippov et al. (1972) | V | 1968 | 4086 | 81 | – | 20 | 2.0 |
| 26 | Moscow | U.S.S.R. | 156 | 55°N | 38°E | Serploov (1967) | V | 1964-65 | 441 | 17 | 28 | – | 2.4 |
| 27 | Leningrad | U.S.S.R. | 4 | 60°N | 30°E | Serploov (1967) | V+FC | 1959-64 | 573 | 23 | 15 | – | 1.6 |
| 28 | Uppsala | Sweden | 16 | 60°N | 18°E | Muller-Hillebrand (1963) | FC | 1960-61 | 318 | – | – | 11 | 1.6 |
| 29 | Murmansk | U.S.S.R. | 46 | 69°N | 33°E | Serploov (1969) | V | 1964-65 | 140 | 7 | 6 | – | 0.9 |

(1) V = visual; FC = field change; LFC = lightning flash counter.
(2) Long-period averages for annual thunderdays obtained from World Meteorological Organization (1956).
† Station in vicinity of Missoula.

Ref: from Mackerras and Prentice, 1977.

\* Private communication (1972).
\*\* Private communication (1971).
\*\*\* Omitted from computer data for % versus T regression analysis.

127

# Table 7.7

## Frequencies of Thunderstorm Days in Florida

(a) FREQUENCIES OF OBSERVED NUMBER OF DAYS THAT EXPERIENCED x THUNDERSTORM EVENTS AT KSC FOR THE 11-YEAR PERIOD JANUARY 1957 THROUGH DECEMBER 1967

| x | Jan | Feb | Mar | Apr | May | Jun | Jul | Aug | Sep | Oct | Nov | Dec | Spring | Summer | Fall |
|---|---|---|---|---|---|---|---|---|---|---|---|---|---|---|---|
| 0 | 335 | 295 | 308 | 299 | 266 | 187 | 177 | 185 | 228 | 311 | 321 | 334 | 873 | 540 | 860 |
| 1 | 4 | 9 | 20 | 18 | 43 | 77 | 80 | 89 | 54 | 17 | 6 | 3 | 81 | 246 | 77 |
| 2 | 2 | 4 | 9 | 10 | 25 | 40 | 47 | 30 | 33 | 9 | 3 | 2 | 44 | 117 | 45 |
| 3 |  | 2 | 3 | 3 | 3 | 17 | 26 | 24 | 12 | 4 |  | 2 | 9 | 67 | 16 |
| 4 |  |  | 1 |  | 3 | 6 | 9 | 10 | 3 |  |  |  | 4 | 25 | 3 |
| 5 |  |  |  |  | 0 | 2 | 2 | 3 |  |  |  |  | 0 | 7 |  |
| 6 |  |  |  |  | 1 | .1 |  |  |  |  |  |  | 1 | 1 |  |
| n | 341 | 310 | 341 | 330 | 341 | 330 | 341 | 341 | 330 | 341 | 330 | 341 | 1,012 | 1,012 | 1,001 |

(b) RELATIVE FREQUENCY OF DAYS THAT EXPERIENCED AT LEAST ONE THUNDERSTORM AT KSC

| Jan | Feb | Mar | Apr | May | Jun | Jul | Aug | Sep | Oct | Nov | Dec | Spring | Summer | Fall |
|---|---|---|---|---|---|---|---|---|---|---|---|---|---|---|
| 0.018 | 0.048 | 0.097 | 0.094 | 0.220 | 0.433 | 0.481 | 0.457 | 0.309 | 0.088 | 0.027 | 0.021 | 0.137 | 0.458 | 0.141 |

Ref: from Proceedings of 4th Annual Workshop on Meterological and Environmental Inputs to Aviation System, March 1980.

# Table 7.8
## Annual Variation in Occurrences of Lightning and Rainfall, Brisbane*

| | JUL | AUG | SEP | OCT | NOV | DEC | JAN | FEB | MAR | APR | MAY | JUN |
|---|---|---|---|---|---|---|---|---|---|---|---|---|
| Thunderdays per month | 0.3 | 0.4 | 0.6 | 2.4 | 4.4 | 5.1 | 2.7 | 3.2 | 1.7 | 0.6 | 0.3 | 0.2 |
| Thunderstorms per thunderday | 1 | 1 | 1 | 1.12 | 1.05 | 1.08 | 1.15 | 1.1 | 1.06 | 1 | 1 | 1 |
| Flashes per thunderstorm | 5 | 36 | 73 | 250 | 267 | 300 | 233 | 120 | 70 | 47 | 71 | 27 |
| Flashes per month | 2 | 15 | 44 | 676 | 1,235 | 1,645 | 725 | 418 | 126 | 28 | 21 | 5 |
| Rainfall (mm) per month | 49 | 30 | 45 | 77 | 92 | 136 | 142 | 183 | 147 | 77 | 67 | 56 |

*Visual observations (mean values for all recorded thunderstorms, 1958-68).
Ref: from Golde, 1977.

Figure 7.1

Thunderstorm Days (Isokeraunic Level)*
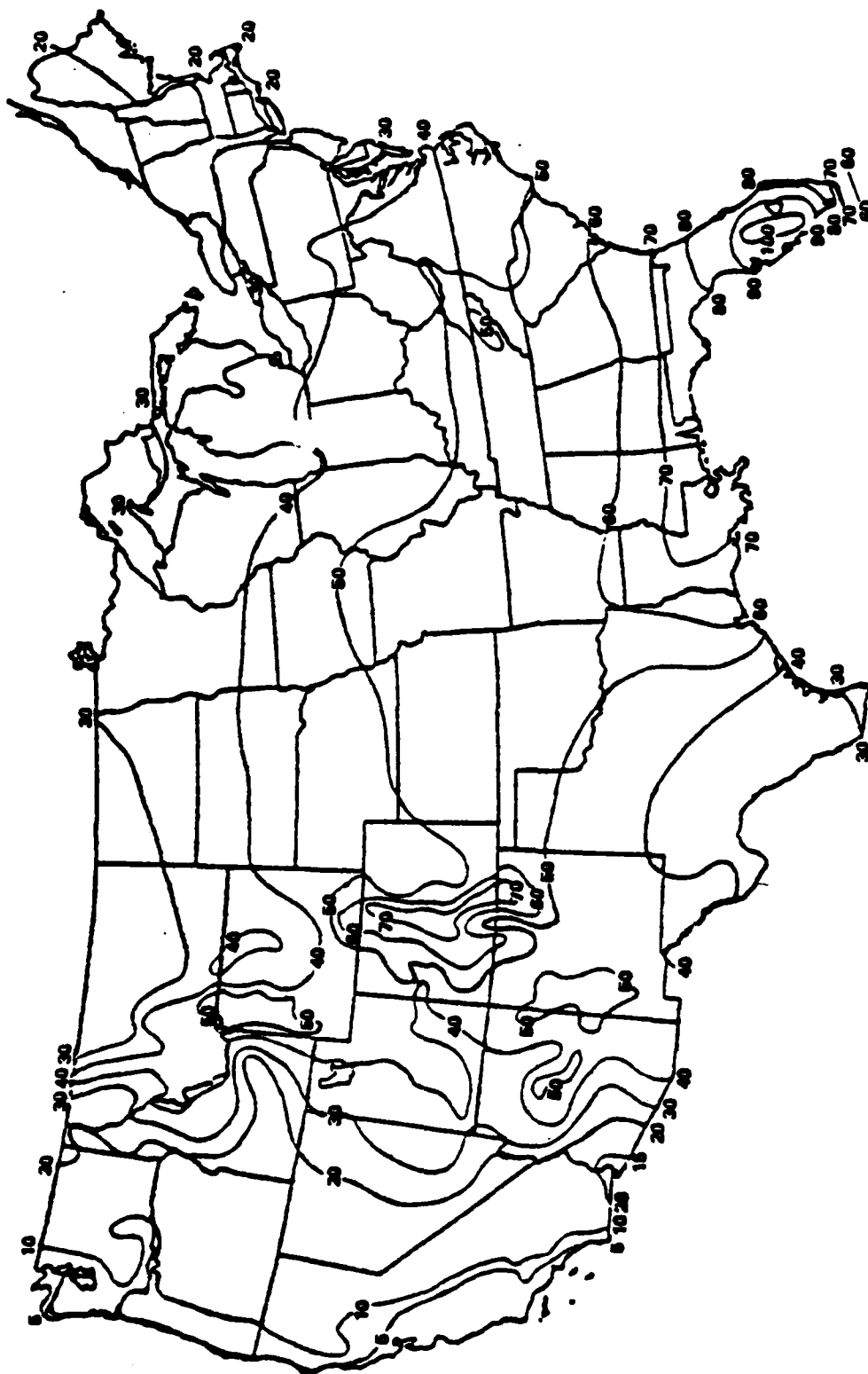
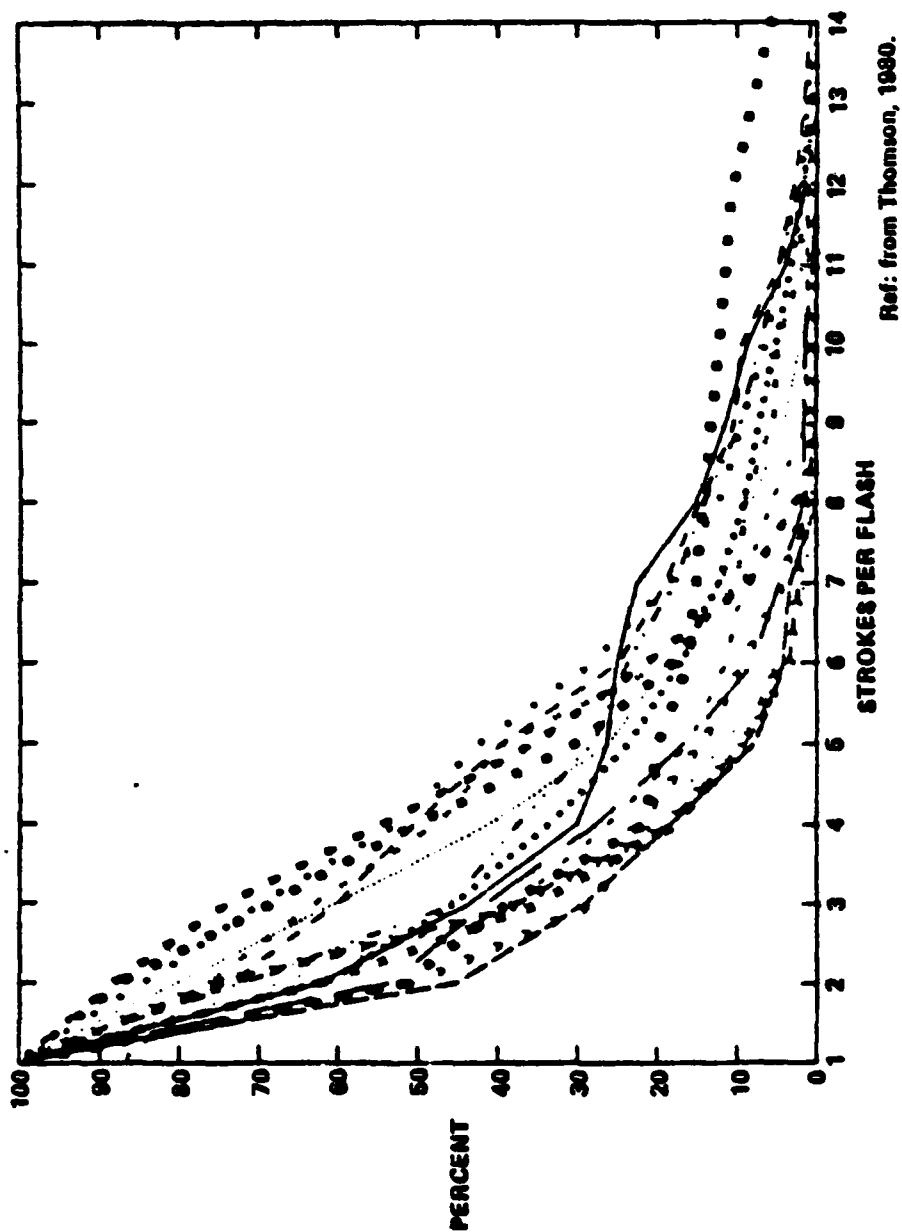*Within the continental United States, as reported by U.S. Weather Bureau. (Mean annual number of days with thunderstorms.)

Figure 7.2
Cumulative Frequency Distributions—
Number of Strokes per Flash
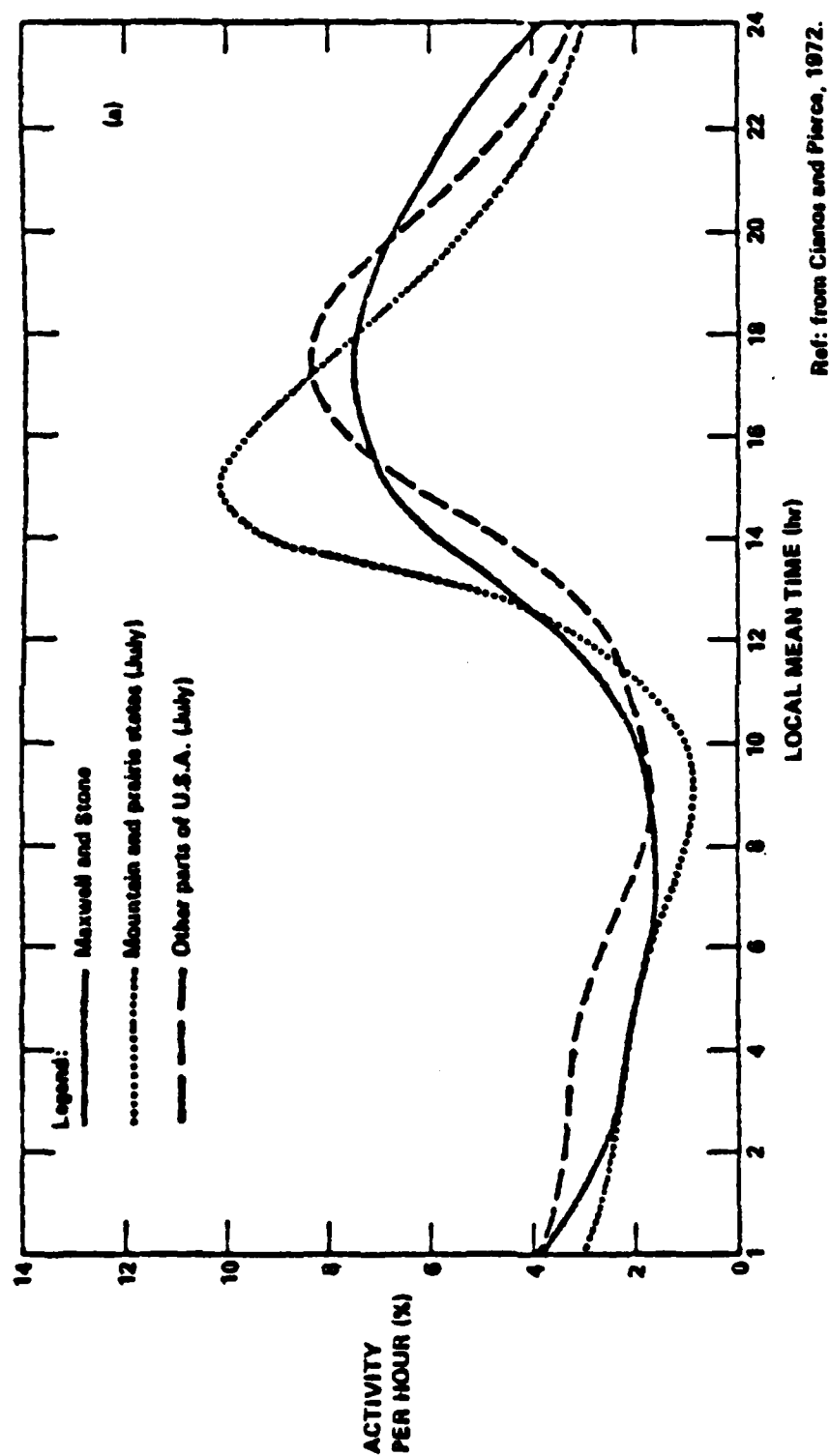
Figure 7.3

Diurnal Variation of Thunderstorm Activity

PERCENTAGE OF STRIKES

(km)

THOUSANDS OF FEET

USA
(NEWMAN 1950-61)

UK/EUROPE
(PERRY 1959-75)

USSR
(TURNOV 1969-74)

EUROPE/SA
(ANDERSON 1965-74)

USA
(PLUMER 1971-75)

(PISTON)

(TURBOJET AND TURBOPROP)
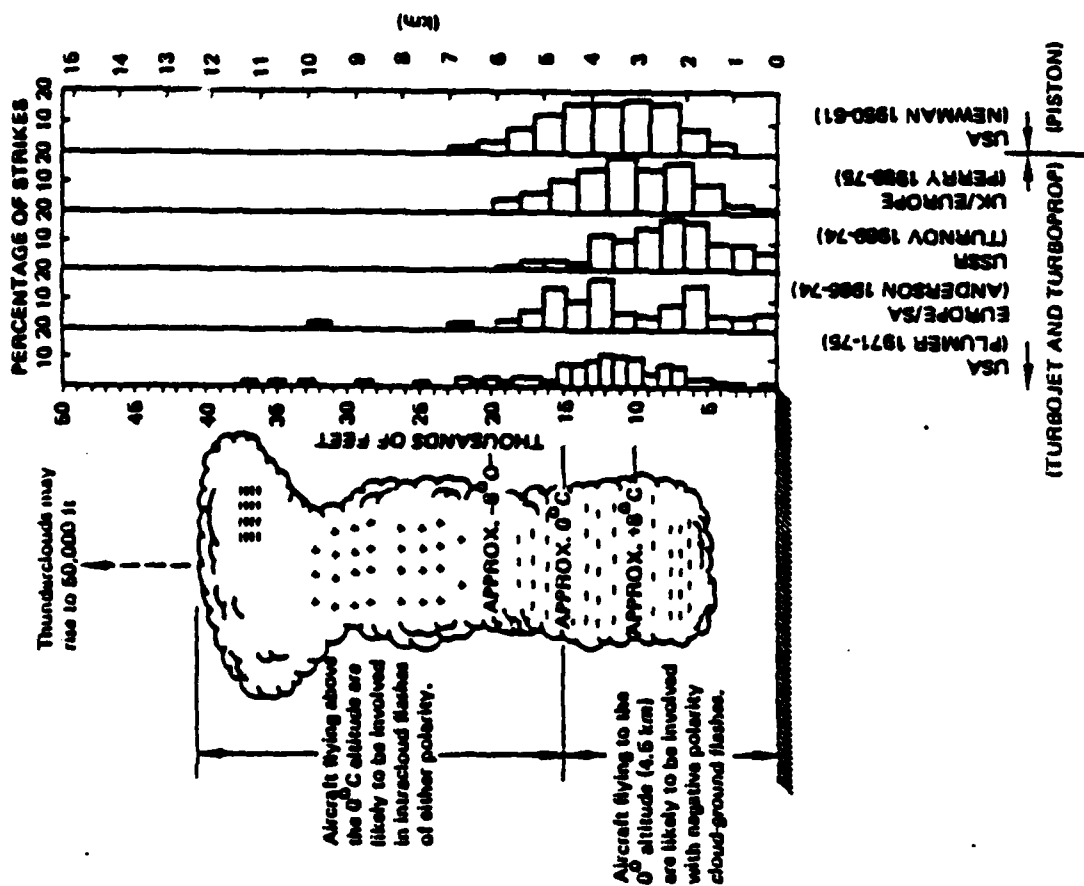
Ref: from Fisher and Plumer, 1977.

Thunderclouds may rise to 60,000 ft.

APPROX. -8 °C

APPROX. 0 °C

APPROX. 8 °C

Aircraft flying above the 0° C altitude are likely to be involved in intracloud flashes of either polarity.

Aircraft flying to the 0° altitude (4.5 km) are likely to be involved with negative polarity cloud-ground flashes.

8401B4-14

Figure 7.4
Aircraft Lightning Strike Incidents
as a Function of Altitude

133
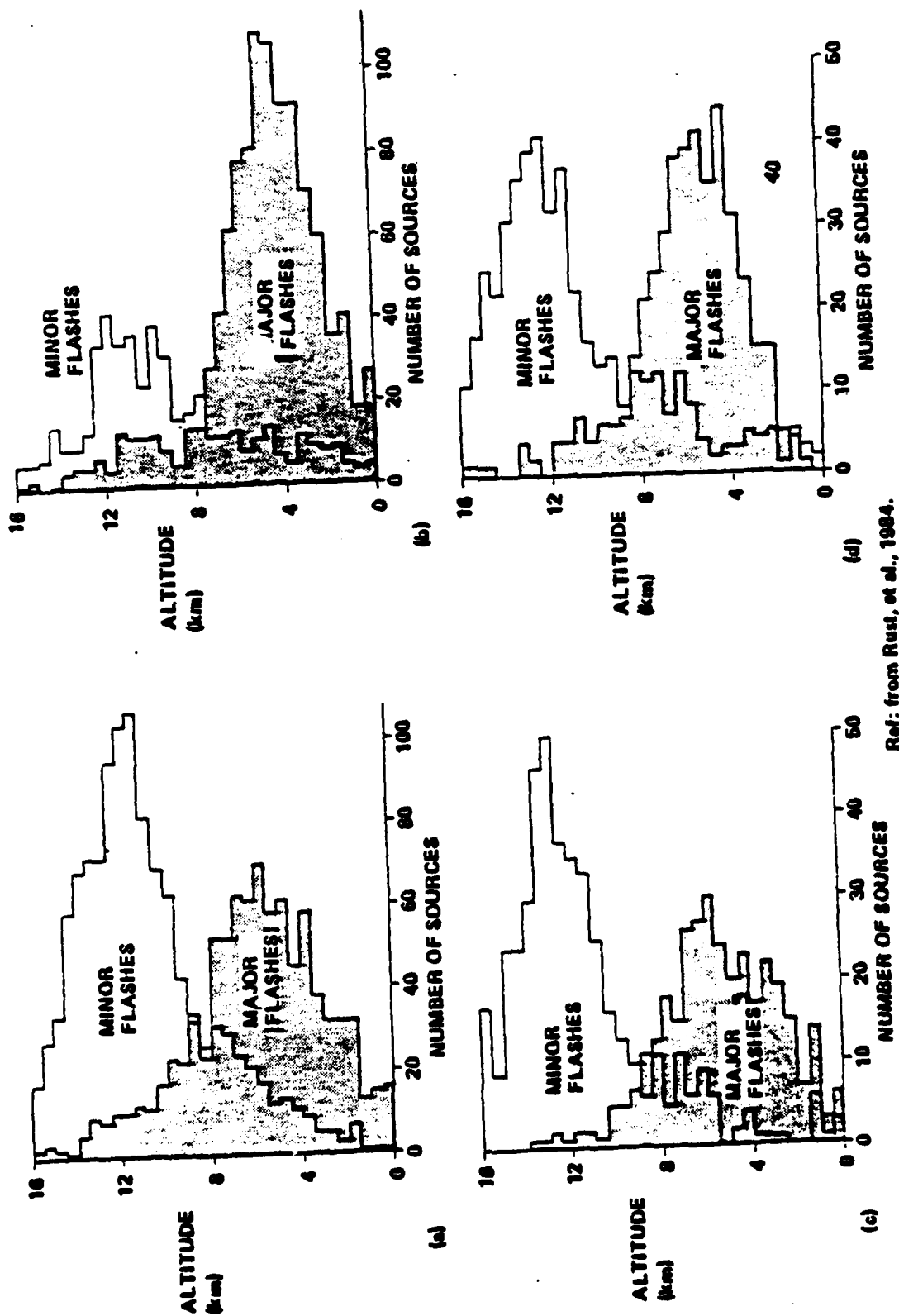
Figure 7.5

Altitude Distributions of VHF Lightning Impulse Sources,
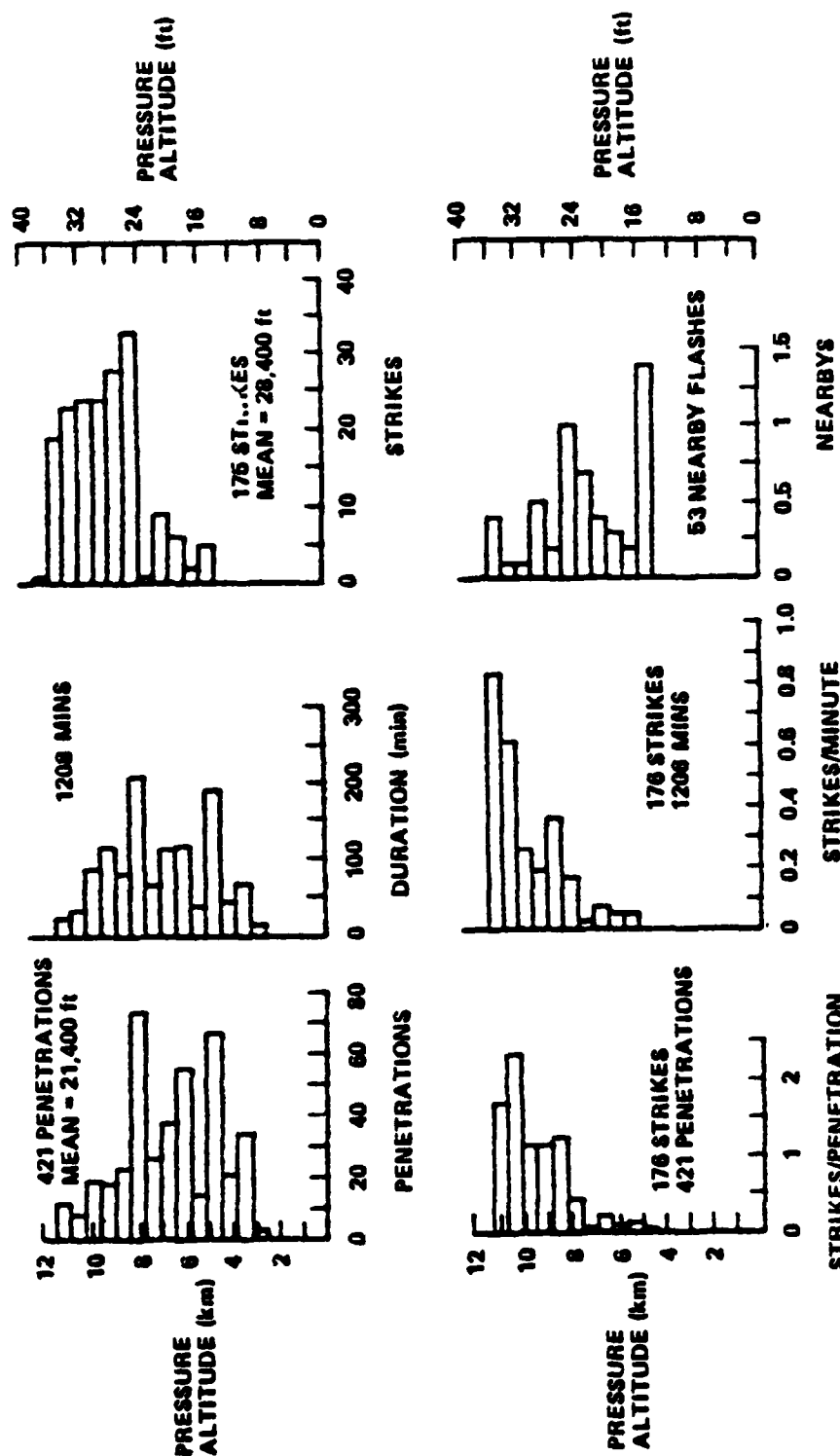19 June 1980

Ref: from Rust, et al., 1984.

Figure 7.6

Thunderstorm Penetrations and Lightning Statistics*
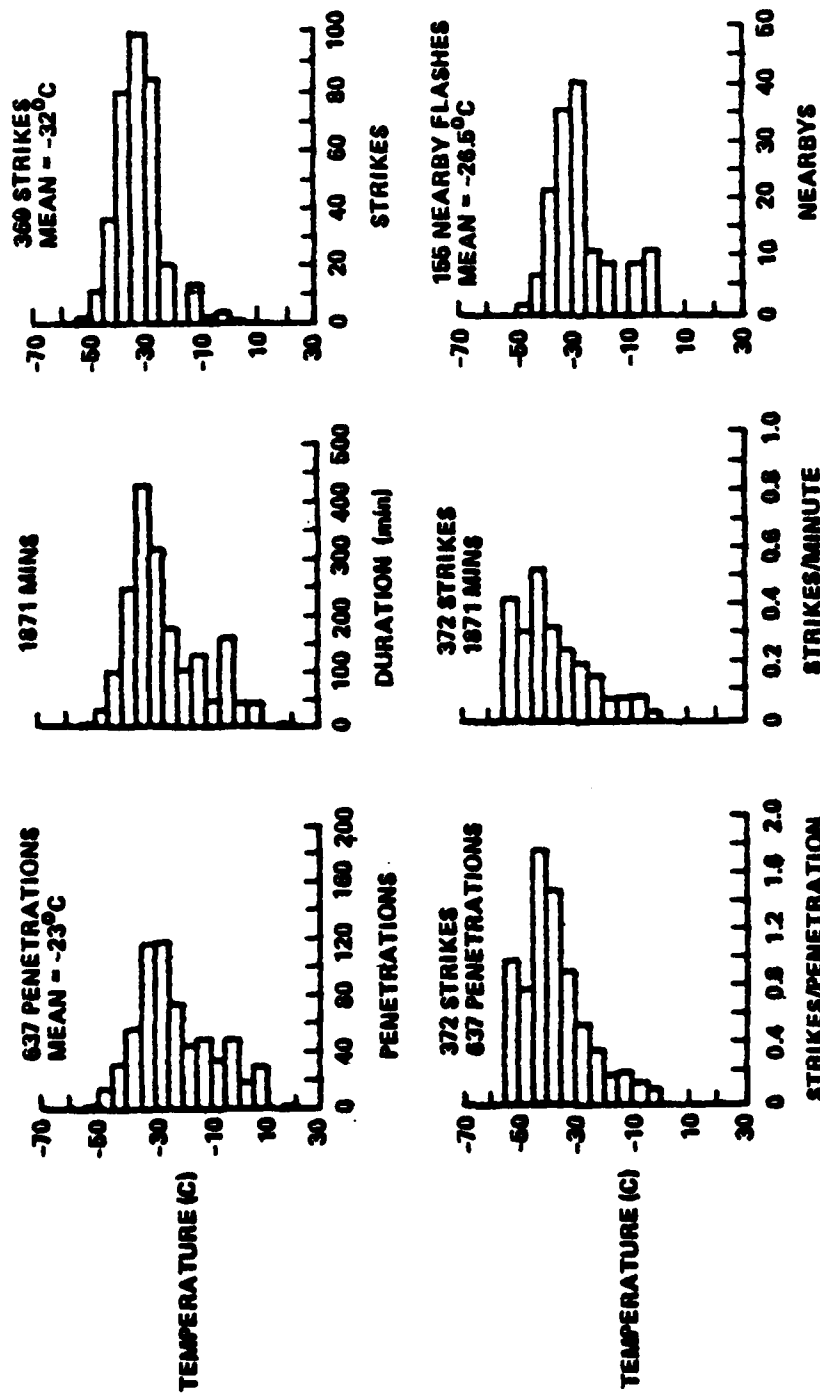
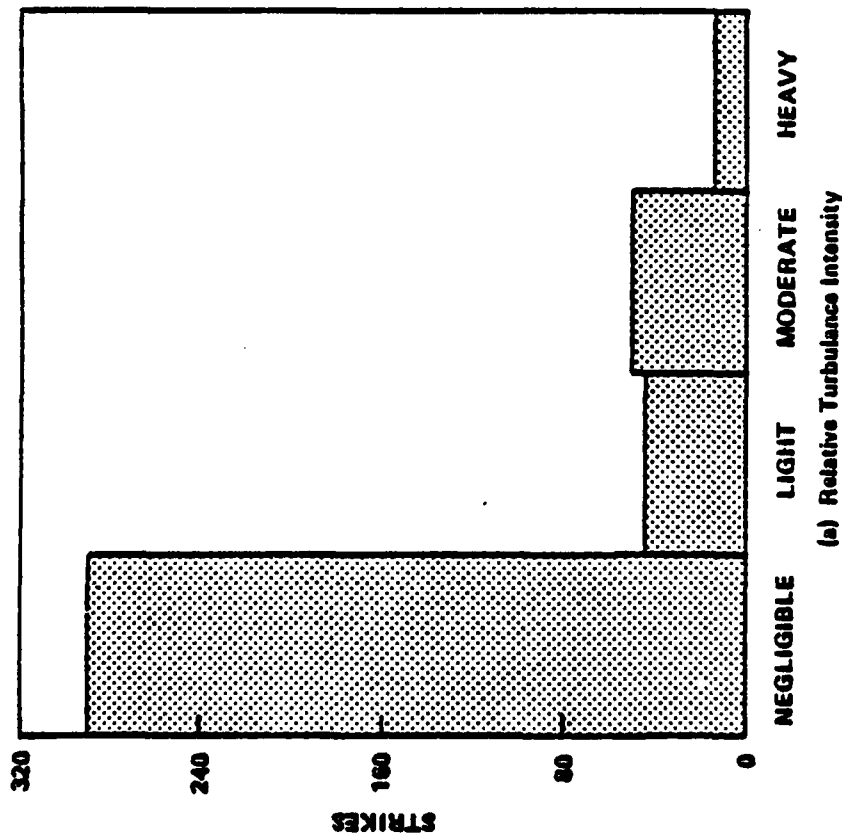*As a function of ambient temperature for storm hazards 1980-83.

Ref: Fisher, et al., 1984.

Figure 7.7

Thunderstorm Penetrations and Lightning Statistics*

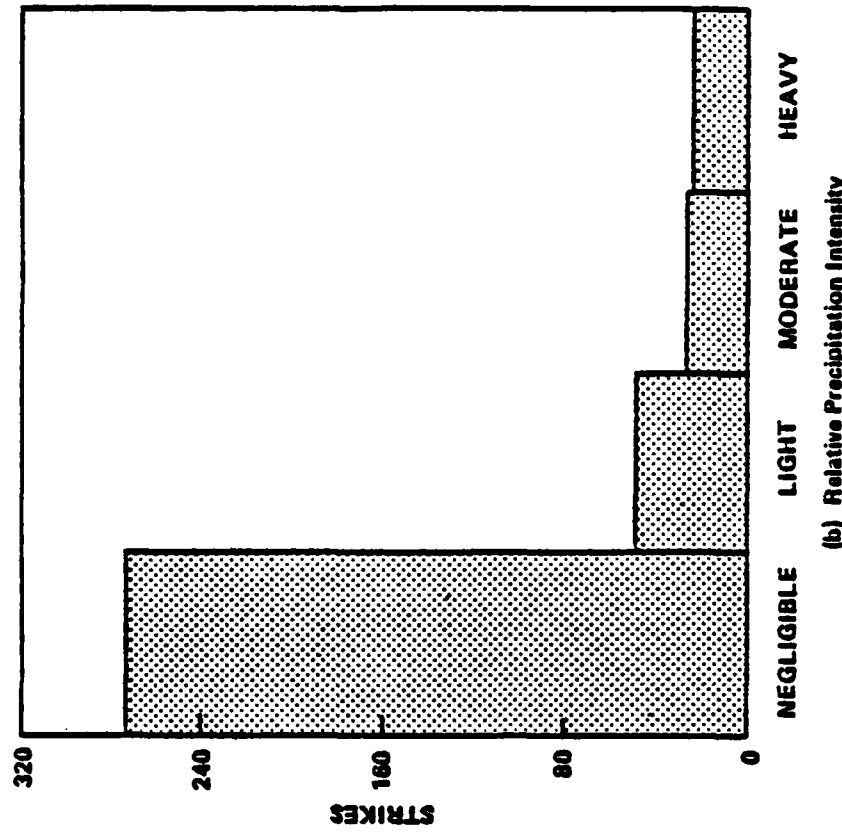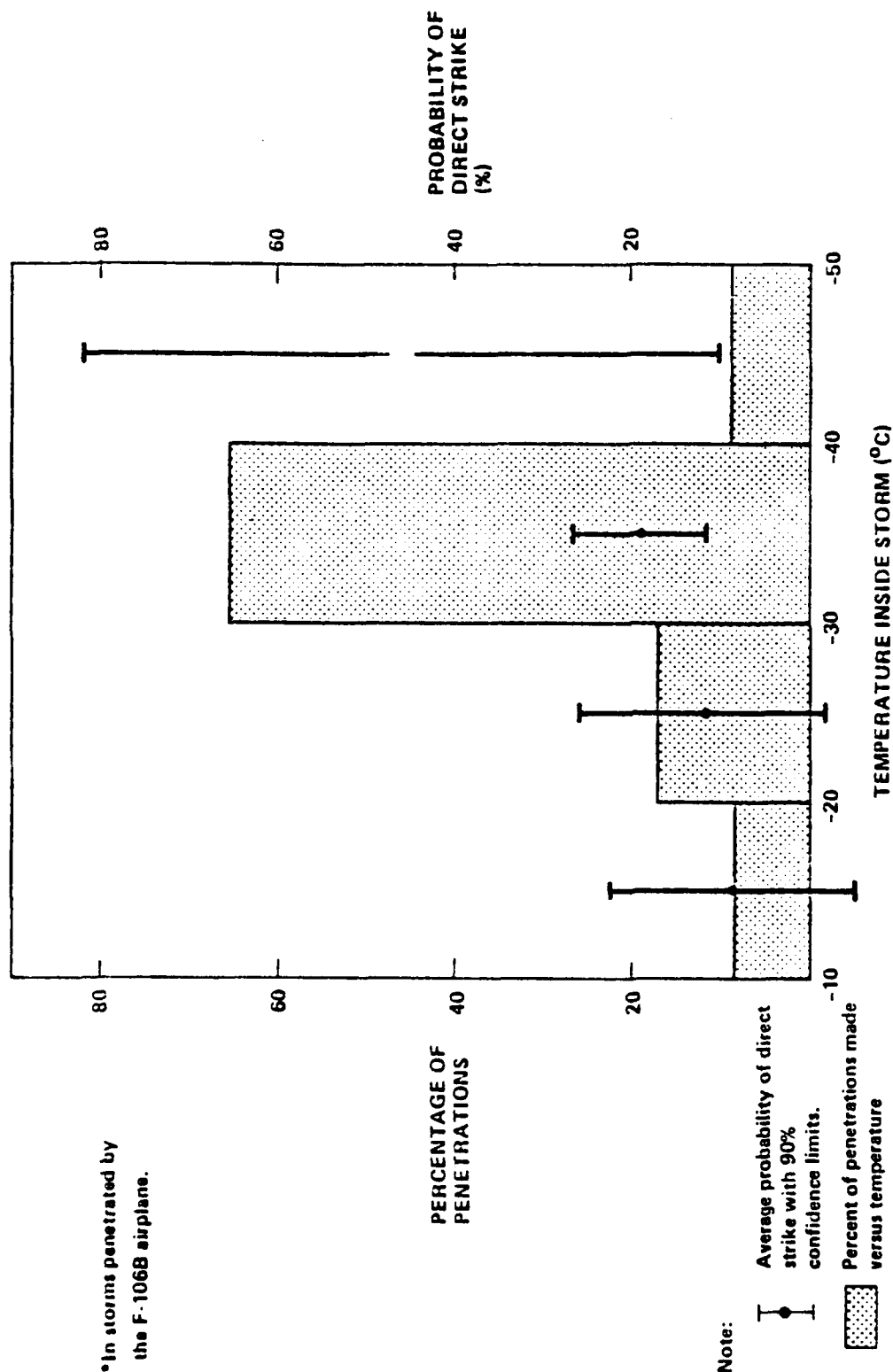*As a function of pressure altitude for storm hazards 1980-82.

Ref: Fisher, et al., 1984.

Figure 7.8
Relationship of Lightning Strikes to Relative Turbulence and
Precipitation Intensities*

137

Figure 7.9
Temperature Inside Storms
and Probability of Direct Strike *
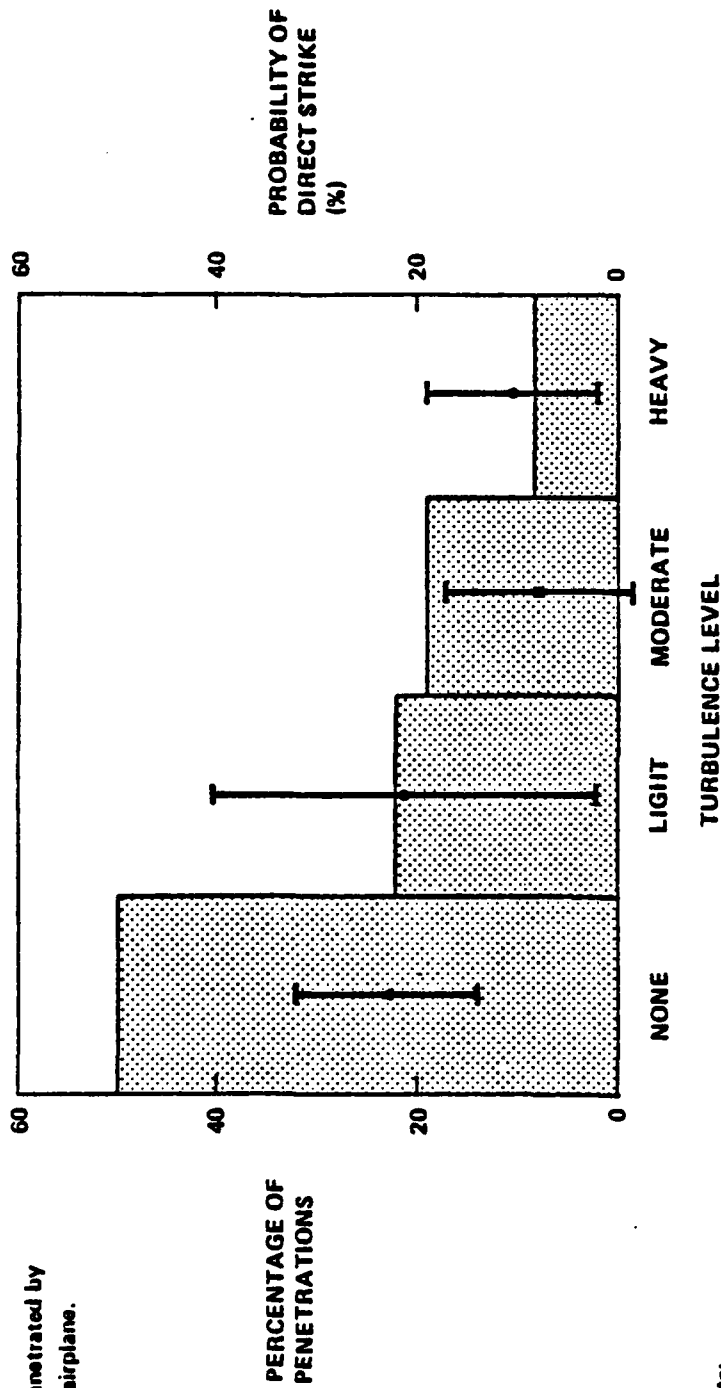
Ref: Mazur et al., 1984.

Figure 7:10
Turbulence Level and
Probability of Direct Strike*

139

Figure 7.11

Rain Intensity and Probability of Direct Strike *

Figure 7.12

Lightening Flash Rate and Probability of Direct Strike*
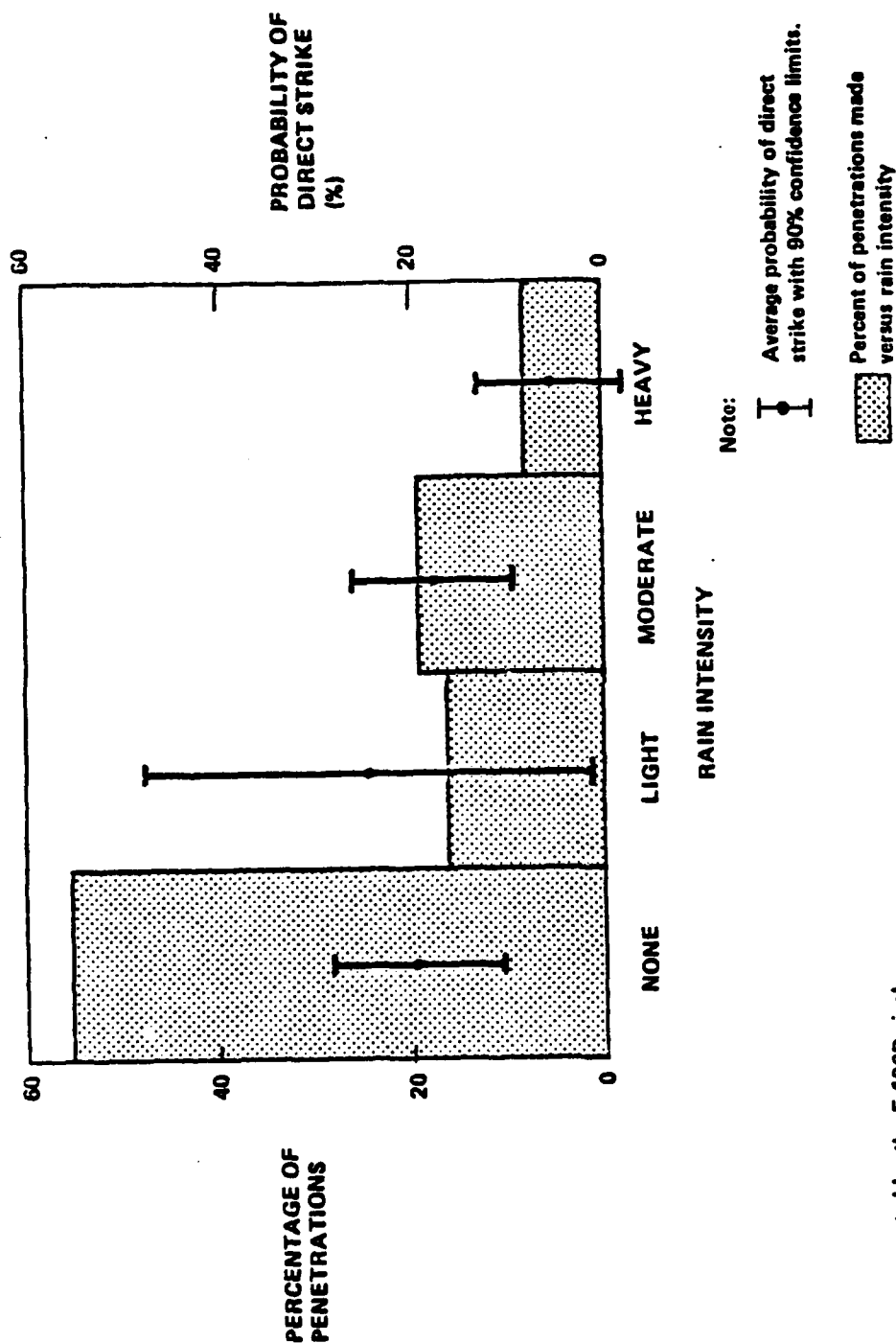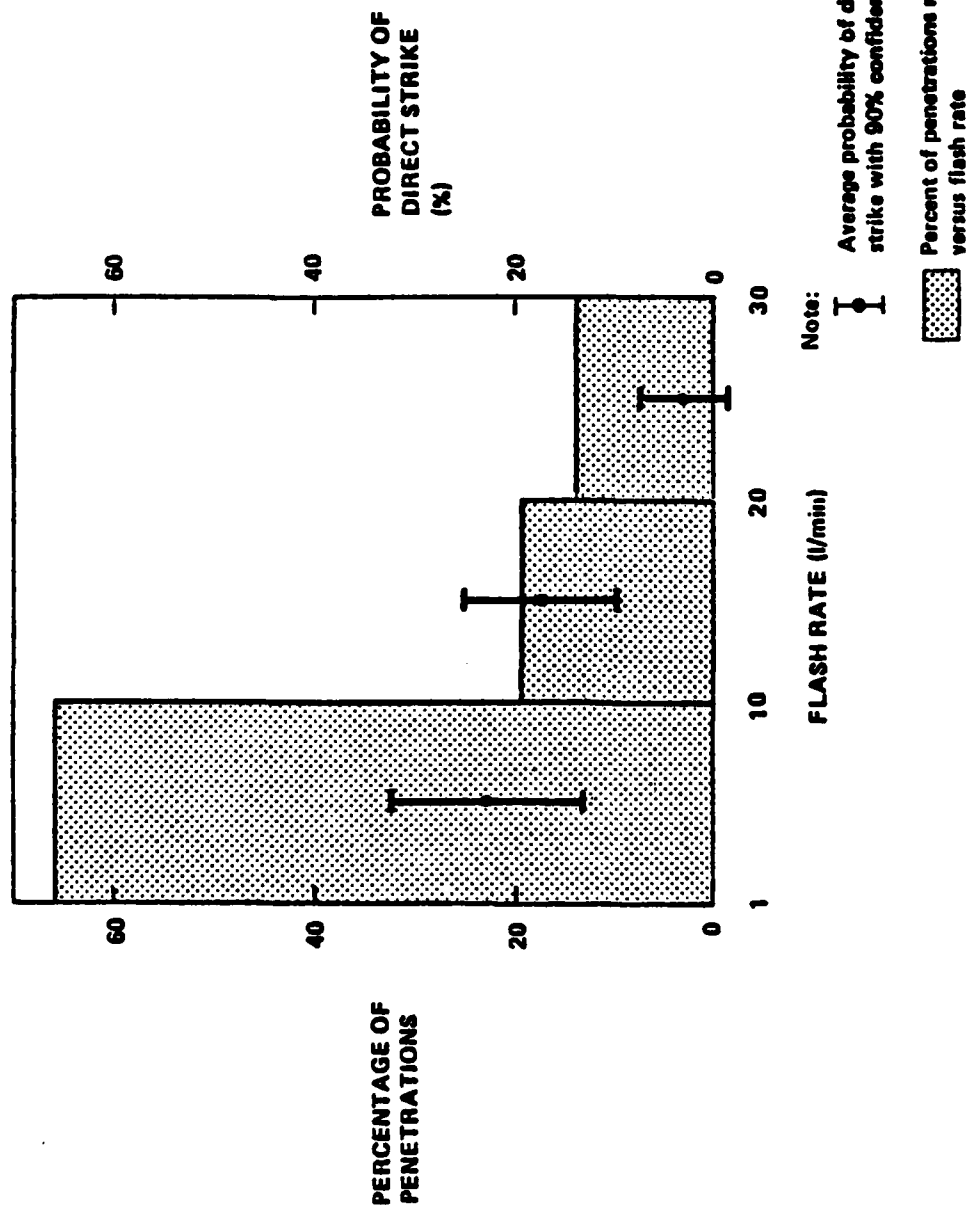
*In storms penetrated by the F-106 airplane.

# 8.0 SUMMARY

This document provides definition of the AEHP program threat environment. The threat document will be revised periodically to provide the "best" current definition of AEH threats. This issue summarizes the initial atmospheric electricity threat to be used for the AEHP program. The experimental basis for this threat was critically reviewed. Comparisons with measured statistical data were made as well an assessment of the validity of the data. Comments on on-going lightning data collection programs are made. This data will impact the final threat definition. The initial AEH threat definition is needed to support the Phase I environmental impact tests. A final AEH threat definition will arise out of additional studies of existing data as well as new data as it becomes available.

The topics included in this document are definition and review of lightning data sources, data comparison with the initial lightning threat parameters, lightning model review and discussion, static electrification threat levels, parametric threat levels of both lightning and static electricity, and comparison of lightning with NEMP and EMI threats. A discussion on meterological environment effects will be added in the next issue.

## 8.1 CONCLUSIONS

The initial definition of the AEHP lightning threat is compared to ground-based direct current tower measurements. The validity of the measured data was critically reviewed. To refine the ground lightning threat, the available statistical data sets (including Berger, Garbagnati, Uman, Eriksson, Cianos and Pierce and Popalansky) must be critically assessed and quantitatively as to accuracy and experimental limitations. The earlier data (Cianos and Pierce and Popalansky) do not reflect the fast rise times recently measured and thus the data base is biased toward longer rise times. Both the tower current data and the lightning current values derived from field measurements are subject to uncertainties. These uncertainties need to be quantitatively assessed for use in an updated current threat level.

The static electrification threat is based on published measurements of streamer and corona noise. Static electrification threat levels may change in the future as new avionic/electronic technology (fly-by-wire) and materials

(graphite/epoxy, Kevlar, etc.) are used in newer aircraft. Charging rates and locations of corona and streamers may change as well as the coupling to aircraft systems. As advanced technology aircraft are designed, static electrification threat levels may have to be updated.

The conclusions reached to date in defining an appropriate atmospheric electricity threat are:

1. Present lightning threat is based on currently available industry draft standards and Boeing interpretation of newer high rate of rise data. Static electrification is defined from prior measurements of corona and streamer noise.

2. Newer measurements of lightning current trends toward higher current rise rates. Reinterpretation of older tower data, newer instrumentation and derivation current parameters from field measurements generally point to faster current rise times and higher current rise rates.

3. Airborne data indicates lightning current amplitudes smaller than ground based measurements but rates of rise may be the same.

4. Technical problems arise in assessing old and new lightning measurements:

   a. Experimental limitations difficult to quantify from published results.

   b. Sample size of data from each experimenter is too small for a reasonable statistical confidence level.

   c. Data is often not presented in form to correlate lightning parameters of interest (e.g. amplitude vs. rate of rise).

   d. Tower measurements may underestimate current rise rates due to impedance and leader effects.

e. Current parameters derived from field measurements are subject to a variety of uncertainties. Velocity of propagation assumed can introduce large uncertainty. A factor of two may also arise from assuming the stroke initites at the ground and propagates upward.
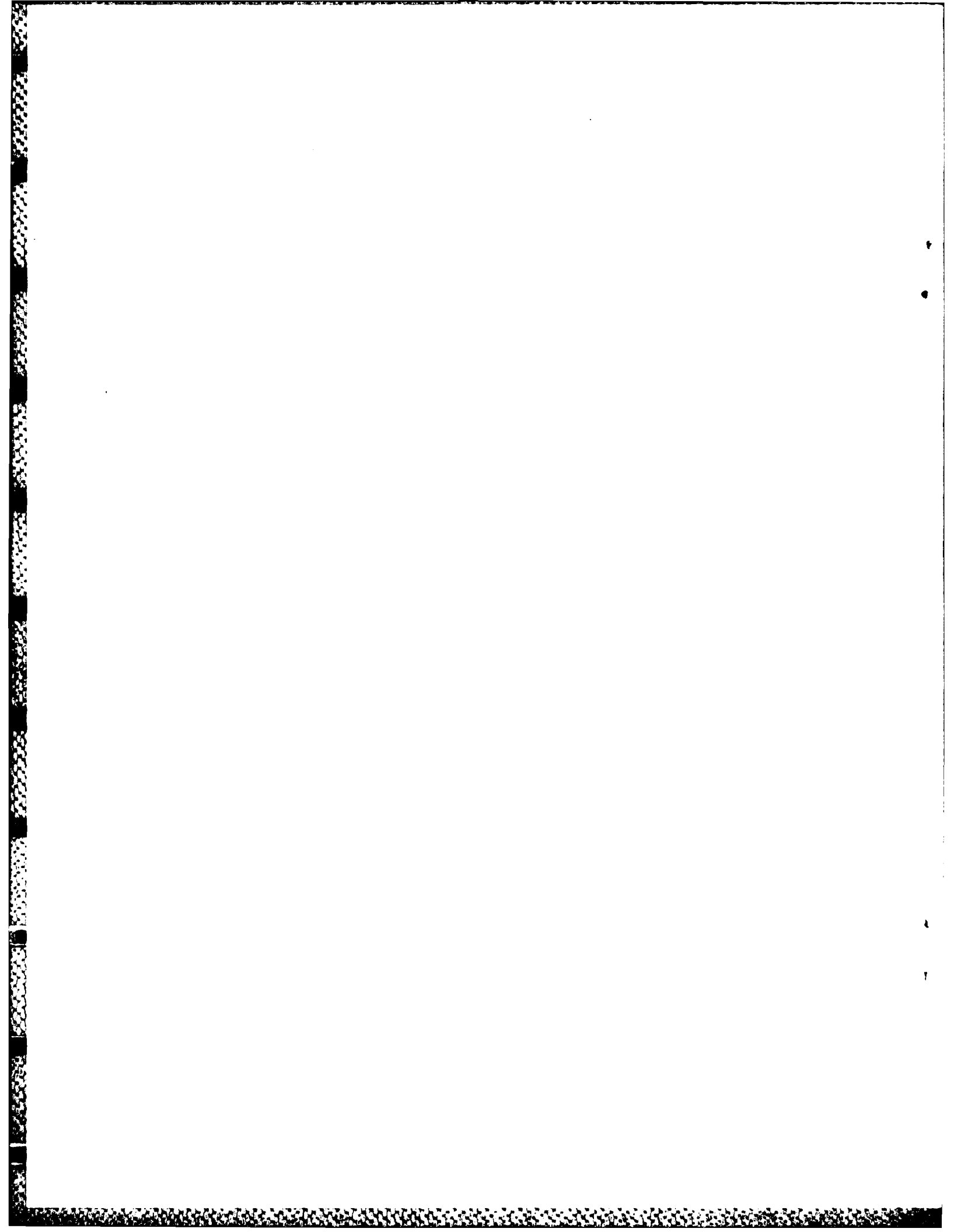
## 8.2 RECOMMENDATIONS

The atmospheric electricity threat directly affects aircraft protection. Uncertainty in the threat level imposes a penalty factor for all future technology aircraft. New materials (graphite composite, Kevlar, etc), fly-by-wire flight control and increased systems integration introduce new requirements for protection. An accurate atmospheric threat level imposes the least overprotection requirements with consequent lower cost and weight penalties. The present uncertainty in the atmospheric electricity threat is estimated to be within a factor of two from the present AEH threat definition. The only way to increase the accuracy of the threat is by obtaining more data. This objective can be accomplished in the following ways:

1. Airborne data collection. This is the most critical need for defining an airborne threat level. Flight tests should be continued to establish a future data base. This method is expensive and will not yield a large enough volume of data for many years. The immediate benefit would be better understanding of the interaction between naturally occurring lightning and aircraft in flight.

2. Ground strike current measurements. Continuation of studies similar to Berger, Garbagnati and Eriksson on towers. The towers need calibration to establish effects of the tower inductance and local ground impedance on the lightning current waveforms. Geographical effects on lightning could be established by a network of towers. Rocket triggered lightning experiments offer the advantage of near certain strikes.

3. Simultaneous measurements. This would allow correlation of fields, visual pictures of the stroke, and luminosity measurements as a function of time. These would help establish a more accurate means of deriving current parameters from field data. The pictures would establish orientation and tortuosity profiles. The luminosity data would establish the velocity of propagation more accurately.

4. <u>Luminosity measurements</u>. More data is needed to establish velocities of propagation near the ground as a function of distance away from the initiation point. Velocities are needed to establish more reliable means of obtaining current parameters from field data and for checking theoretical lightning models.

5. <u>Reprocess the existing data base</u>. The most effective way to establish a more accurate AEH threat is to compile and evaluate all existing lightning data to date. This approach could bring the uncertainty down to within a factor of two from the present AEHP threat. To analyze the presently available data more appropriately:

   a. Raw data must be collected and experimental setups and limitations established from unpublished sources.

   b. Quantify errors/uncertainties to put the experimental data on a common basis.

   c. Derive the statistical threat levels from the total data base accumulated.

A complete lightning definition program would pursue all the items listed above as cost allowed. The most effective approach, however, is item (5). This approach also has the possible advantage of establishing future calibration needs for various types of experiments. This could lead to better quality data being obtained from future efforts to quantify naturally occurring electricity environments.

*U.S. GPO 559-065*

# END

# FILMED

11-85

# DTIC